Sleeping on the Job: How studying sleep and circadian rhythm disturbances in a mouse model of Dravet syndrome kept me up at night

Raymond Sanchez

A dissertation

submitted in partial fulfillment

of the requirements for the degree of

Doctor of Philosophy

University of Washington

2020

Reading Committee:

Horacio O. de la Iglesia, Chair

Ethan Buhr

Franck Kalume

Program Authorized to Offer Degree:

Neuroscience

University of Washington

Abstract

Sleeping on the Job: How studying sleep and circadian rhythm disturbances in a mouse model of Dravet syndrome kept me up at night

Raymond EA Sánchez

Chair of Supervisory Committee: Horacio O. de la Iglesia

Department of Biology

Epilepsies are among the most common neurological disorders in the world, and sleep disturbances are highly comorbid with many forms of epilepsy. Dravet syndrome (DS) is a severe form of childhood onset epilepsy caused by haploinsufficiency of the *Scn1a* gene encoding the pore-forming alpha subunit of the $Na_V1.1$ sodium channel, which is expressed primarily in GABAergic neurons. In addition to intractable seizures, DS is characterized by severe sleep disturbances and high risk of sudden death during sleep. Previous characterizations of a mouse model of DS containing a heterozygous deletion of *Scn1a* demonstrated that these mice display deficits in the circadian regulation of locomotor activity. We predicted that DS mice would also display impaired circadian regulation of sleep and hypothesized that these disturbances are caused by loss of neuronal excitability resulting from reduced $Na_V1.1$ expression in the suprachiasmatic nucleus (SCN), the master circadian clock. Through a combination of genetic, physiological and behavioral experiments, we provide novel insights into the role of $Na_V1.1$ sodium channel expression in the SCN in circadian sleep regulation and the nature of sleep disturbances in this debilitating disease. In addition, we leverage our data to develop novel methods for the analysis of sleep data and encourage more researchers to study the circadian regulation of sleep in pre-clinical models of disease.

Table of Contents

Acknowledgments

I cannot overstate how fortunate I've been to have found such an amazing community of colleagues, mentors and friends during my PhD. First and foremost, I need to thank my thesis mentor **Dr. Horacio de la Iglesia**. Your endless patience, compassionate mentorship and incredible Argentinian-style barbecue have gotten me through what would have otherwise been a rough 5 years. I'm constantly inspired by your intelligence and creativity in the lab and I'm so grateful for the time I've had to work with you.

I want to thank my committee, **Drs. Franck Kalume, Bill Catterall, Richard Palmiter, Ethan Buhr** and **David Gire**, all of whom have provided me with invaluable guidance over these last few years. Thanks especially to Franck and Bill, who opened their labs to me for rotations, and have continued to be mentors to me long after those rotations ended. Franck, I'd have no idea how to spot an interictal spike if it wasn't for you! Finally, without **Dr. Bing Brunton**, the entirety of my Chapter 3 would not have been possible. She is brilliant and I'm deeply grateful to her for patient explanations of the ins and outs of digital signal processing and machine learning. I also want to thank the UW Neuroscience program, especially **Lucia Wisdom, Kyle Shea, Dr. David Perkel,** and **Dr. Jane Sullivan**, and my funding sources at the Washington Research Foundation Institute for Neuroengineering.

The de la Iglesia lab has been a second family to me and made coming into work every day so much fun. I want to thank every member of the lab I've worked with over the last 5 years, past and present, but especially the following people: **Dr. Ivana Bussi**, one of the absolute best scientists and human beings I know, thanks for sticking out the ups and downs of being on Team

Scn1a with me and for the countless hours of laughs and commiseration in the lab; **Dr. Miriam Ben-Hamo**, an inspiring scientist and future physician from whom I learned so much; **Dr. Leandro Casiraghi**, for demystifying actiwatches and being a fantastic scientist and great friend; **Dr. Gideon Dunster**, for sharing the ups and downs of being a grad student with me and (usually) making all those times you got me off-task at work worth it with your sense of humor and love of bringing the lab together; **Dr. Macarena Aloi**, for being such a fun collaborator and introducing me to the wonderful worlds of Alzheimer's disease and microglia; **Luis Salazar** for being a great friend and mouse colony dad; **Kaitlyn McGlothlen**, for diving into the human side of science with me in our conversations with homeless study participants; (soon-to-be Dr.) **Jazmine Perez**, for being my first friend in the lab and teaching me to do ECoG/EMG surgeries, which became the bread and butter of my thesis; and **Tenley Weil** for giving me my first real experience being a research mentor. I'm hopeful that the next generation of de la Iglesia labbies will have the same positive experience that I did.

Many of my colleagues at UW have become lifelong friends, and for no one is this truer than for **Aaron Garcia, Mohammad Tariq, Rapheal Williams** and **Ryan Farero.** The four of you have become my family and none of this would have been possible without freestyle Fridays/jam sessions, late nights out and soft committing to just about everything we do. Y'all are the absolute best humans.

My family hasn't always understood what it is I do, but they have been unbelievably supportive every step of the way. To my **Mom and Dad**, thank you both for providing me with such powerful examples of what can be accomplished through perseverance and determination, and

for always putting my needs before your own. To my **sisters Tiare and Aubrianna**, thanks for putting up with me talking about brain stuff at holidays when I know you probably couldn't care less! I love you all very much.

To **Andrea**, my fiancé and partner of almost 8 years, I don't have enough words to express how incredibly grateful I am to you. Your love, kindness, patience and understanding during my PhD have been what's kept me going, and I can't thank you enough for everything you've done for me. I'm sorry for all those hours I made you wait in the car on the weekends while I went to check on the mice, but I promise in the end it will have all been worth it! I love you so much.

I want to dedicate this thesis to my grandfather **Gilbert Sanchez**, my grandmother **Leilah Green**, my aunt **Shirley Caramella** and cousin **Gavin Caramella**. Your experiences with mental health, whether trying to help others improve their mental health or struggling with your own, opened my eyes to the urgency with which we desperately need to understand more about how the brain works to alleviate the suffering of countless people around the world. You are loved and missed.

Finally, I'd be remiss not acknowledging that I am completing my PhD at a time when the United States is reckoning with its long history of systemic racism, especially anti-Black racism, in the midst of a world-changing pandemic that is disproportionately affecting people of color. Academia has a history of being oppressive to people from underrepresented groups. When I started the graduate school interview process, a Latino faculty member told me that as a PhD student of Latino and Pacific Islander descent, I'd need to work extra hard to stand

out because my representation in academia would be important for other people of color to see. I don't know whether I've succeeded in this, but I do know that no matter what comes next in my career, I will commit myself to continuing the work necessary to make STEM fields more equitable, inclusive and welcoming to researchers from underrepresented and marginalized groups.

Introduction

Biological Clocks and Rhythms

The success of a species is highly dependent on its ability to adapt to environmental pressures. As a consequence of the rotation of the Earth around its own axis and the sun, life evolved under multiple rhythmic environmental regimes, including both seasonal and daily changes in light exposure, temperature and weather conditions. It should come as no surprise then that nearly every species on Earth has developed a biological timekeeping system that can anticipate these changes and organize physiology and behavior in a way that is advantageous for the organism[1]. Life forms as seemingly disparate as plants[2], humans[3], fungi[4], cavefish[5], and bees[6], to name a few, all have biological clocks in common. Decades of investigation into these biological timekeeping systems have revealed them to be among the most important and highly conserved characteristics of life on our planet.

These nearly ubiquitous biological clocks have three key characteristics: they are endogenous to the organism, they can synchronize to environmental cycles (entrainable), and they continue functioning regardless of external temperature (temperature conserved)[1]. These characteristics allow organisms to both adjust their biological rhythms to align with environmental cycles, a process called entrainment, and to maintain rhythmicity in the absence of environmental stimuli. This process is illustrated in a diagram called the eskinogram shown in Figure 1, here in the context of light stimuli entraining the rhythms of rest and activity.

Although the precise construction varies slightly between species, the molecular mechanisms of the core clockwork are well characterized (Figure 2). Biological rhythms of approximately 24 hours, or circadian rhythms, are generated by a transcriptional-translational feedback loop (TTFL) in which translated proteins act to inhibit their promoters, thus halting

their continued production[7]. Once these proteins are degraded, expression of their corresponding genes is once again promoted, and this cycle continues. In mammals, the positive arm of this feedback loop consists of two proteins called CLOCK and BMAL. These proteins bind to form heterodimers that bind to E-box enhancer elements of the Period (PER1, PER2, PER3) and Cryptochrome (CRY1, CRY2) genes to activate their transcription. PER and CRY proteins then heterodimerize and inhibit the activity of CLOCK/BMAL heterodimers, thus negatively regulating their own transcription[7]. This primary clock mechanism is supported by a secondary feedback loop, in which retinoic acid receptor-related orphan receptors (RORs) and the transcriptional repressor REV-ERBα activate and inhibit the expression of BMAL1, respectively. Post-translational modifications of these core clock proteins can affect the period of the rhythm, or the length of time required for one cycle of the rhythm to be complete[7]. Indeed, mutations in core clock genes are associated with dramatic changes in this temporal regulation. For example, mutations in CRY1 have recently been connected to Delayed Sleep Phase Disorder in humans, in which sleep onset and offset times become progressively later relative to societal norms[8]. In mammals, every cell contains its own intrinsic circadian oscillator generated by this molecular clockwork, and the coordination of these clocks drives the temporal regulation of behavior and physiology.

The master circadian clock responsible for this coordination is the suprachiasmatic nucleus (SCN), a small bundle of neurons located at the base of the brain in the hypothalamus[9] (Figure 3). The SCN synchronizes circadian oscillators throughout the body to environmental light-dark (LD) cycles by way of light input from the retina. In addition to the photosensitive rod and cone cells responsible for mediating visual perception, the mammalian retina contains intrinsically photosensitive retinal ganglion cells (ipRGCs) that can receive light input in the

absence of rods and cones[10]. These neurons make up about 2-4% of cells in the retina and are unique in their expression of the photopigment melanopsin, which responds primarily to 480 nanometer wavelength light. These ipRGCs project primarily to neuronal populations in the brain that are not involved in image-forming visual perception, including the SCN, via the retinohypothalamic tract (RHT)[10].

Although over 90% of SCN neurons express the inhibitory small neurotransmitter GABA[11], the SCN is highly heterogeneous and is roughly divided into two functional and anatomical subregions: the ventro-lateral SCN (vlSCN) or "core", which expresses the neuropeptide vasoactive intestinal polypeptide (VIP) and is highly light-responsive; and the dorsal-medial SCN (dmSCN) or "shell", containing arginine vasopressin (AVP) neurons that are strong intrinsic circadian oscillators[9]. VIP neurons in the vlSCN receive dense glutamatergic inputs from ipRGCs, providing information about the presence or absence of environmental light. The vlSCN then relays light information to AVP neurons in the vlSCN, synchronizing their intrinsic oscillations to external environmental light and maintaining synchrony of the SCN neural network. Although this coupling mechanism between vl- and dmSCN is incompletely understood, evidence suggests that both GABA[12] and VIPergic signaling[13,14] are critically important for maintaining network synchrony. Neurons in the dmSCN both send axonal projections to nuclei throughout the brain and release humoral factors[15], signals which together provide a temporal order for processes including metabolism[16], hormone release[17], and daily cycles of sleep and wake[18].

Mammalian Sleep and the Two-Process Model of Sleep Regulation

The most overt output of the circadian clock is sleep, which is a reversible state of unconsciousness characterized by inactivity and reduced responsiveness to external sensory stimuli[19]. Sleep is ubiquitous throughout the animal kingdom and is observed in nearly every animal species that has been studied, making it one of the most highly evolutionary conserved behaviors[20]. In mammals, sleep is classified as being one of two primary stages: rapid eye-movement (REM) sleep and non-rapid eye-movement (NREM) sleep. These two stages have distinct physiological signatures which can be measured using a combination of electroencephalography (EEG) and electromyography (EMG) in both humans and animals. NREM sleep is characterized by synchronous, high voltage amplitude waves oscillating in the 0.5-4 Hz frequency range (hereafter referred to as the delta band) as measured by EEG, and reduced muscle tone as measured by EMG. A final key feature of NREM sleep is the presence of sleep spindles, waxing and waning 10-15 Hz oscillations hypothesized to be important in the consolidation of memory during sleep[21,22]. REM sleep is characterized by mixed frequency, low voltage amplitude waves, high power in the 6-10 Hz frequency range (here after referred to as the theta band), and complete muscle atonia[19].

In most mammals, sleep is consolidated into a single primary bout happening at approximately the same time of day, in which NREM sleep is highly concentrated at the beginning of the sleep cycle, and REM sleep at the end[19]. This sleep architecture is highly consistent and critical for a variety of physiological processes including memory consolidation[21], and its disruption underlies neurological disorders like narcolepsy[23].

Our understanding of sleep stages and their timing is often framed in the context of the two-process model of sleep regulation, which posits that sleep is controlled by the interactions of

separate circadian and homeostatic processes[24,25] (Figure 4). Homeostatic regulation of sleep (Process S) is driven by sleep debt, or how long an individual has been awake. Sleep propensity increases with time spent awake until the individual falls asleep and decreases the longer an individual has been asleep. The key marker of functional homeostatic sleep regulation is an increased amount of NREM sleep, and especially slow-wave sleep (SWS) characterized by oscillations of 1 Hz or less, during which electrographic delta band power is at its highest. Indeed, it is well documented in both human[26] and animal models[27,28] that sleep drive increases during periods of sleep deprivation, and that the amount of SWS observed during the rebound bout of sleep is proportional to the length of the deprivation period.

Circadian regulation of sleep (Process C) is driven by the circadian pacemaker in the SCN, such that sleep drive oscillates with a periodicity that is typically entrained to the environmental LD cycle. Landmark studies by Tobler et al.[29] and Trachsel et. al[30] provided key evidence that these two processes are distinct by demonstrating that in SCN-lesioned nocturnal rats, the rhythmicity of sleep-wake cycles was abolished without altering the total amount of daily sleep time. Remarkably, the integrity of Process S was left intact. Similarly, Albers et al. demonstrated that diurnal squirrel monkeys with lesions of the SCN lost behavioral circadian rhythmicity[31]. Multiple studies of human sleep performed by Derk-Jan Dijk and Charles Czeisler led to the development of a forced-desynchrony protocol in which participants are placed in a LD cycle that the circadian pacemaker cannot entrain to, leading to sleep occurring at different times of the day[26], a model later emulated in rodents[32–34]. This paradigm provided an experimental framework in which to test predictions of the two-process model and provide evidence that Processes S and C are separate sleep regulatory mechanisms in humans and animal models.

Neural Circuitry of Homeostatic and Circadian Sleep Regulation

Although the neural circuitry underlying both sleep regulatory processes is well studied, it remains incompletely understood. The master circadian pacemaker in the SCN is at the core of Process C (Figure 5). While there is heterogeneity in the activity rhythms of both single neurons and neuronal ensembles, on average SCN neurons display peak firing rates during the subjective day in both diurnal and nocturnal mammals[35]. SCN neurons are themselves autonomous oscillators and express circadian rhythmicity in both neuronal firing and clock gene expression[9,36,37]. Through a mechanism that has yet to be fully characterized but likely depends on a combination of gap junction-mediated electrical coupling[38], neuropeptide[9] and conventional neurotransmitter signaling[9,11], individual neuronal oscillators are able to synchronize so that the entire SCN network can maintain synchrony.

While there is debate about whether SCN neuronal activity promotes wakefulness or sleep, it is generally agreed upon that the SCN relays temporal information to downstream targets regulating sleep and wakefulness via efferent axonal projections and diffusible humoral factors[18]. Indeed, a landmark study by Silver et al. demonstrated that SCN grafts housed in a semi-permeable capsule that prevented axonal outgrowth were able to restore behavioral circadian rhythmicity in SCN-lesioned animals, suggesting that diffusible factors play a key role in circadian sleep regulation[39]. Although the SCN sends relatively sparse projections to both sleep- and wake-active neuronal populations, it makes indirect contacts with these regions via dense projections to the subparaventricular zone (SPZ) and the dorsomedial hypothalamus (DMH)[18]. The SPZ and DMH then project to NREM sleep-active regions including the ventrolateral preoptic nucleus (VLPO) and median preoptic nucleus (MnPO) of the

hypothalamus, as well as orexinergic and cholinergic populations that play key roles in initiating both wakefulness and REM sleep[18,19,40].

While the SCN and the targets of its efferent projections are clearly associated with Process C, Process S lacks a clear and comparable neural correlate (Figure 6). An important consideration is the mechanism by which the brain can enter a state of NREM sleep. One key player in this mechanism is the VLPO, which sends inhibitory GABAergic projections to hypothalamic and brainstem nuclei that promote wakefulness as part of the ascending arousal system[40,41]. Lesions of the VLPO result in sleep loss[42] and chemogenetic activation of the VLPO has been demonstrated to promote NREM sleep[43]. Additionally, populations of neurons in the VLPO express receptors for the sleep-promoting nucleoside adenosine, and these neurons fire faster during rebound sleep relative to their activity during a typical bout of NREM sleep[44]. However, these neurons do not appear to accumulate sleep need as their firing rate is normal during sleep deprivation[40], suggesting that while the VLPO promotes NREM sleep after periods of deprivation, it likely does not contain the sleep homeostat.

Although the precise mechanisms of homeostatic sleep regulation remain unknown, the circuitry underlying its key observable features – increases in sleep spindles and SWS duration – is well-characterized. At the core of both spindle and slow wave oscillations is a series of interconnected cortical and thalamic nuclei[45]. In the cortex, slow wave oscillations are generated by reciprocal connections between excitatory pyramidal cells and inhibitory interneurons cycling between "Up" states, in which cortical neurons fire fast and synchronously, and "Down" states, in which they are quiescent[46]. In the thalamus, the reciprocally connected GABAergic thalamic reticular nucleus (TRN) and glutamatergic thalamocortical (TC) neurons of the dorsal thalamic nuclei generate the sleep spindle oscillation (Figure 7). Briefly, action potentials from cortical

pyramidal neurons during SWS excite TRN neurons, which then inhibit TC neurons via a combination of $GABA_A$ and $GABA_B$ post-synaptic receptors. After a period of inhibition of TC neurons, they initiate a post-inhibitory rebound burst of action potentials, exciting TRN neurons again. Electrical coupling of TRN neurons results in synchronous firing across the thalamus, giving rise to the spindle oscillation. TC neurons project to and excite cortical pyramidal neurons, relaying information about the state of the spindle network, underlying the coincident nature of SWS and spindles[45,46]. The spindle oscillation is eventually terminated by an intra-TRN inhibition mechanism by which TRN neurons inhibit each other to desynchronize firing[45,47–49]. Importantly, the TRN can initiate and maintain sleep spindle-like oscillations in thalamic slice preparations[47], and optogenetic stimulation of TRN in behaving mice results in the generation of spindle oscillations[50], local cortical slow waves and transition from wakefulness to NREM sleep[51].

Although much remains to be elucidated about the cellular and molecular mechanisms underlying the two-process model, the SCN and the TRN as substrates of circadian and homeostatic sleep regulation, respectively will provide a useful framework to explore sleep regulation in neurological disease in this thesis.

Circadian Rhythms, Sleep and Epilepsy

Sleep and circadian rhythm disturbances are often comorbid in neurological diseases, and poor circadian rhythm and sleep quality can have important consequences for neurological health[52–55]. Epilepsies are among the most common neurological disorders in the U.S.[56], and often go hand-in-hand with sleep disorders[45,57,58]. Sleep disturbances in epilepsy patients are associated with increased seizure incidence and severity, greater cognitive disturbances and reduced quality

of life[57]. Nocturnal seizures are prevalent in many forms of epilepsy[48], and sudden unexpected death in epilepsy (SUDEP) often occurs during sleep, especially in pediatric patients[59]. Additionally, patients often experience increased risk of seizure occurrence following sleep deprivation[60]. Finally, it is well documented that propensity for seizures and interictal epileptic spiking events shows both circadian and multi-day rhythms[61–68].

While the mechanisms underlying the close relationship between sleep disturbances and epilepsy is incompletely understood, one potential explanation is the common neuronal substrates implicated in generating both healthy neural oscillations during sleep and pathological oscillations during seizures[45]. A striking example of one such substrate is the TRN[48]. In slice preparations, spindle-like oscillations generated by the TRN can be turned into epileptiform oscillations characteristic of absence seizures[45] by applying $GABA_A$ receptor antagonists to the slice[69,70]. The same phenomenon can be observed *in vivo* by injecting $GABA_A$ receptor antagonists directly into the thalamus of behaving rats[71]. More recently, it was demonstrated that absence seizures could be interrupted by reducing the excitability of TRN neurons *in vivo* in a mouse model of epilepsy in which TRN neurons are hyperexcitable[72]. Yet another example is the hippocampus, which normally generates the highly synchronous sharp-wave ripple oscillation observed during NREM sleep, but is at the heart of dysfunction seen in medial temporal lobe epilepsies, which are highly common[45,73]. While the SCN itself is unlikely to underlie seizure generation per se, it is well documented that neuronal membrane excitability displays circadian modulation[74,75], and it has also been proposed that the SCN may modulate excitability of the hippocampal network via long-range efferent projections[63,76], both of which could contribute to seizure generation and propagation. These changes in normal brain function are further

confounded by the complex effects that commonly prescribed anti-epileptic drugs have on sleep timing, duration and quality[57,77].

Taken together, the aforementioned work highlights the need for a more comprehensive and mechanistic understanding of the relationship between sleep, circadian rhythms and epilepsy.

Sleep Disturbances in Dravet Syndrome

Dravet syndrome (DS) is a rare and severe form of treatment-resistant, childhood-onset epilepsy with a high mortality rate[78,79]. DS usually manifests at six-nine months of age with fever and hyperthermia-induced seizures, and gradually progresses to include to spontaneous myoclonic, tonic–clonic, absence, and partial seizures[80]. During this time, DS patients develop several other co-morbidities including autism-like behaviors[80,81], ataxia[80,82], psychomotor regression[80] and high risk for SUDEP[80,83]. Sleep disruptions are reported by more than 70% of DS patients[84], and DS patients report more frequent nighttime awakenings and greater daytime sleepiness than patients with other forms of epilepsy[85]. Disturbances including sleep onset insomnia, difficulty maintaining sleep and frequent nocturnal seizures are well documented, and these disturbances are described as highly disruptive to quality of life for both patients and caregivers[86,87].

DS is caused by loss-of-function mutations in one allele of the *SCN1A* gene[88], which codes for the pore-forming alpha subunit of the $Na_V1.1$ sodium channel[89]. $Na_V1.1$ is widely expressed throughout the brain, primarily in GABAergic interneurons. Previous work in a mouse model of DS, in which the *Scn1a* gene is heterozygously deleted ($Scn1a^{+/-}$), has shown that the mutation causes a selective reduction in the excitability of inhibitory interneurons[90,91]. Several

characterizations of DS mice have revealed that, like human patients, they display both spontaneous and thermally-induced seizures[90,92], ataxia[82], autism-like cognitive and social deficits[81,93], SUDEP[94], and sleep disturbances[95–97]. Specific heterozygous deletion of the Scn1a gene in forebrain interneurons recapitulates the epilepsy, SUDEP, cognitive impairment, autistic-like behaviors, and homeostatic sleep disruption observed in DS mice[81,95,96,98]. This work has led to the unified hypothesis that hyperexcitability of different neural circuits due to the loss of functional $Na_V1.1$ channels underlies the co-morbidities of DS[99].

In previous studies, our lab identified circadian behavioral deficits in DS mice including reduced circadian amplitude of wheel-running activity (WRA), elongated endogenous WRA period under conditions of constant darkness (DD), delayed activity onset, and increased time to re-entrainment of WRA to a new LD cycle[95]. These deficits were correlated with poor network synchrony and reduced photoresponsiveness in the SCN. Later work showed that DS mice also lack normal homeostatic NREM sleep rebound in response to sleep deprivation, as well as fragmented NREM sleep under baseline conditions[96]. This was associated with reduced excitability of GABAergic inhibitory neurons in the TRN.

These results form the foundation for my thesis, in which I will conduct an investigation into the nature and mechanisms of sleep and circadian rhythm disturbances in DS. This avenue of inquiry provides an important opportunity to both further our understanding of the basic biology underlying sleep regulation and provide greater insight into debilitating sleep-related comorbidities of DS that deeply impact patients and their caregivers.

Specific Aims of Thesis

For this thesis, I hypothesized that the *Scn1a*$^{+/-}$ mouse model of DS would display circadian sleep disturbances as the result of reduced expression of the $Na_V1.1$ sodium channel in SCN neurons. By using a combination of genetic and viral manipulations, behavioral assays, in vivo electrophysiology and novel data analysis techniques, my thesis explores unanswered questions related to sleep disturbances in Dravet syndrome that simultaneously address the pathophysiology of this debilitating neurological disease and reveal greater insight about the neural substrates of the two-process model of sleep regulation. The following work tests predictions of my central hypothesis by addressing three primary specific aims:

1. **The circadian regulation of sleep in a mouse model of Dravet syndrome**. Here, I will describe how we performed long-term continuous recordings of sleep to reveal deficits in circadian sleep regulation in Dravet syndrome mice that were independent of epileptic activity.
2. **The role of $Na_V1.1$ sodium channel expression in the circadian regulation of sleep.** Here, I will describe experiments we performed to selectively delete the $Na_V1.1$ sodium channel from SCN neurons to examine their contribution to the intrinsic daily timing of sleep.
3. **Novel supervised machine learning-based methods for sleep stage classification to aid in studies of circadian sleep regulation.** Here I will describe our efforts to develop supervised machine learning-based analysis tools for automatic sleep stage classification, which aided in our long-term continuous recordings of sleep in Dravet syndrome.

Taken together, the results presented in this thesis further our understanding of sleep disturbances in Dravet syndrome, suggest targets for therapies aimed at addressing these disturbances, and provide novel analysis tools and insights for researchers studying the neurobiology of sleep regulation.

Figures

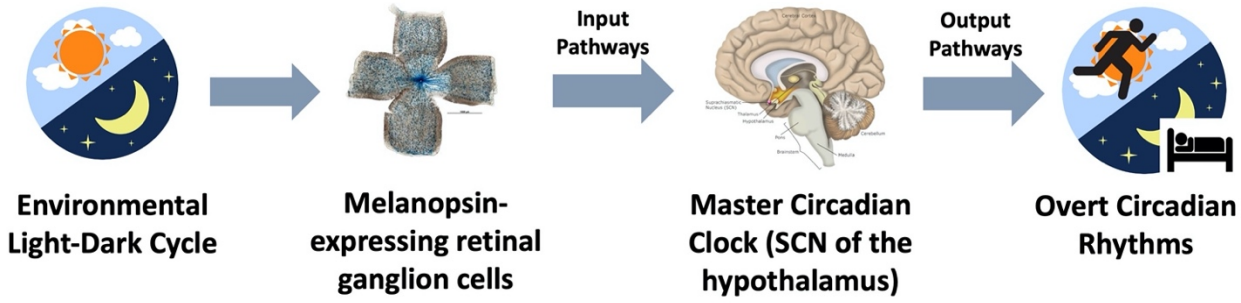

Figure 1. Core components of the mammalian circadian system. This diagram, called an eskinogram, outlines the essential components of the mammalian circadian system. The intrinsic circadian oscillator in the suprachiasmatic nucleus (SCN) is entrained by the environmental light-dark cycle, although other environmental factors can also act on the master clock and its subordinate oscillators, including food availability and social cues. The SCN then regulates the timing of overt circadian rhythms, including the sleep-wake cycle.

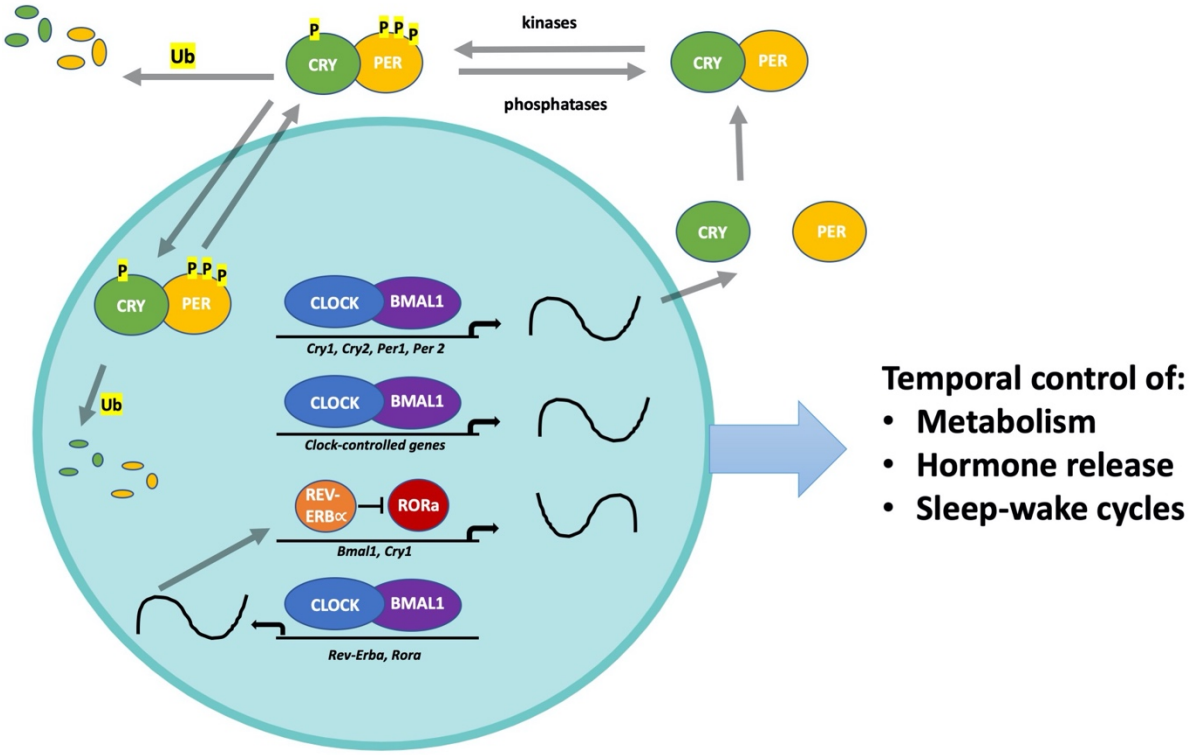

Figure 2. Core circadian clock gene transcriptional-translational feedback (TTFL) loops. Two connected TTFL loops are responsible for generating circadian rhythmicity in mammalian cells. The core TTFL is driven by four integral clock proteins: two activators (CLOCK and BMAL1) and two repressors (PER and CRY), as well as kinases and phosphatases that regulate the localization and stability of these integral clock proteins. This mechanism is described in detail in the main manuscript. This figure is adapted from Partch et al., 2015.

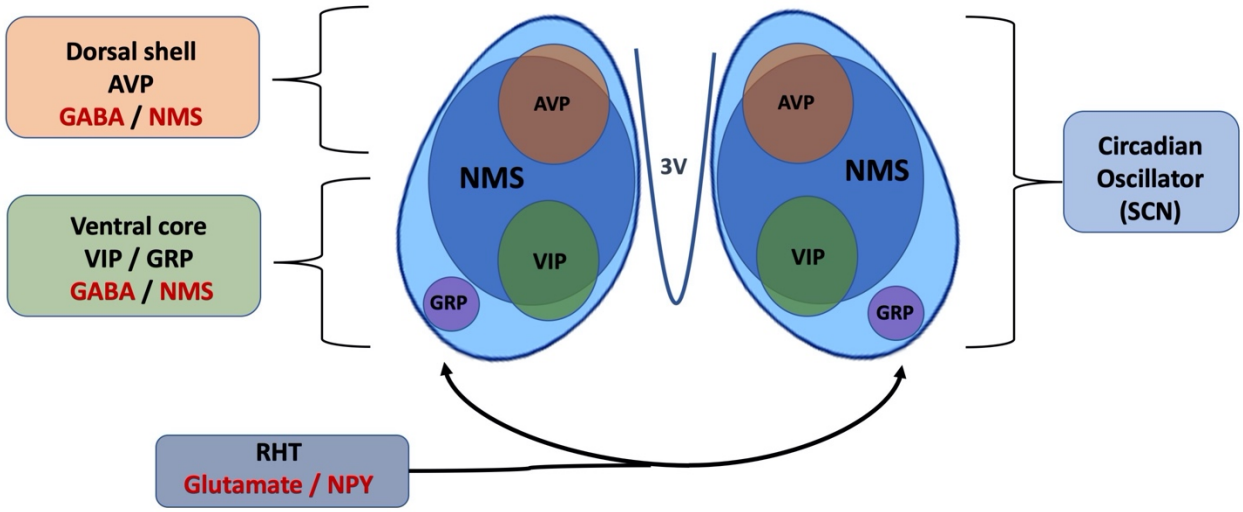

Figure 3. The mammalian suprachiasmatic nuclei. The SCN is a highly heterogeneous population of hypothalamic neurons that comprise the master circadian clock. Subpopulations of the SCN are typically identified by the neuropeptide they predominantly express, though nearly all SCN neurons are GABAergic. AVP neurons in the dorsal SCN are endogenous oscillators, while VIP neurons in the ventral SCN receive light information from the retina via the RHT. These subregions are hypothesized to be coupled by GABAergic and VIPergic signaling mechanisms. Abbreviations: AVP – arginine vasopressin, NMS – Neuromedin S, VIP – vasoactive intestinal polypeptide, GRP – gastrin-releasing peptide, RHT – retinohypothalamic tract, 3V – third ventricle, NPY – Neuropeptide Y.

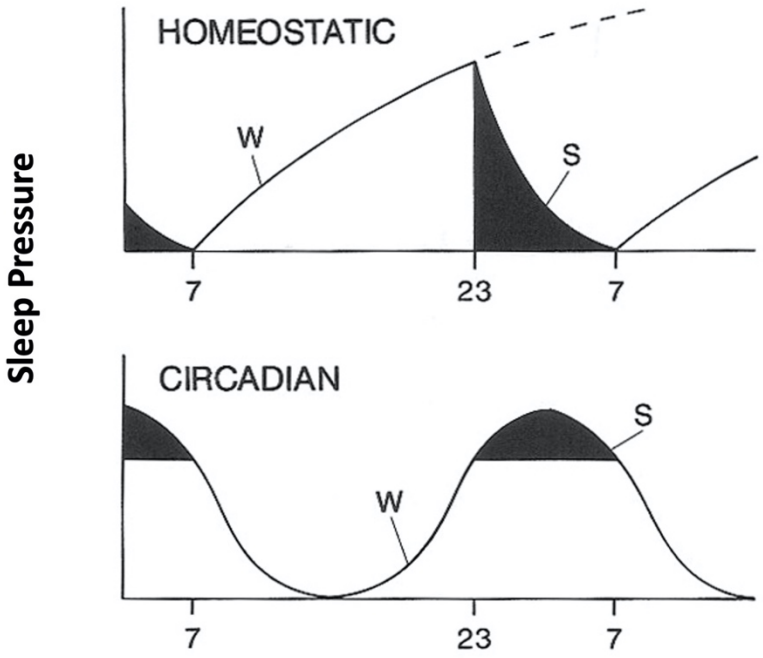

Figure 4. The two-process model of sleep regulation. Homeostatic sleep regulation (top panel) describes the process by which sleep need increases with time spent awake, while circadian sleep regulation (bottom panel) describes how sleep pressure increases during specific times of the day as determined by the circadian clock. The time at which sleep pressure is highest for both processes is the time at which sleep is most likely to occur. Figure adapted from Borbely and Achermann, 1999.

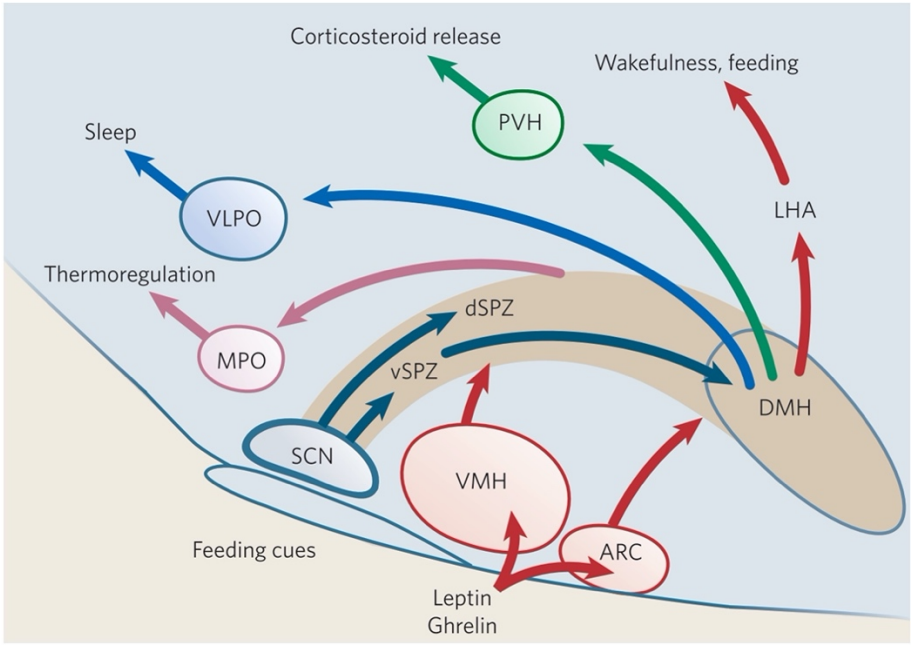

Figure 5. Hypothalamic circuitry underlying the circadian regulation of sleep and behavior. The SCN sends direct and indirect projections to numerous other hypothalamic neuronal populations involved in the regulation of sleep/wake cycles, feeding, hormone release and core body temperature. The most numerous of these projections go to the dorsal medial hypothalamus (DMH) by way of the subparaventricular zone (SPZ), which then sends projects to regions critical for sleep regulation including the lateral hypothalamic area (LHA) and ventrolateral preoptic nucleus (VLPO). Other abbreviations: MPO – median preoptic area, VMH – ventral medial hypothalamus, PVH – paraventricular hypothalamus, ARC – arcuate nucleus. This figure is adapted from Saper et al., 2005.

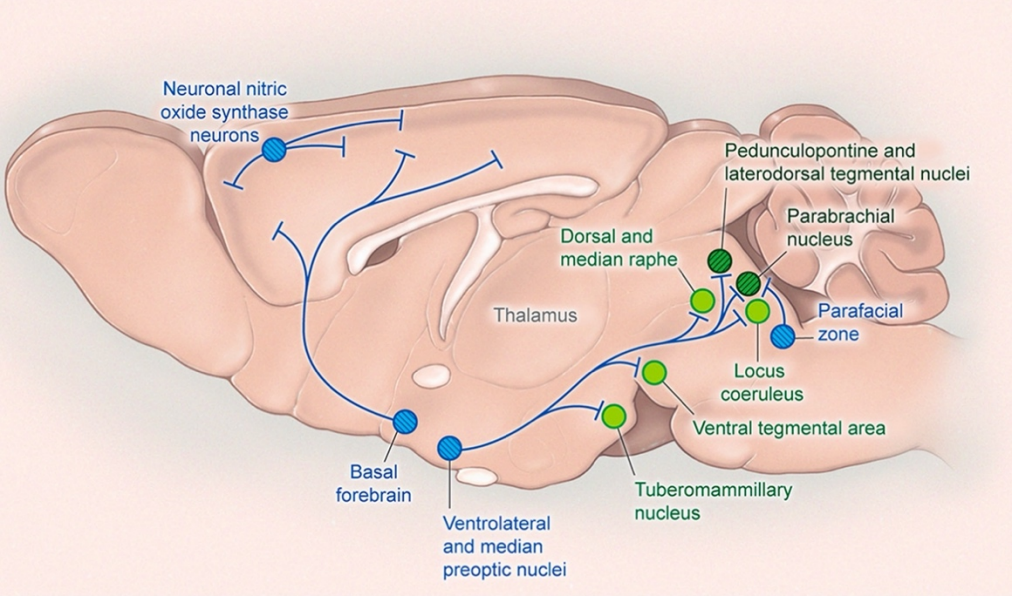

Figure 6. Neural circuitry involved in the regulation of NREM sleep. Unlike the circadian regulation of sleep, the circuitry regulating the promotion of NREM and the homeostatic sleep is response is diffuse. Blue shaded areas are sleep-promoting, while green shaded areas are wake-promoting. This figure is adapted from Scammell et al., 2017.

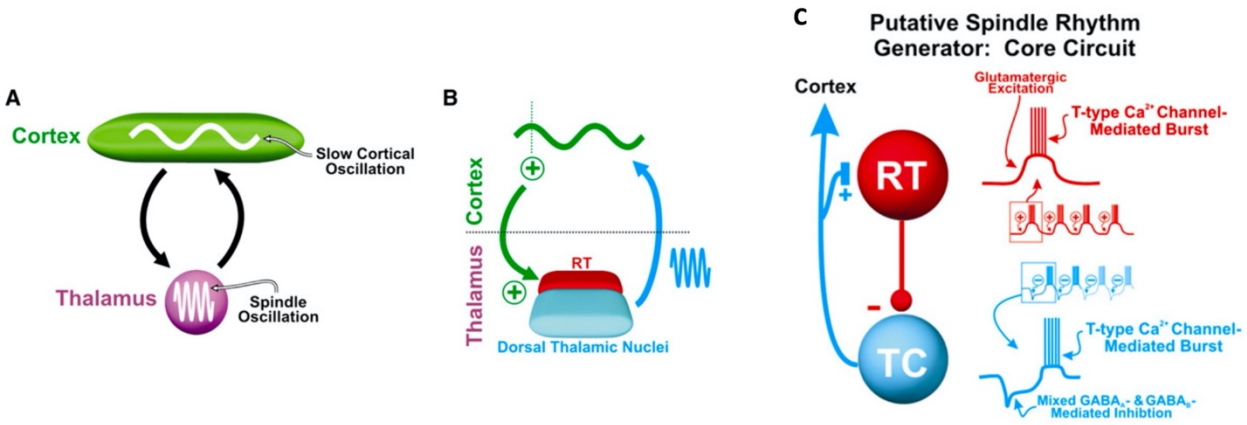

Figure 7. Thalamocortical circuitry underlying the slow cortical and thalamic sleep spindle oscillations during NREM sleep. A) Slow waves and sleep spindles during NREM sleep are generated by interconnected populations of neurons in cortex and thalamus, depicted in B and described in more detail in the main text. C) Zoomed-in view of the bottom panel of B, showing the core circuit underlying spindle rhythm generation. The thalamic reticular nucleus is critical in this process. This figure was adapted from Beenhakker & Huguenard, 2009.

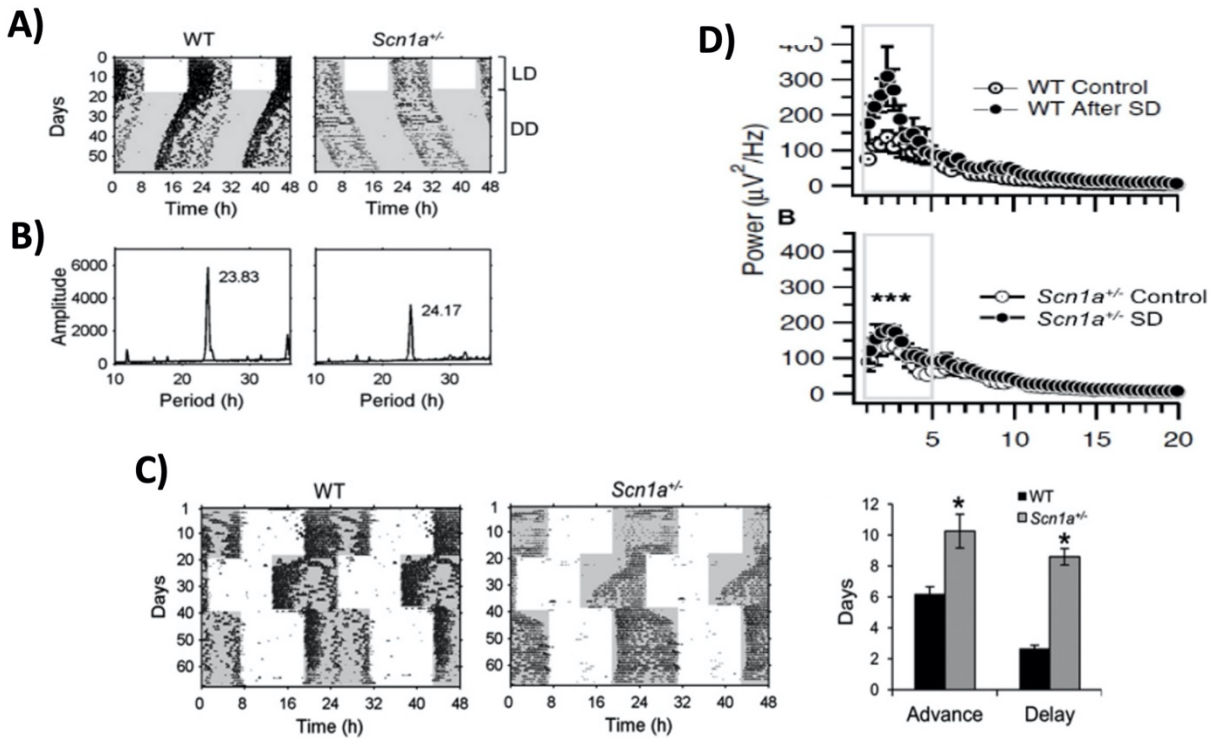

Figure 8. Sleep and circadian rhythm disturbances in Dravet syndrome mice. DS mice have a longer circadian period of locomotor activity **(A and B),** take longer to re-entrain to phase-shifts of the light-dark (LD) cycle **(C)**, and have blunted homeostatic sleep rebound following sleep deprivation **(D).** This figure adapted from Han et al., 2012 and Kalume et al., 2015.

References

1 Merrow M, Spoelstra K, Roenneberg T. The circadian cycle: Daily rhythms from behaviour to genes. *EMBO Rep* 2005:930–5. https://doi.org/10.1038/sj.embor.7400541.

2 Salomé PA, McClung CR. The Arabidopsis thaliana clock. *J Biol Rhythms* 2004;**19**:425–35. https://doi.org/10.1177/0748730404268112.

3 Panda S, Hogenesch JB, Kay SA. Circadian rhythms from flies to human. *Nature* 2002:329–35. https://doi.org/10.1038/417329a.

4 Dunlap JC, Loros JJ. The neurospora circadian system. *J Biol Rhythms* 2004;**19**:414–24. https://doi.org/10.1177/0748730404269116.

5 Cavallari N, Frigato E, Vallone D, Fröhlich N, Lopez-Olmeda JF, Foà A, *et al*. A Blind Circadian Clock in Cavefish Reveals that Opsins Mediate Peripheral Clock Photoreception. *PLoS Biol* 2011;**9**:e1001142. https://doi.org/10.1371/journal.pbio.1001142.

6 Moore D. Honey bee circadian clocks: Behavioral control from individual workers to whole-colony rhythms. *J Insect Physiol* 2001:843–57. https://doi.org/10.1016/S0022-1910(01)00057-9.

7 Partch CL, Green CB, Takahashi JS. Molecular architecture of the mammalian circadian clock. *Trends Cell Biol* 2014:90–9. https://doi.org/10.1016/j.tcb.2013.07.002.

8 Patke A, Murphy PJ, Onat OE, Krieger AC, Özçelik T, Campbell SS, *et al*. Mutation of the Human Circadian Clock Gene CRY1 in Familial Delayed Sleep Phase Disorder. *Cell* 2017;**169**:203-215.e13. https://doi.org/10.1016/j.cell.2017.03.027.

9 Hastings MH, Maywood ES, Brancaccio M. Generation of circadian rhythms in the suprachiasmatic nucleus. *Nat Rev Neurosci* 2018:453–69. https://doi.org/10.1038/s41583-018-0026-z.

10 Hattar S, Liao HW, Takao M, Berson DM, Yau KW. Melanopsin-containing retinal ganglion cells: Architecture, projections, and intrinsic photosensitivity. *Science (80-)* 2002;**295**:1065–70. https://doi.org/10.1126/science.1069609.

11 Albers HE, Walton JC, Gamble KL, McNeill JK, Hummer DL. The dynamics of GABA signaling: Revelations from the circadian pacemaker in the suprachiasmatic nucleus. *Front Neuroendocrinol* 2017:35–82. https://doi.org/10.1016/j.yfrne.2016.11.003.

12 Albus H, Vansteensel MJ, Michel S, Block GD, Meijer JH. A GABAergic mechanism is necessary for coupling dissociable ventral and dorsal regional oscillators within the circadian clock. *Curr Biol* 2005;**15**:886–93. https://doi.org/10.1016/j.cub.2005.03.051.

13 Harmar AJ, Marston HM, Shen S, Spratt C, West KM, Sheward WJ, *et al*. The VPAC2 receptor is essential for circadian function in the mouse suprachiasmatic nuclei. *Cell* 2002;**109**:497–508. https://doi.org/10.1016/S0092-8674(02)00736-5.

14 Aton SJ, Colwell CS, Harmar AJ, Waschek J, Herzog ED. Vasoactive intestinal polypeptide mediates circadian rhythmicity and synchrony in mammalian clock neurons. *Nat Neurosci* 2005;**8**:476–83. https://doi.org/10.1038/nn1419.

15 LeSauter J, Silver R. Output signals of the SCN. *Chronobiol Int* 1998;**15**:535–50. https://doi.org/10.3109/07420529808998706.

16 Panda S. Circadian physiology of metabolism. *Science (80-)* 2016:1008–15. https://doi.org/10.1126/science.aah4967.

17 Gamble KL, Berry R, Frank SJ, Young ME. Circadian clock control of endocrine factors. *Nat Rev Endocrinol* 2014:466–75. https://doi.org/10.1038/nrendo.2014.78.

18 Mistlberger RE. Circadian regulation of sleep in mammals: Role of the suprachiasmatic

nucleus. *Brain Res Rev* 2005:429–54. https://doi.org/10.1016/j.brainresrev.2005.01.005.
19 Scammell TE, Arrigoni E, Lipton JO. Neural Circuitry of Wakefulness and Sleep. *Neuron* 2017;**93**:747–65. https://doi.org/10.1016/j.neuron.2017.01.014.
20 Allada R, Siegel JM. Unearthing the Phylogenetic Roots of Sleep. *Curr Biol* 2008:R670–9. https://doi.org/10.1016/j.cub.2008.06.033.
21 Rasch B, Born J. About sleep's role in memory. *Physiol Rev* 2013;**93**:681–766. https://doi.org/10.1152/physrev.00032.2012.
22 Watson BO, Buzsáki G. Sleep , Memory & Brain Rhythms 2015:67–82. https://doi.org/10.1162/DAED_a_00318.
23 Akintomide GS, Rickards H. Narcolepsy: A review. *Neuropsychiatr Dis Treat* 2011;**7**:507–18. https://doi.org/10.2147/ndt.s23624.
24 Borbély AA, Daan S, Wirz-Justice A, Deboer T. The two-process model of sleep regulation: A reappraisal. *J Sleep Res* 2016;**25**:131–43. https://doi.org/10.1111/jsr.12371.
25 Borbély AA. A Two Process Model of Sleep Regulation. *Hum Neurobiol* 1982;**1**:.
26 Dijk DJ, Czeisler CA. Contribution of the circadian pacemaker and the sleep homeostat to sleep propensity, sleep structure, electroencephalographic slow waves, and sleep spindle activity in humans. *J Neurosci* 1995;**15**:3526–38. https://doi.org/10.1523/jneurosci.15-05-03526.1995.
27 Rechtschaffen A, Bergmann BM, Gilliland MA, Bauer K. *Effects of Method, Duration, and Sleep Stage on Rebounds from Sleep Deprivation in the Rat STATE OF THE ART REVIEWS*. vol. 22. 1999.
28 Huber R, Deboer T, Tobler I. Topography of EEG Dynamics After Sleep Deprivation in Mice. *J Neurophysiol* 2000;**84**:1888–93. https://doi.org/10.1152/jn.2000.84.4.1888.
29 Tobler I, Borbély AA, Groos G. The effect of sleep deprivation on sleep in rats with suprachiasmatic lesions. *Neurosci Lett* 1983;**42**:49–54. https://doi.org/10.1016/0304-3940(83)90420-2.
30 Trachsel L, Edgar DM, Seidel WF, Craig Heller H. Sleep homeostasis in suprachiasmatic nuclei-lesioned rats: effects of sleep deprivation and triazolam administration. *Brain Res* 1992;**589**:253–61. https://doi.org/10.1016/0006-8993(92)91284-L.
31 Albers HE, Lydic R, Gander PH, Moore-Ede MC. Role of the suprachiasmatic nuclei in the circadian timing system of the squirrel monkey. I. The generation of rhythmicity. *Brain Res* 1984;**300**:275–84. https://doi.org/10.1016/0006-8993(84)90837-0.
32 De La Iglesia HO, Cambras T, Schwartz WJ, Díez-Noguera A. Forced desynchronization of dual circadian oscillators within the rat suprachiasmatic nucleus. *Curr Biol* 2004;**14**:796–800. https://doi.org/10.1016/j.cub.2004.04.034.
33 Cambras T, Weller JR, Anglès-Pujoràs M, Lee ML, Christopher A, Díez-Noguera A, *et al*. Circadian desynchronization of core body temperature and sleep stages in the rat. *Proc Natl Acad Sci U S A* 2007;**104**:7634–9. https://doi.org/10.1073/pnas.0702424104.
34 Lee ML, Swanson BE, de la Iglesia HO. Circadian Timing of REM Sleep Is Coupled to an Oscillator within the Dorsomedial Suprachiasmatic Nucleus. *Curr Biol* 2009;**19**:848–52. https://doi.org/10.1016/j.cub.2009.03.051.
35 Schaap J, Pennartz CMA, Meijer JH. Electrophysiology of the circadian pacemaker in mammals. *Chronobiol Int* 2003:171–88. https://doi.org/10.1081/CBI-120019311.
36 Herzog ED, Geusz ME, Khalsa SBS, Straume M, Block GD. Circadian rhythms in mouse suprachiasmatic nucleus explants on multimicroelectrode plates. *Brain Res* 1997;**757**:285–90. https://doi.org/10.1016/S0006-8993(97)00337-5.

37 Welsh DK, Logothetis DE, Meister M, Reppert SM. *Individual Neurons Dissociated from Rat Suprachiasmatic Nucleus Express Independently Phased Circadian Firing Rhythms*. vol. 14. 1995.

38 CS C. Rhythmic Coupling Among Cells in the Suprachiasmatic Nucleus. *J Neurobiol* 2000;**43**:. https://doi.org/10.1002/1097-4695(20000615)43:4<379::AID-NEU6>3.0.CO;2-0.

39 Silver R, LeSauter J, Tresco PA, Lehman MN. A diffusible coupling signal from the transplanted suprachiasmatic nucleus controlling circadian locomotor rhythms. *Nature* 1996;**382**:810–3. https://doi.org/10.1038/382810a0.

40 Saper CB, Scammell TE, Lu J. Hypothalamic regulation of sleep and circadian rhythms. *Nature* 2005;**437**:1257–63. https://doi.org/10.1038/nature04284.

41 Saito YC, Tsujino N, Hasegawa E, Akashi K, Abe M, Mieda M, *et al*. GABAergic neurons in the preoptic area send direct inhibitory projections to orexin neurons. *Front Neural Circuits* 2013;**7**:192. https://doi.org/10.3389/fncir.2013.00192.

42 von Economo C. Sleep as a problem of localization. *J Nerv Ment Dis* 1930;**71**:.

43 Zhang Z, Ferretti V, Güntan I, Moro A, Steinberg EA, Ye Z, *et al*. Neuronal ensembles sufficient for recovery sleep and the sedative actions of α 2 adrenergic agonists. *Nat Neurosci* 2015;**18**:553–61. https://doi.org/10.1038/nn.3957.

44 Alam MA, Kumar S, McGinty D, Alam MN, Szymusiak R. Neuronal activity in the preoptic hypothalamus during sleep deprivation and recovery sleep. *J Neurophysiol* 2014;**111**:287–99. https://doi.org/10.1152/jn.00504.2013.

45 Beenhakker MP, Huguenard JR. Neurons that Fire Together Also Conspire Together: Is Normal Sleep Circuitry Hijacked to Generate Epilepsy? *Neuron* 2009;**62**:612–32. https://doi.org/10.1016/j.neuron.2009.05.015.

46 Neske GT. The slow oscillation in cortical and thalamic networks: Mechanisms and functions. *Front Neural Circuits* 2016:88. https://doi.org/10.3389/fncir.2015.00088.

47 Fuentealba P, Steriade M. The reticular nucleus revisited: Intrinsic and network properties of a thalamic pacemaker. *Prog Neurobiol* 2005:125–41. https://doi.org/10.1016/j.pneurobio.2005.01.002.

48 Steriade M. Sleep, epilepsy and thalamic reticular inhibitory neurons. *Trends Neurosci* 2005;**28**:317–24. https://doi.org/10.1016/j.tins.2005.03.007.

49 Timofeev I, Steriade M. Cellular Mechanisms Underlying Intrathalamic Augmenting Responses of Reticular and Relay Neurons. *J Neurophysiol* 1998;**79**:2716–29. https://doi.org/10.1152/jn.1998.79.5.2716.

50 Halassa MM, Siegle JH, Ritt JT, Ting JT, Feng G, Moore CI. Selective optical drive of thalamic reticular nucleus generates thalamic bursts and cortical spindles. *Nat Neurosci* 2011;**14**:1118–20. https://doi.org/10.1038/nn.2880.

51 Lewis LD, Voigts J, Flores FJ, Ian Schmitt L, Wilson MA, Halassa MM, *et al*. Thalamic reticular nucleus induces fast and local modulation of arousal state. *Elife* 2015;**4**:. https://doi.org/10.7554/eLife.08760.

52 Anderson K. Sleep disturbance and neurological disease. *Clin Med J R Coll Physicians London* 2011:271–4. https://doi.org/10.7861/clinmedicine.11-3-271.

53 Videnovic A, Lazar AS, Barker RA, Overeem S. 'The clocks that time us' - Circadian rhythms in neurodegenerative disorders. *Nat Rev Neurol* 2014:683–93. https://doi.org/10.1038/nrneurol.2014.206.

54 Turek FW, Dugovic C, Zee PC. Current Understanding of the Circadian Clock and the

Clinical Implications for Neurological Disorders.
55 Videnovic A, Zee PC. Consequences of circadian disruption on neurologic health. *Sleep Med Clin* 2015:469–80. https://doi.org/10.1016/j.jsmc.2015.08.004.
56 Helmers SL, Thurman DJ, Durgin TL, Pai AK, Faught E. Descriptive epidemiology of epilepsy in the U.S. population: A different approach. *Epilepsia* 2015;**56**:942–8. https://doi.org/10.1111/epi.13001.
57 Bazil CW. Sleep and epilepsy. *Curr Opin Neurol* 2000:171–5. https://doi.org/10.1097/00019052-200004000-00010.
58 Méndez M, Radtke RA. Interactions between sleep and epilepsy. *J Clin Neurophysiol* 2001:106–27. https://doi.org/10.1097/00004691-200103000-00003.
59 Carreño M, Fernández S. Sleep-Related Epilepsy. *Curr Treat Options Neurol* 2016. https://doi.org/10.1007/s11940-016-0402-9.
60 Malow BA. Sleep Deprivation and Epilepsy. *Epilepsy Curr* 2004;**4**:193–5. https://doi.org/10.1111/j.1535-7597.2004.04509.x.
61 Shouse MN, Silva AM Da, Sammaritano M. Circadian rhythm, sleep, and epilepsy. *J Clin Neurophysiol* 1996:32–50. https://doi.org/10.1097/00004691-199601000-00004.
62 Hofstra WAe, de Weerd AW. The circadian rhythm and its interaction with human epilepsy: A review of literature. *Sleep Med Rev* 2009:413–20. https://doi.org/10.1016/j.smrv.2009.01.002.
63 Cho CH. Molecular mechanism of circadian rhythmicity of seizures in temporal lobe epilepsy. *Front Cell Neurosci* 2012;**6**:55. https://doi.org/10.3389/fncel.2012.00055.
64 Baud MO, Kleen JK, Mirro EA, Andrechak JC, King-Stephens D, Chang EF, *et al*. Multi-day rhythms modulate seizure risk in epilepsy. *Nat Commun* 2018;**9**:1–10. https://doi.org/10.1038/s41467-017-02577-y.
65 Mirzoev A, Bercovici E, Stewart LS, Cortez MA, Snead OC, Desrocher M. Circadian profiles of focal epileptic seizures: A need for reappraisal. *Seizure* 2012:412–6. https://doi.org/10.1016/j.seizure.2012.03.014.
66 Sánchez Fernández I, Ramgopal S, Powell C, Gregas M, Zarowski M, Shah A, *et al*. Clinical evolution of seizures: Distribution across time of day and sleep/wakefulness cycle. *J Neurol* 2013;**260**:549–57. https://doi.org/10.1007/s00415-012-6675-3.
67 Karoly PJ, Freestone DR, Boston R, Grayden DB, Himes D, Leyde K, *et al*. Interictal spikes and epileptic seizures: Their relationship and underlying rhythmicity. *Brain* 2016;**139**:1066–78. https://doi.org/10.1093/brain/aww019.
68 Karoly PJ, Ung H, Grayden DB, Kuhlmann L, Leyde K, Cook MJ, *et al*. The circadian profile of epilepsy improves seizure forecasting n.d. https://doi.org/10.1093/brain/awx173.
69 Huguenard JR, Prince DA. Clonazepam suppresses GABA(B)-mediated inhibition in thalamic relay neurons through effects in nucleus reticularis. *J Neurophysiol* 1994;**71**:2576–81. https://doi.org/10.1152/jn.1994.71.6.2576.
70 Kim U, Sanchez-Vives M V., McCormick DA. Functional dynamics of GABAergic inhibition in the thalamus. *Science (80-)* 1997;**278**:130–4. https://doi.org/10.1126/science.278.5335.130.
71 Castro-Alamancos MA. Neocortical synchronized oscillations induced by thalamic disinhibition in vivo. *J Neurosci* 1999;**19**:RC27–RC27. https://doi.org/10.1523/jneurosci.19-18-j0005.1999.
72 Ritter-Makinson S, Clemente-Perez A, Higashikubo B, Cho FS, Holden SS, Bennett E, *et al*. Augmented Reticular Thalamic Bursting and Seizures in Scn1a-Dravet Syndrome. *Cell*

Rep 2019;**26**:54-64.e6. https://doi.org/10.1016/j.celrep.2018.12.018.
73 Buzsáki G. Hippocampal sharp wave-ripple: A cognitive biomarker for episodic memory and planning. *Hippocampus* 2015;**25**:1073–188. https://doi.org/10.1002/hipo.22488.
74 Allen CN, Nitabach MN, Colwell CS. Membrane currents, gene expression, and circadian clocks. *Cold Spring Harb Perspect Biol* 2017;**9**:a027714. https://doi.org/10.1101/cshperspect.a027714.
75 Flourakis M, Kula-Eversole E, Hutchison AL, Han TH, Aranda K, Moose DL, *et al*. A Conserved Bicycle Model for Circadian Clock Control of Membrane Excitability. *Cell* 2015;**162**:836–48. https://doi.org/10.1016/j.cell.2015.07.036.
76 Smarr BL, Jennings KJ, Driscoll JR, Kriegsfeld LJ. A time to remember: The role of circadian clocks in learning and memory. *Behav Neurosci* 2014;**128**:283–303. https://doi.org/10.1037/a0035963.
77 Legros B, Bazil CW. Effects of antiepileptic drugs on sleep architecture: A pilot study. *Sleep Med* 2003;**4**:51–5. https://doi.org/10.1016/s1389-9457(02)00217-4.
78 Dravet C, Oguni H. Dravet syndrome (severe myoclonic epilepsy in infancy). *Handb. Clin. Neurol.*, vol. 111. Elsevier B.V.; 2013. p. 627–33.
79 Fujiwara T. Clinical spectrum of mutations in SCN1A gene: severe myoclonic epilepsy in infancy and related epilepsies. *Epilepsy Res* 2006;**70 Suppl 1**:S223-30. https://doi.org/10.1016/j.eplepsyres.2006.01.019.
80 Dravet C. The core Dravet syndrome phenotype. *Epilepsia* 2011;**52**:3–9. https://doi.org/10.1111/j.1528-1167.2011.02994.x.
81 Han S, Tai C, Westenbroek RE, Yu FH, Cheah CS, Potter GB, *et al*. Autistic-like behaviour in Scn1a +- mice and rescue by enhanced GABA-mediated neurotransmission. *Nature* 2012;**489**:385–90. https://doi.org/10.1038/nature11356.
82 Kalume F, Yu FH, Westenbroek RE, Scheuer T, Catterall WA. Reduced sodium current in Purkinje neurons from Nav1.1 mutant mice: Implications for ataxia in severe myoclonic epilepsy in infancy. *J Neurosci* 2007;**27**:11065–74. https://doi.org/10.1523/JNEUROSCI.2162-07.2007.
83 Kalume F, Scheuer T, Catterall WA, Kalume F, Westenbroek RE, Cheah CS, *et al*. Sudden unexpected death in a mouse model of Dravet syndrome Find the latest version : Sudden unexpected death in a mouse model of Dravet syndrome 2013;**123**:1798–808. https://doi.org/10.1172/JCI66220.1798.
84 Licheni SH, Mcmahon JM, Schneider AL, Davey MJ, Scheffer IE. Sleep problems in Dravet syndrome: a modifiable comorbidity. *Dev Med Child Neurol* 2018;**60**:. https://doi.org/10.1111/dmcn.13601.
85 Schoonjans AS, De Keersmaecker S, Van Bouwel M, Ceulemans B. More daytime sleepiness and worse quality of sleep in patients with Dravet Syndrome compared to other epilepsy patients. *Eur J Paediatr Neurol* 2019;**23**:61–9. https://doi.org/10.1016/j.ejpn.2018.09.012.
86 Nolan K, Camfield CS, Camfield PR. Coping With a Child With Dravet Syndrome: Insights From Families 2008. https://doi.org/10.1177/0883073808314162.
87 Villas N, Meskis MA, Goodliffe S. Dravet syndrome: Characteristics, comorbidities, and caregiver concerns. *Epilepsy Behav* 2017;**74**:81–6. https://doi.org/10.1016/j.yebeh.2017.06.031.
88 Claes L, Del-Favero J, Ceulemans B, Lagae L, Van Broeckhoven C, De Jonghe P. De novo mutations in the sodium-channel gene SCN1A cause severe myoclonic epilepsy of

infancy. *Am J Hum Genet* 2001;**68**:1327–32. https://doi.org/10.1086/320609.
89 Catterall WA, Kalume F, Oakley JC. NaV1.1 channels and epilepsy. *J Physiol* 2010:1849–59. https://doi.org/10.1113/jphysiol.2010.187484.
90 Yu FH, Mantegazza M, Westenbroek RE, Robbins CA, Kalume F, Burton KA, *et al*. Reduced sodium current in GABAergic interneurons in a mouse model of severe myoclonic epilepsy in infancy. *Nat Neurosci* 2006;**9**:1142–9. https://doi.org/10.1038/nn1754.
91 Ogiwara I, Miyamoto H, Morita N, Atapour N, Mazaki E, Inoue I, *et al*. Nav1.1 localizes to axons of parvalbumin-positive inhibitory interneurons: A circuit basis for epileptic seizures in mice carrying an Scn1a gene mutation. *J Neurosci* 2007;**27**:5903–14. https://doi.org/10.1523/JNEUROSCI.5270-06.2007.
92 Oakley JC, Kalume F, Yu FH, Scheuer T, Catterall WA. Temperature- and age-dependent seizures in a mouse model of severe myoclonic epilepsy in infancy. *Proc Natl Acad Sci U S A* 2009;**106**:3994–9. https://doi.org/10.1073/pnas.0813330106.
93 Tatsukawa T, Ogiwara I, Mazaki E, Shimohata A, Yamakawa K. Impairments in social novelty recognition and spatial memory in mice with conditional deletion of Scn1a in parvalbumin-expressing cells. *Neurobiol Dis* 2018;**112**:24–34. https://doi.org/10.1016/j.nbd.2018.01.009.
94 Kalume F, Westenbroek RE, Cheah CS, Yu FH, Oakley JC, Scheuer T, *et al*. Sudden unexpected death in a mouse model of Dravet syndrome. *J Clin Invest* 2013;**123**:1798–808. https://doi.org/10.1172/JCI66220.
95 Han S, Yu FH, Schwartz MD, Linton JD, Bosma MM, Hurley JB, *et al*. Na V 1.1 channels are critical for intercellular communication in the suprachiasmatic nucleus and for normal circadian rhythms n.d. https://doi.org/10.1073/pnas.1115729109.
96 Kalume F, Oakley JC, Westenbroek RE, Gile J, de la Iglesia HO, Scheuer T, *et al*. Sleep impairment and reduced interneuron excitability in a mouse model of Dravet Syndrome. *Neurobiol Dis* 2015;**77**:141–54. https://doi.org/10.1016/j.nbd.2015.02.016.
97 Papale LA, Makinson CD, Christopher Ehlen J, Tufik S, Decker MJ, Paul KN, *et al*. Altered sleep regulation in a mouse model of SCN1A -derived genetic epilepsy with febrile seizures plus (GEFS+). *Epilepsia* 2013;**54**:625–34. https://doi.org/10.1111/epi.12060.
98 Cheah CS, Yu FH, Westenbroek RE, Kalume FK, Oakley JC, Potter GB, *et al*. Specific deletion of NaV1.1 sodium channels in inhibitory interneurons causes seizures and premature death in a mouse model of Dravet syndrome. *Proc Natl Acad Sci U S A* 2012;**109**:14646–51. https://doi.org/10.1073/pnas.1211591109.
99 Catterall WA. Dravet syndrome: a sodium channel interneuronopathy. *Curr Opin Physiol* 2018. https://doi.org/10.1016/j.cophys.2017.12.007.

Chapter 1

Circadian Regulation of Sleep in a Pre-Clinical Model of Dravet Syndrome: Dynamics of Sleep Stage and Siesta Re-entrainment

(Note to reader: the following was published in the journal SLEEP in July 2019 and is available online or upon request as a journal article in PDF format).

Abstract

Study Objectives:

Sleep disturbances are common co-morbidities of epileptic disorders. Dravet syndrome (DS) is an intractable epilepsy accompanied by disturbed sleep. While there is evidence that daily sleep timing is disrupted in DS, the difficulty of chronically recording polysomnographic sleep from patients has left our understanding of the effect of DS on circadian sleep regulation incomplete. We aim to characterize circadian sleep regulation in a mouse model of DS.

Methods:

Here we exploit long-term electrocorticographic recordings of sleep in a mouse model of DS in which one copy of the *Scn1a* gene is deleted. This model both genocopies and phenocopies the disease in humans. We test the hypothesis that the deletion of *Scn1a* in DS mice is associated with impaired circadian regulation of sleep.

Results:

We find that DS mice show impairments in circadian sleep regulation including a fragmented rhythm of NREM sleep and an elongated circadian period of sleep. Next, we characterize re-entrainment of sleep stages and siesta following jet lag in the mouse. Strikingly, we find that re-entrainment of sleep following jet lag is normal in DS mice, in contrast to previous demonstrations of slowed re-entrainment of wheel-running activity. Finally, we report that DS mice are more likely to have an absent or altered daily "siesta".

Conclusions:

Our findings support the hypothesis that the circadian regulation of sleep is altered in DS and highlight the value of long-term chronic polysomnographic recording in studying the role of the circadian clock on sleep/wake cycles in pre-clinical models of disease.

Introduction

Sleep disturbance is common in epilepsy, and is associated with reduced seizure control, poor cognitive outcomes, and decreased quality of life[1]. The prevalence of nocturnal seizures in several forms of epilepsy[2], increased risk of seizure occurrence following sleep deprivation[3] and evidence that seizure propensity shows daily rhythms[4-9] highlights the need for a better understanding of the relationship between sleep, epilepsy and the circadian clock.

Dravet syndrome (DS) is a severe form of treatment-resistant, childhood-onset epilepsy with a high mortality rate[10]. DS usually manifests at six-nine months of age with fever and hyperthermia-induced seizures, and gradually progresses to include to spontaneous myoclonic, tonic–clonic, absence, and partial seizures[10,11]. During this time, DS patients develop several other co-morbidities including autism-like behaviors, ataxia, psychomotor regression and high risk of sudden unexpected death (SUDEP). Sleep disruptions are reported by more than 70% of DS patients[12], and DS patients report more frequent nighttime awakenings and greater daytime sleepiness than patients with other forms of epilepsy[13]. Disturbances including sleep onset insomnia, difficulty maintaining sleep and frequent nocturnal seizures are well documented, and these disturbances are described as highly disruptive to quality of life for both patients and caregivers[14-16].

DS is caused by loss-of-function mutations in one allele of the *SCN1A* gene[17], which codes for the pore-forming alpha subunit of the $Na_V1.1$ sodium channel[18]. $Na_V1.1$ is widely expressed throughout the brain, primarily in GABAergic interneurons. Previous work in a mouse model of DS, in which the *Scn1a* gene is heterozygously deleted, has shown that the mutation causes a selective reduction in the excitability of inhibitory interneurons[19-20]. Several characterizations of DS mice have revealed that, like human patients, they display both

spontaneous and thermally-induced seizures[19,21], ataxia[22], autism-like cognitive and social deficits[23,24], SUDEP[25], and sleep disturbances[26-28]. Specific heterozygous deletion of the Scn1a gene in forebrain interneurons recapitulates the epilepsy, SUDEP, cognitive impairment, autistic-like behaviors, and homeostatic sleep disruption observed in DS mice[23,26,28.29]. This work has led to the unified hypothesis that hyperexcitability of different neural circuits due to the loss of functional $Na_V1.1$ channels underlies the co-morbidities of DS[30].

The two-process model of sleep regulation proposes both homeostatic and circadian drives that influence the timing and consolidation of sleep[31]. While the neural circuitry underlying these sleep regulatory processes is multi-faceted, reliant on multiple neurotransmitter systems, and widely diffuse across the brain, many of the most important nodes in these circuits are GABAergic[32,33]. In previous studies, we identified circadian behavioral deficits in DS mice including reduced circadian amplitude of wheel-running activity (WRA), elongated endogenous WRA period under conditions of constant darkness (DD), and increased time to re-entrainment of WRA to a new light-dark (LD) cycle[26]. These deficits were correlated with poor network synchrony and reduced photoresponsiveness in the GABAergic suprachiasmatic nucleus (SCN) of the hypothalamus, the master circadian clock in mammals and a critical component of daily sleep timing[34]. Later work showed that DS mice also lack normal homeostatic non-rapid eye movement (NREM) sleep rebound in response to sleep deprivation, as well as fragmented NREM sleep under baseline conditions[28]. This was associated with reduced excitability of GABAergic inhibitory neurons in the thalamic reticular nucleus (TRN), a brain region which contributes to maintaining the slow oscillations characteristic of NREM sleep and the homeostatic sleep response[2]. Based on these findings, we hypothesized that DS mice would also display deficits in the circadian regulation of sleep.

Here we leverage long-term electrocorticographic (ECoG) recordings to characterize the circadian regulation of sleep in DS mice. We hypothesized that DS mice would have disturbances in circadian sleep regulation due to reduced GABAergic tone in the SCN caused by the heterozygous deletion of the *Scn1a* gene. We report disturbances in circadian sleep behavior of DS mice including elongated circadian period of sleep, a fragmented rhythm of NREM sleep that was not correlated with epileptiform interictal activity and fragmented or absent siesta, a short bout of sleep under the control of the circadian clock. Interestingly, DS mice displayed no deficits in re-entrainment of sleep acrophase following jet lag, and similar total sleep time during each phase of the LD cycle when compared to wild type (WT) controls. These results highlight the value of coupling long-term sleep recordings with locomotor activity monitoring to more comprehensively disentangle the effects of environmental manipulations on different outputs of the circadian clock, and provide a novel approach to studying the circadian regulation of sleep in preclinical models of disease.

Methods

Animals and Housing Conditions

All experiments with animals were performed in accordance with animal protocols approved by the Office of Animal Welfare at the University of Washington. Mice with a heterozygous deletion of the *Scn1a* gene (*Scn1a*$^{+/-}$), hereafter referred to as DS mice, were generated by targeted deletion of the last exon, encoding domain IV from the S3 to S6 segment and the entire C-terminal tail of $Na_V1.1$ channels, as previously described[19]. The mice used in this study were generated by crossing heterozygous mutant mice of C57BL/6 background with wild type (WT)

C57BL/6 mice (both males and females of each genotype), resulting in only WT or heterozygous *Scn1a* mutant offspring. Mice were genotyped as previously described[28].

Electrocorticographic Recordings

Sleep was recorded as previously described[35]. Briefly, mice were anesthetized with isoflurane and placed into a stereotaxic device where isoflurane anesthesia continued throughout surgery. Each mouse was implanted with ECoG electrodes, consisting of dental screws (Pinnacle Technology, Lawrence, KS; No. 8209: 0.10-in.). A midline incision was made above the skull. Recording electrodes were screwed through cranial holes as follows: over the left frontal cortex (1.5 mm lateral and 2 mm anterior to bregma) and over the right parietal cortex (1.5 mm lateral and 2 mm posterior to bregma), a ground electrode was placed over the visual cortex (1.5 mm lateral and 4.0 mm posterior to bregma), and a reference electrode was placed over the cerebellum (1.5 mm lateral and 6.5 mm posterior to bregma). Electromyogram (EMG) signals were obtained by placing a pair of silver wires into the neck muscles. The screws were connected, through silver wires, to a common 6-pin connector compatible with the Pinnacle recording device. The screws and connector were fixed to the skull with dental cement. Mice were implanted at between 3 and 4 months of age to account for the long duration of circadian sleep experiments. After surgery, mice were housed in single recording cages under a 12:12 LD cycle.

Mice had a recovery period of 1 week and were then fitted with a preamplifier and tether, and connected to the Pinnacle Technology recording system, where they were allowed 1 day to acclimate before recording started. The ECoG and EMG signals were sampled at 400 Hz with low-pass filters of 80 Hz and 100 Hz, respectively.

Sleep Scoring and Processing

Raw ECoG/EMG data were automatically classified in 10-second bouts as either wake, NREM sleep or REM sleep using a previously described custom algorithm implemented in Python v2.7[35]. Briefly, the power spectrums of the ECoG and EMG signals are calculated using Welch's method with an overlap window of 50%. Then, the following features for each 10-second epoch of sleep are calculated: delta power, the sum of ECoG power at frequencies ranging between 0.5 and 4 Hz; theta power, the sum of ECoG power at frequencies ranging between 6 and 12 Hz; and EMG RMS, the mean square root of the raw EMG signal. If EMG RMS was higher than a visually determined threshold for each 24-h recording session, typically set at 0.4 standard deviations above the mean, the epoch was classified as wake, otherwise it was classified as sleep. Next, sleep stage was classified as REM whenever the theta to delta power ratio during the epoch was higher than the average theta to delta ratio—over the whole 24-h recording session—plus 1 standard deviation. The remaining epochs were classified as NREM sleep. This scoring method was based on heuristics for manually scoring sleep in previous studies, and validated by 2 independent experimenters that visually scored 10-second bins as previously described[36-38], with a minimum of 90% score agreement in both cases.

The 10-s scored epochs were further binned into 1- or 60-min bins, for which we calculated the percentage of each sleep state. A 1- or 60-min bin was classified as REM when more than 20% of the bin was spent in REM sleep. If REM sleep was lower than 20% during the bin, it was classified as either wake or NREM sleep, depending on which of the 2 brain states contributed to a higher percentage of the 1- or 60-min bin. Hypnograms were generated with 10-second bins of sleep scores using a custom R code. NREM and REM intensities were calculated

as the product of sleep stage percentage and either delta or theta power within each 1- or 60-min bin. Statistical analysis was performed for both 1- and 60-min bins and yielded similar results; 1-minute bins are reported for total sleep time, sleep re-entrainment, rhythm intra-daily variability and circadian sleep period analyses, while 60-min bin results are reported for daily sleep stage intensity scores under baseline conditions.

During long-term recording, the recording software was restarted every 24 hours to account for potential software or hardware failures, resulting in a loss of approximately 10-30 seconds of recording time each day. To account for this, missing data points were imputed after scoring by taking the mean of the values for delta, theta and sleep stage calls in the 60 seconds following and preceding the gap using a custom R code. This facilitated the combination of sleep scores into larger bins and enhanced the continuity of the recording.

Interictal Spike Quantification

Epileptiform interictal spikes were identified semi-automatically over a 24-hour recording session with the Sirenia Seizure software (Pinnacle Technology, Lawrence, KS) using a line length threshold[39] established for both ECoG channels, then confirmed visually by a manual scorer blind to experimental conditions. Spikes were then classified as occurring during either Wake, NREM or REM based on scores obtained through automated sleep classification.

Behavioral Experiments and Analysis

Our recordings were maintained in a ventilated, light-tight room under either a 12:12 LD cycle with 200-lux intensity or DD. To determine the effect of abrupt LD phase shifts on the phase of the circadian rhythm of sleep, we used a delay and advance “jetlag” protocol[26]. After

mice were entrained to a 12:12 LD cycle, a delay jetlag was initiated by extending the light phase by 6 hours (i.e., delaying the time of lights-off by 6 hours). The mice stayed under this new 12:12 LD cycle until they re-entrained to the new cycle. The advance jetlag was initiated by shortening the light phase by 6 hours (i.e., advancing the time of lights off by 6 hours). For each day of recording, acrophase was determined for both NREM and REM sleep using the El Temps software package (Dr. Toni Diéz-Noguera, Universidad de Barcelona), and time to re-entrainment was calculated as the number of days necessary for sleep stage acrophase to return to mean baseline levels within a 95% confidence interval.

To assess the endogenous circadian period of sleep, we released mice into DD for at least 14 days after they had synchronized to a 12:12 LD cycle. Free running period of NREM, REM and total sleep were assessed using 1-minute bins and Sokolove-Bushell periodogram analysis in El Temps and R version 3.1.2 as previously described[40]. Waveforms of total sleep in DD were generated using El Temps as previously described[26], and adjusted for the circadian period of each animal.

We defined the "siesta" as a brief (<2 hours) bout of sleep occurring primarily during the dark phase of the LD cycle that is visually discernible from the main bout and occurs with a regular onset each day. To compare the re-entrainment of the siesta and the main bout of sleep, we used total sleep (both NREM and REM), due to the brevity of the siesta and the limited number of REM bouts within it. We calculated the re-entrainment speed (RS) in minutes per day for both sleep bouts individually by extracting the slope of a line fitted to sleep offset for delays and onset for advances using actograms of sleep by three manual scorers blind to experimental conditions. RS was determined to the average slope calculated from the three manual scorers.

Wake after sleep onset (WASO)[41] was defined as the percentage of total time spent awake during the time of lights on in the chamber, as sleep onset occurred within minutes of lights on. WASO was calculated for each DS mouse during the same 24-hour recording period used for the interictal spike analysis.

Data Analysis and Statistics

Data are presented as mean ± SEM, and typically analyzed using one-, two- or three-way ANOVA followed by Tukey, or Student's t-tests for comparisons in which type I error was not possible. Chi-squared tests were used to assess differences in the occurrence of siesta between genotypes. The 24-h distributions of REM and NREM intensity were compared between genotypes using a 2-sample Kolmogorov-Smirnov test, as the data were not normally distributed. Sleep stage bout durations from both genotypes were not normally distributed and were analyzed using a 2-way ANOVA of the aligned rank transform of the data with the ARTool R package[42]. Occurrences of interictal spikes were analyzed using the Kruskal-Wallis test, and post-hoc pairwise comparisons made with the Wilcoxon rank sum test. $P < 0.05$ was considered as statistically significant. Intradaily variability (IV) index was calculated as previously described[43,44]. Briefly, IV is the ratio of the mean square of the difference between all the successive hours on each day, and the same calculation around the overall mean:

$$IV = \frac{n \sum_{i=2}^{n} (x_i - x_{i-1})^2}{(n-1) \sum_{i=1}^{n} (x_i - \bar{x})^2}$$

Where n is the total number of data points, x_i is each individual data point, and $\bar{x}$ is the mean of all the data points. An IV index of 0 represents a perfect sinusoid, while an IV index of 2 represents Gaussian noise. Interictal spiking frequency was correlated with sleep IV or WASO

using Spearman's rank correlation. All statistical tests were done with GraphPad Prism 6 (GraphPad Software, Inc., La Jolla, CA) or R version 3.1.2.

Results

DS Mice Show Similar Total Amounts of Sleep Compared to WT Mice under Baseline Conditions

We first sought to determine whether total sleep duration differed between WT and DS mice over the 24-hour day. We implanted WT and DS mice with ECoG/EMG electrodes and recorded continuously under 12:12 LD conditions. We then assessed total sleep time and intensity during the light and dark phases.

Sleep bouts of both genotypes synchronized to a 12:12 LD cycle. While representative hypnograms of 24-hours of baseline data (Fig. 1A) reflect previously observed sleep fragmentation of DS mice[28], mean daily sleep time calculated from 48 consecutive hours of recording shown in Figure 1B reveal that WT and DS sleep time is comparable and highly consolidated during the light phase (2-way ANOVA: genotype [$F_{1,44} = 0$, $p = 1$]; light phase [$F_{1,44} = 686.11$, $p < 0.001$], n = 10 DS mice, 15 WT mice) (data not shown). We next generated daily waveforms of 1-hour bins of NREM and REM sleep intensity, defined as the product of the amount of time spent in each sleep stage per hour and the average delta or theta power, respectively (Fig. 1B). The distribution of sleep intensity did not differ between genotypes for NREM (Kolmogorov-Smirnov test, $p = 0.45$) or REM (Kolmogorov-Smirnov test, $p = 0.686$). Finally, we found that, in agreement with previous reports[28], mean NREM and REM sleep bout duration is comparable between genotypes (Fig. 1C), during both the light phase (2-way ANOVA of aligned rank transform data; effect of sleep stage [$F_{1,44} = 128.15$, $p > 0.001$] but not

genotype [$F_{1,44} = 3.04$, $p > 0.05$], and no interaction [$F_{1,44} = 0.25$, $p = 0.62$]) and the dark phase (2-way ANOVA of aligned rank transform data; effect of sleep stage [$F_{1,44} = 121.59$, $p < 0.001$] but not genotype [$F_{1,44} = 0.01$, $p = 0.92$] and no interaction [$F_{1,44} = 0.87$, $p = 0.35$]).

DS Mice Display Altered Intradaily Variability of NREM Sleep That is Not Correlated with Interictal Activity

Previous work has demonstrated that DS mice display reduced circadian amplitude of locomotor activity under baseline 12:12 LD conditions[26], and highly fragmented NREM but not REM sleep[28]. We predicted that DS mice would also display a less stable daily rhythm of NREM and REM sleep and assessed the integrity of sleep rhythms using intradaily variability (IV), a non-parametric index of rhythm fragmentation. We found that IV index (Fig, 2A) was significantly higher in DS mice for NREM sleep (unpaired two-tailed t-test, $p = 0.04$), but not REM sleep (unpaired two-tailed t-test, $p = 0.32$), indicating that DS mice have a fragmented daily rhythm of NREM sleep under baseline conditions.

It has been shown that interictal spiking events occur during NREM sleep in DS mice and these spikes are associated with an increased number of awakenings from NREM sleep[28]. We predicted that spiking frequency would also be positively correlated with NREM IV. We quantified the presence of interictal spikes during wake, NREM and REM sleep over a 24-hour recording session under baseline 12:12 LD conditions. In agreement with previous work, we found that interictal spiking occurs primarily during NREM sleep in DS mice (Kruskal-Wallis rank sum test, $\chi^2 = 18.051$, df = 2, $p < 0.001$) (Fig. 2B). Some spikes were observed during wake, and rarely during REM sleep (pairwise comparisons using Wilcoxon rank sum test; NREM-Wake, $p = 0.001$; NREM-REM, $p < 0.001$, REM-Wake, $p = 0.27$). Spontaneous seizures

were occasionally observed in DS mice during wake. Interictal spikes were not observed in WT mice. Interestingly, we found no significant correlation between NREM IV and interictal spike frequency during NREM sleep (Spearman's rank correlation, $r_s = 0.19$, $p = 0.6$) (Fig. 2C).

Previous reports have indicated that DS mice have highly fragmented sleep, and we predicted that wake after sleep onset (WASO), a measure of sleep fragmentation commonly used in studies of human sleep, would also be positively correlated with interictal spiking activity in DS mice. Interestingly, we found no correlation between WASO and interictal spike frequency across behavioral states (Spearman's rank correlation, $r_s = 0.19$, $p = 0.61$) (Fig. 2D).

Sleep Bouts Take Longer to Re-entrain to Phase Advances Than Phase Delays, and DS Mice Display Normal Re-entrainment

We previously demonstrated that DS mice take longer to re-entrain to abrupt phase advances and delays of the LD cycle simulating jet lag than WT mice, as measured by WRA[26]. We predicted that the acrophase of sleep stages of DS mice would also take longer to re-entrain to abrupt phase shifts of the LD cycle. DS and WT mice were implanted with ECoG/EMG electrodes, recorded from continuously for 3-5 days and subjected to either delay or advance jet lags (Fig. 3). To our knowledge, continuous polysomnographic sleep recordings during single transient jet lags have not been performed in mice, so we first set out to determine the re-entrainment time of NREM and REM sleep stage acrophases following both phase delays and advances in WT mice.

We find that following phase delays, WT NREM and REM sleep took an average of 4.5 ± 0.4 and 5.1 ± 5 days to re-entrain, respectively (n = 14). Following phase advances, NREM and REM re-entrained in 6.9 ± 0.5 and 7.8 ± 0.6 days, respectively (n = 16). Fig. 3A shows a

representative double-plotted actogram from one WT mouse, with acrophase overlaid in red on the left side. DS mice displayed comparable re-entrainment times for both delays (NREM = 5.3 ± 0.4 days, REM = 5.9 ± 1 days, n = 7) and advances (NREM = 5.9 ± 6 days, REM = 7.3 ± 0.9 days, n = 9). Three-way ANOVA with genotype, sleep stage and jet lag direction as factors reveals an effect of jet lag direction ($F_{1,84} = 27.93$, $p < 0.001$), where advances took longer to re-entrain to than delays, but no difference between genotypes ($F_{1,84} = 0.003$, $p = 0.96$) and no effect of the interaction (Fig. 4). Interestingly, there was a trend for NREM sleep to re-entrain faster than REM sleep that reached the borderline of statistical significance ($F_{1,84} = 3.9$, $p = 0.051$).

These results indicate that in both WT and DS mice, sleep bouts take longer to re-entrain to advances than delays, as expected based on an abundance of previous work demonstrating the same result in mice using WRA. Furthermore, there was no significant difference in re-entrainment time between NREM and REM sleep stages, unlike previous demonstrations of this phenomenon from similar experiments in the rat[37]. Finally, we found that despite differences in re-entrainment times as measured by WRA[26], there was no difference in re-entrainment time of sleep bouts between WT and DS mice in our ECoG experiments.

DS Mice Have an Elongated Circadian Period of Sleep

We predicted that like WRA, DS mice would display an elongated circadian period of sleep relative to WT controls. To test this prediction, we recorded sleep from WT and DS mice continuously for at least 14 days under conditions of constant darkness (Fig. 5A and B). We found that the daily period of total sleep time in DD is significantly longer in DS (23.83 ± 0.04 hours, n = 5) than WT (23.64 ± 0.03 hours, n = 3) mice (two-tailed Student t-test, $p = 0.01$) (Fig.

5E). However, this difference was smaller than that measured from WRA[26]. To determine if there were any differences in the circadian period of NREM and REM sleep between and within genotypes, we also performed a 2-way ANOVA with genotype and sleep stage as factors. While we found a strong effect of genotype ($F_{1,17} = 19.96$, $p < 0.001$), we found no effect of sleep stage ($F_{1,17} = 0.15$, $p = 0.86$) or the interaction ($F_{1,17} = 0.5$, $p = 0.62$) (data not shown). These results suggest that, in agreement with previous findings[57], the rhythm of both NREM and REM sleep are under strong control of the circadian clock in free-running conditions.

DS Mice Are More Likely to Have an Absent or Fragmented Daily "Siesta"

The "siesta" is a brief bout of sleep during the active period commonly observed to occur in WT mice[45-49]. Recent work has demonstrated that the daily timing of the siesta is under control of vasoactive intestinal polypeptide (VIP) neurons in the SCN[49], suggesting it as an important output of the circadian system's regulation of sleep. Our continuous ECoG/EMG recording paradigm offered a unique opportunity to directly assess how the timing of the siesta in mice responds to manipulations of the LD cycle, and to determine if the siesta is disrupted in DS mice.

We first asked whether DS mice also display a consolidated siesta akin to that seen in WT mice (Figure 6). We found that DS mice were nearly 40% less likely to have a consolidated siesta than WT controls (Chi-Squared test, $\chi^2(1) = 4.768$, $p = 0.02$) (Fig. 6B, top left panel).We then set out to determine if there were any differences between the re-entrainment dynamics of the siesta and the main bout of sleep following phase shifts in WT mice. Here, we define the siesta as a brief (<2 hours) bout of sleep occurring primarily during the active period (dark phase) of the LD cycle that is visually discernible from the main bout and occurs with a regular

onset each day. We first calculated the re-entrainment speed in minutes per day for both sleep bouts individually by extracting the slope of a line fitted to sleep offset for delays and onset for advances using actograms of sleep by manual scorers blind to experimental conditions. In WT mice, we find that re-entrainment of the siesta is slower than the primary bout of sleep for both advances and delays (2-way ANOVA: sleep bout [$F_{1,54} = 65.88$, $p < 0.001$], jet lag condition [$F_{1,54} = 3.953$, $p = 0.052$] and effect of the interaction [$F_{1,54} = 4.023$, $p < 0.05$], n = 14 mice for delays, 16 for advances) (Fig. 6A).

Strikingly, for those DS mice that did display a siesta, a 2-way ANOVA with Tukey post-hoc comparisons revealed a significant difference in RS between the siesta and main sleep bout following delays ($p < 0.001$), but not advances ($p = 0.25$) (Fig. 6B, bottom left panel). Therefore, we conclude that DS mice have a disrupted daily siesta relative to their WT counterparts.

Discussion

Here we show that DS mice have impairments in the circadian regulation of sleep including fragmented rhythm of NREM sleep, elongated endogenous period of sleep and a disrupted daily siesta. These findings are consistent with our previous characterization of circadian wheel-running behavioral deficits in DS mice and suggest that a global heterozygous loss-of-function mutation in the $Na_V1.1$ sodium channel is sufficient to cause disturbances in the circadian regulation of sleep. However, in contrast to our previous report, both NREM and REM sleep acrophase in DS mice re-entrain normally to phase shifts of the LD cycle simulating jet lag. Moreover, while the endogenous period of both WRA and sleep was significantly longer in DS mice, the magnitude of this difference is more pronounced in WRA than sleep[26]. This could be in

part due to the fact that DS mice were previously documented to display less wheel-running activity in general than WT mice.

Despite these discrepancies, our results are consistent with reports of disturbed sleep in DS patients[14,15]. We found that the endogenous period of both NREM and REM sleep is longer in DS mice than their WT counterparts. As noted previously[26], the elongation of circadian period in DS mice is striking, as period lengthening is typically only seen in clock gene or clock-related gene mutants such as *Clock*[50], *Rorβ*[51], and *CK1ε*[52]. A similar phenomenon in DS patients could explain complaints of delayed sleep onset and difficulty maintaining sleep, as a longer endogenous period of sleep would result in a delayed phase of circadian entrainment. DS mice also showed rhythm fragmentation in NREM but not REM sleep. We hypothesize that disturbances to NREM sleep we report here and have reported previously[28] are caused by reduced excitability of GABAergic TRN neurons as a result of heterozygous deletion of *Scn1a*. Of note, recent work has demonstrated that another mouse model of DS displays hyperexcitability of TRN neurons due to compensation by calcium-activated SK potassium channels, leading to excessive burst firing and non-convulsive seizures[53]. However, the aforementioned DS mouse contains a human *Scn1a* mutation and is bred on a different genetic background than the DS model presented here, suggesting a number of different explanations for the discrepancies in TRN properties. Still, these results raise the possibility that cellular and/or network changes outside the TRN may contribute to the NREM sleep disturbances observed in DS. Interestingly, although interictal spiking during NREM sleep in DS mice has been associated with increased awakenings[28], we observed no correlation between interictal spiking frequency and both NREM intradaily variability and WASO. While we cannot completely rule out the contribution of epileptic activity to sleep disturbances in DS mice, our data suggest that epileptic

activity identified at the recording sites in our experimental setup alone is unlikely to fully account for the fragmentation of sleep rhythms in DS. It is possible that the combination of epileptic activity and sleep rhythm fragmentation with a potentially independent etiology leads to the frequent nighttime awakenings reported by DS patients.

While most patients diagnosed with DS have a mutation in the *SCN1A* gene, these mutations exist on a spectrum, and the type and severity of symptoms seen in patients with DS and other *SCN1A*-related epilepsies can vary widely[18]. For example, a mouse model of generalized epilepsy with febrile seizures plus (GEFS+), which is the result of a different *Scn1a* mutation, was shown to have reduced NREM and REM sleep and normal homeostatic sleep rebound, in contrast to this and previous descriptions of sleep in the DS mouse studied here[27]. Continuing to characterize sleep and other co-morbidities in these different pre-clinical models of *SCN1A*-related epilepsies could be informative in helping to identify and more effectively address different manifestations of symptoms in patients.

The contradictions between the sleep phenotype found in this study and previously identified circadian behavioral phenotypes underscore the value of combining long-term ECoG/EMG recording and activity monitoring in disentangling different behavioral outputs of the circadian clock, particularly in pre-clinical models of disease. It is well-documented that DS mice are susceptible to thermally-induced seizures[19,21], and that exercise such as wheel-running increases core body temperature. The risk of thermally-induced seizures could deter DS mice from running on wheels. Furthermore, like many DS patients, DS mice show spasticity[23], which could reduce their ability to run on a wheel. Similarly, a seizure during WRA might cause premature termination, whereas a seizure before WRA might prevent initiation of a bout of running. Although it remains to be determined why, it is clear that DS mice show reduced wheel-

running and this could in turn affect their ability to achieve normal circadian phase resetting of WRA[26]. Therefore, existing circadian behavioral impairments in DS mice may appear exacerbated when measuring rest-activity cycles by WRA, as opposed to measuring home cage activity or ECoG/EMG.

There is evidence to suggest that the circadian deficits in DS mice are the result of reduced GABAergic neurotransmission caused by the loss-of-function mutation in the $Na_V1.1$ channel, and thus impaired communication between SCN subregions[26]. The mutation reduces excitability of GABAergic neurons specifically[19], and GABA has been proposed as a critical component in coupling both SCN subregions[51], and individual SCN neuronal oscillators[54-56]. This network integrity is key to the maintenance of rhythmic sleep-wake behaviors of the type observed here[57]. Despite this, the possibility remains that neuronal damage sustained as a result of chronic seizures may also contribute to sleep phenotypes. The SCN projects to multiple known sleep-wake maintenance centers[57], as well as to neurons that drive endocrine, metabolic and autonomic functions that affect sleep[34]. Depending on the frequency, severity and origin point of seizures, the SCN and its myriad downstream targets may be differentially affected. Though we are unaware of any evidence that seizures in DS directly affect the integrity of these areas, future work could incorporate histological evaluation of DS mouse brain tissue to determine if and how such centers are affected. This could also help to explain the high degree of inter-individual differences seen in circadian sleep behaviors in DS mice, such as rate of re-entrainment to jet lag (Fig. 4). Although such an analysis is beyond the scope of the present study, previous histological work has confirmed a reduction in the expression of the $Na_V1.1$ channel in GABAergic neurons in the SCN[26], TRN[28], hippocampus[19], cortex[19-20,24] and sleep-related hypothalamic nuclei[26-27] of DS mice, suggesting the *Scn1a*$^{+/-}$ mutation is highly likely to

contribute to the sleep phenotypes observed here. Of note, our previous study on WRA in DS mice used animals that were typically older than then ones used in the current study; some of the circadian deficits observed in WRA and not in the regulation of polysomnographically recorded sleep could be also due to the history of seizures that could presumably have cumulative neuronal damage in SCN targets. Future work on sleep-related co-morbidities of DS should employ region-specific targeting of the *Scn1a*$^{+/-}$ mutation to the SCN and its downstream targets — many of which also richly express the $Na_V1.1$ channel[27] — in order to characterize their respective contributions to the phenotypes observed in the DS mouse.

While this study is not the first to employ polysomnographic recordings of this length in rodents[59], our results join a short but growing list of successes in using long-term ECoG/EMG recording to study the circadian regulation of sleep. A series of studies from our lab employed long-term continuous sleep recording in rats to demonstrate that under lighting conditions that cause internal circadian desynchrony, the daily rhythms of NREM and REM sleep become uncoupled[36], and that the daily timing of REM sleep specifically is associated with an oscillator in the dorsomedial subregion of the SCN[37]. In mice, long-term sleep recordings have been used to characterize temporal distributions and re-entrainment dynamics of sleep following chronic environmental circadian disruption in the form of serial advance jet lags over 3 months[60], as well as chronic sleep disturbances that occur under LD cycles that cause circadian misalignment[61], highlighting the value of this approach.

In addition to the identification of circadian sleep regulation deficits in DS, our study offers a thorough characterization of re-entrainment dynamics of sleep following a single phase shift of the LD cycle simulating jet lag in WT mice, as well as, to our knowledge, the first direct observation of the effects of LD cycle manipulation on the daily siesta. Interestingly, we found

no significant difference in re-entrainment time between NREM and REM sleep stages. This is in contrast to results from similar experiments in the rat, which demonstrated that REM sleep takes longer to re-entrain to delay jet lags than NREM, and that the timing of REM is associated with the activity of the dorsomedial SCN[37]. A recent study found that under 20-h LD cycles causing circadian desynchrony in the mouse, REM sleep increases during the dark phase during misaligned days—coinciding with the subjective day—, suggesting that REM sleep timing is regulated primarily by the ~24-hour circadian clock, and is dissociated from the LD cycle[61]. This is in agreement with our previous finding in rats that under 22-h LD circadian forced desynchrony, REM is dissociated from LD cycle and displays an endogenous period of approximately 25 hours[36]. Future work seeking to reconcile these findings on the role of the circadian clock in the timing of REM sleep in mice could combine continuous sleep recording and a serial jet lag protocol as used by Casiraghi et al.[62] to examine both re-entrainment dynamics and the resulting period of sleep stages.

Both our protocol and Casiraghi et al.'s serial jet lag paradigm could also be useful in further characterizing the mechanisms underlying both the timing and the re-entrainment dynamics of the siesta, which recent evidence suggests is under control of VIP neurons in the ventral SCN[49]. We previously demonstrated reduced signal propagation from the VIP-rich ventral SCN to the dorsal SCN resulting in poor network connectivity in DS mice[26], which could help to explain the disturbed siesta phenotype reported here. However, NREM sleep rhythm fragmentation was observed in DS mice, and because NREM sleep comprises a sizable portion of the daily siesta, it is possible that the absence or fragmentation of siesta in DS mice is an epiphenomenon of NREM fragmentation in general. Still, the difference in re-entrainment dynamics of siesta, but not the main sleep bout, between WT and DS mice that display a

consolidated siesta, as well as the complete absence of siesta in some animals, suggest that while NREM fragmentation likely contributes, the siesta phenotype cannot be explained by this fragmentation alone. Interestingly, a recent study using a mouse model of Angelman syndrome with a maternal deletion of the *Ube3A* gene, which is expressed in the SCN, found that the daily siesta is lost while circadian rhythmicity remains intact[47], suggesting the siesta may also be regulated by the sleep homeostat. Yet another report found that mice with a deficiency in serotonin synthesis exhibit both abnormal circadian behavior and a complete lack of siesta[48]. Taken together, these data suggest a combination of circadian and homeostatic components are at play in timing the siesta and highlight the need for further study of its regulation.

Long-term sleep experiments of the kind performed here and in previous studies also offer a framework in which to study diseases with circadian and sleep-related co-morbidities where long-term polysomnographic studies are not possible in patients. Additionally, these approaches would be invaluable in determining both efficacy and mechanisms of interventions to improve sleep hygiene, and in turn the core symptoms of these diseases. Pharmacological imposition of sleep improved both circadian and cognitive outcomes in a mouse model of Huntington's disease[63,64]. Non-pharmacological behavioral interventions using circadian entraining cues to improve the temporal organization of sleep-wake cycles have also proven effective in treating disease. For example, social rhythm therapy has shown success in improving both sleep hygiene and symptoms in patients with mood disorders[65], and temporally restricting feeding has been shown to reduce seizure frequency and severity in a rat model of pilocarpine-induced epilepsy[66]. Combining these interventions with continuous sleep monitoring can offer greater insight into how sleep timing and quality is affected and provide clues into how these changes may result in improvement of disease symptoms.

Figures

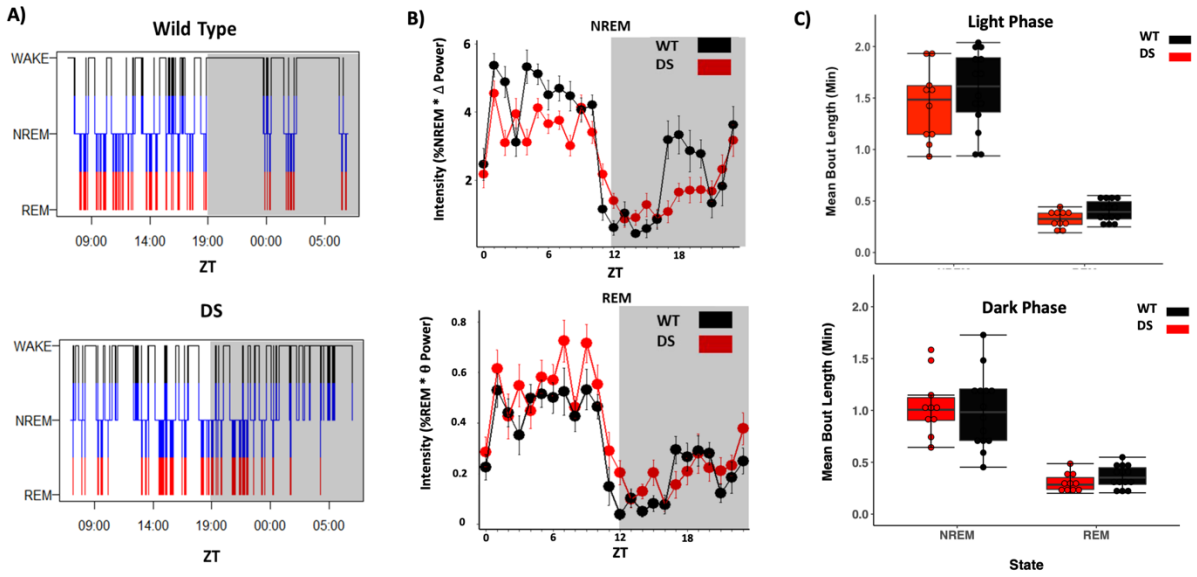

Figure 1. DS mice show similar sleep bout length compared to WT controls. **A)** Representative hypnograms taken from a single day of sleep under a 12:12 LD cycle in wild-type (top) and DS (bottom) mice. **B)** Average waveforms 60-min bins of non-rapid eye movement (NREM) and rapid-eye movement (REM) sleep intensity calculated from normalized power values in WT and DS mice**.** The distribution of sleep intensity did not differ between genotypes for NREM (Kolmogorov-Smirnov test, $p = 0.45$) or REM (Kolmogorov-Smirnov test, $p = 0.686$), and both WT and DS mice show similar total sleep time in both phases of the LD cycle (data not shown, 2-way ANOVA, effect of LD phase ($p < 0.001$) but not genotype ($p = 0.36$)). **C)** Average NREM and REM sleep bouts is comparable between genotypes, during both the light phase (2-way ANOVA of aligned rank transform data; effect of sleep stage ($F_{1,44} = 128.15$, $p > 0.001$) but not genotype ($F_{1,44} = 3.04$, $p > 0.05$), and no interaction ($F_{1,44} = 0.25$, $p = 0.62$)) and the dark phase (2-way ANOVA of aligned rank transform data; effect of sleep stage ($F_{1,44} = 121.59$, $p < 0.001$) but not genotype ($F_{1,44} = 0.01$, $p > 0.05$) and no interaction ($F_{1,44} = 0.87$, $p = 0.35$).

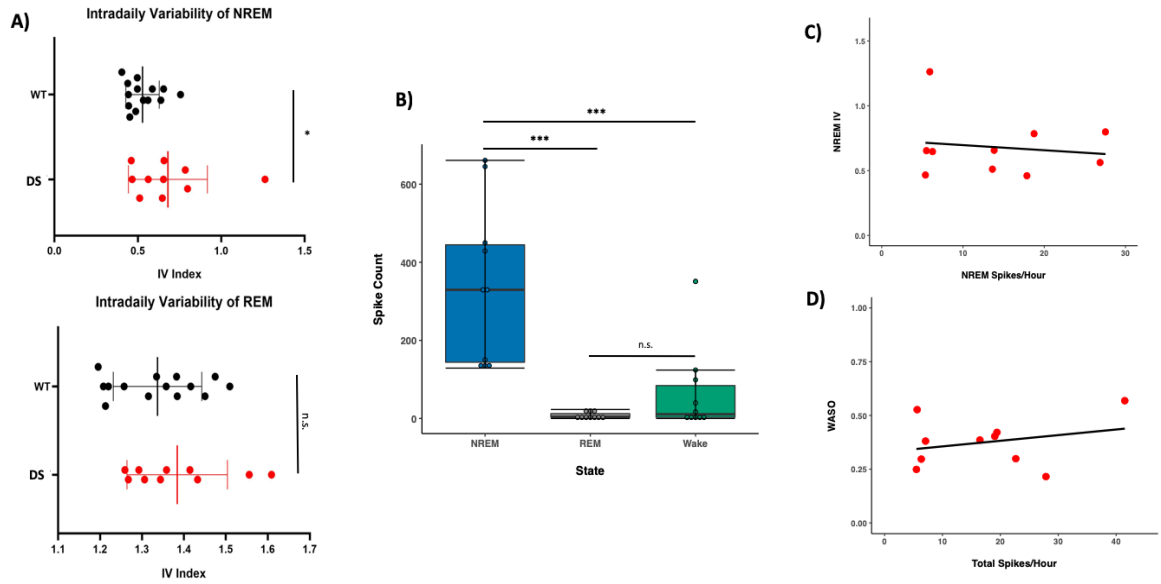

Figure 2. Altered intradaily variability of NREM sleep is not correlated with interictal activity in DS mice. A) Intradaily variability (IV), a non-parametric measure of daily rhythm fragmentation, is higher in DS mice than WT mice for NREM sleep (top panel; unpaired two-tailed t-test, p = 0.04), but not for REM sleep (bottom panel; unpaired two-tailed t-test, p = 0.32). **B)** Interictal spiking occurs primarily in NREM sleep in DS mice (Kruskal-Wallis rank sum test, $\chi^2 = 18.051$, df = 2, p < 0.001), while some spikes were observed during wake and rarely during REM sleep (pairwise comparisons using Wilcoxon rank sum test; NREM-Wake, p = 0.001; NREM-REM, p < 0.001, REM-Wake, p = 0.27). Interictal spiking was not observed in WT mice. **C)** Interictal spike frequency showed no significant correlation with intradaily variability of NREM sleep (Spearman's rank correlation, $r_s = 0.19$, p = 0.6). **D)** Total interictal spike frequency showed no significant correlation with wake after sleep onset (Spearman's rank correlation, $r_s = 0.19$, p = 0.61).

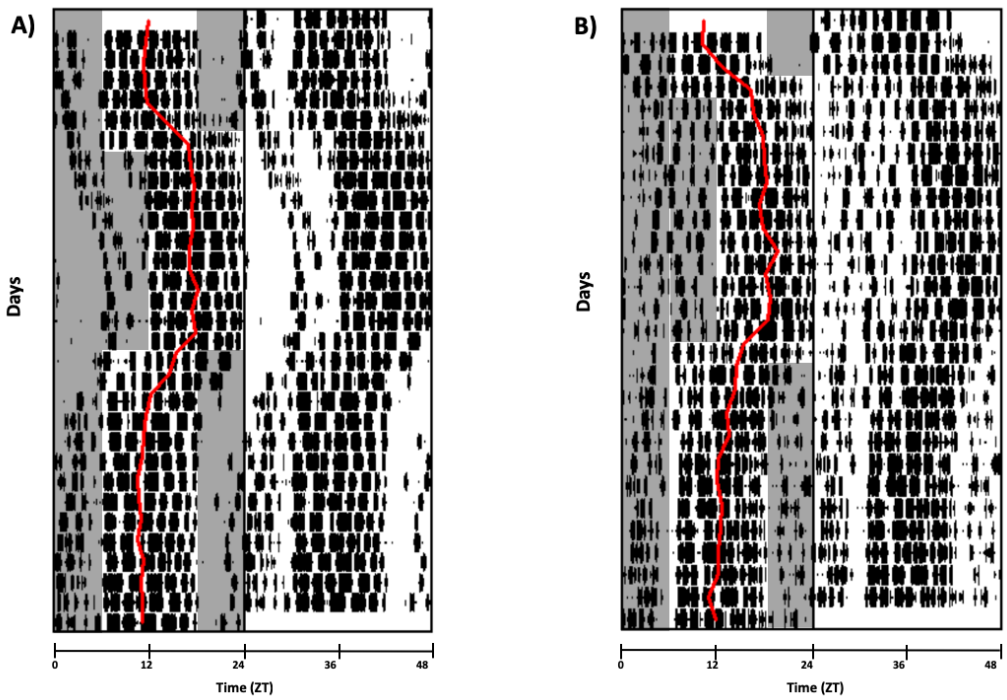

Figure 3. Re-entrainment of WT and DS mice to delay and advance jet lags. **A)** Representative double-plotted actogram of total sleep from a WT control mouse undergoing 30 days of continuous ECoG/EMG recording. Sleep acrophase for each day is overlaid in red on only one side of the actogram. All animals were monitored for 3-5 days under baseline conditions, and then subjected to either delay or advance jet lags. Shaded areas indicate periods of lights off, which are only indicated on the left side of the plots for easy visualization. **B)** Same as **A)** for one DS mouse.

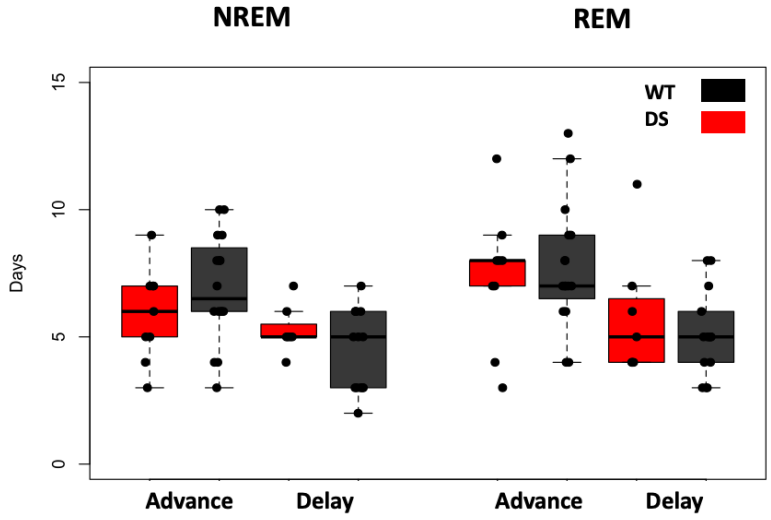

Figure 4. Sleep acrophase takes longer to re-entrain to phase advances than delays, and DS display normal re-entrainment when compared to WT littermates.
Time to re-entrainment is calculated as the number of days necessary for sleep stage acrophase to return to mean baseline levels within a 95% confidence interval. Three-way ANOVA with genotype, sleep stage and jet lag direction as factors reveals a significant effect of jet lag condition ($p < 0.001$, $F_{1,84} = 27.93$), but no difference in re-entrainment time between sleep stages ($p = 0.051$, $F_{1,84} = 3.9$) or between genotypes ($p = 0.96$, $F_{1,84} = 0.003$), and no interactions. n = 14 WT and 7 DS mice for delays, 16 WT and 9 DS mice for advances.

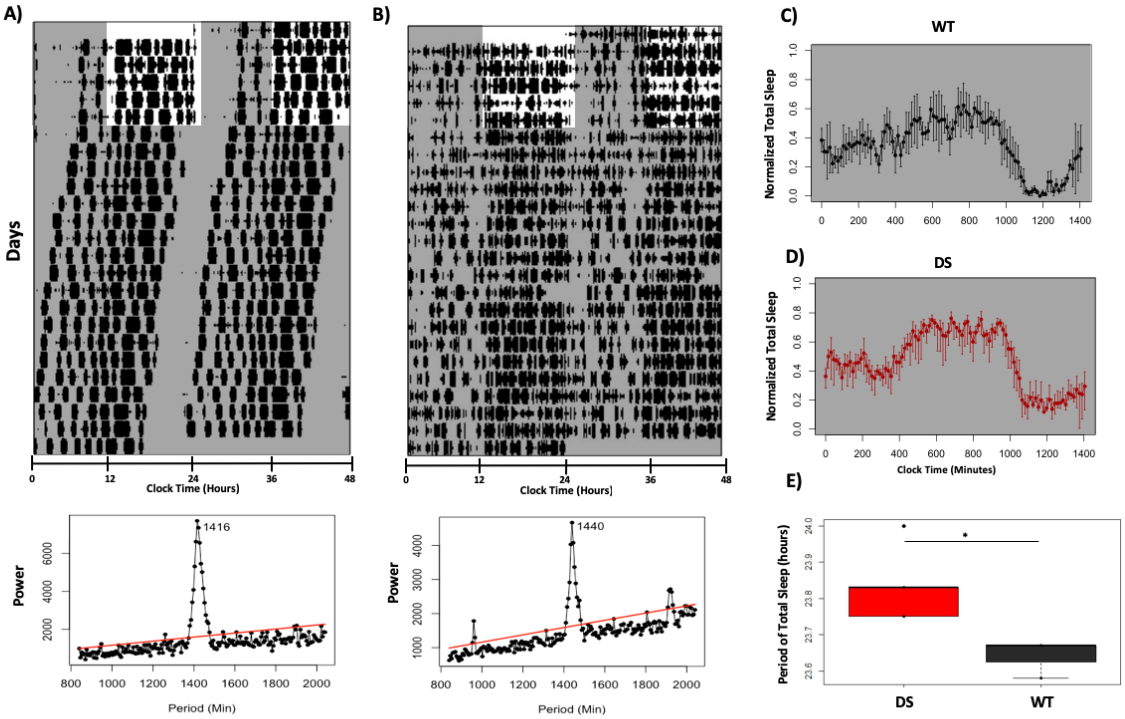

Figure 5. Elongated circadian period of sleep in DS mice under constant conditions. A) Top panel: representative double-plotted actogram of total sleep bouts from a WT mouse. Shaded bars indicate times of lights off. Bottom panel: Sokolov-Bushell periodogram calculated for mouse above revealed an endogenous period of 23.6 hours. Red line indicates threshold of significance for the measured period. WT mice had a mean period of 23.64 hours. **B)** Same as A) for one DS mouse with period of 24 hours. Mean period for DS mice was 23.87 hours. **C)** Mean waveform of sleep bouts under constant darkness for WT mice. **D)** Same as C) for DS mice. **E)** DS mice have a significantly longer period of total sleep in constant darkness than WT mice (two-tailed Student t-test, $p = 0.01$. $n = 3$ WT mice, 5 DS mice).

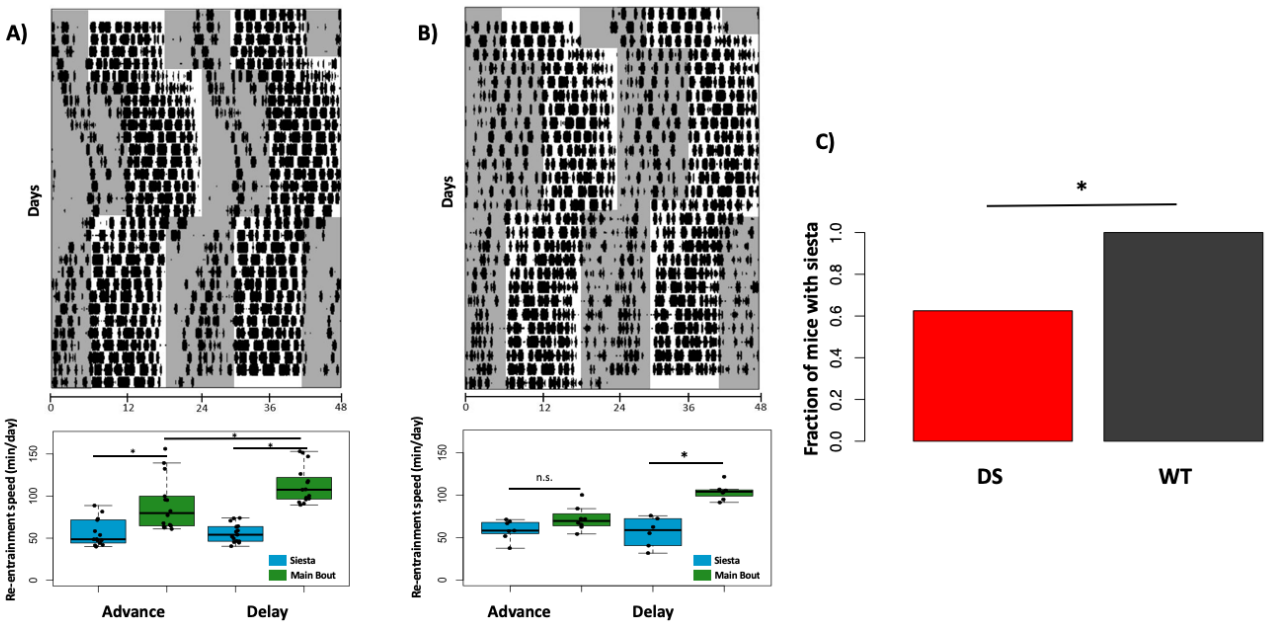

Figure 6. Re-entrainment dynamics of primary sleep bout and siesta. A) Top panel: Representative actogram of total sleep from WT mouse used for siesta scoring. Bottom panel: Re-entrainment speed (minutes/day) of the primary sleep bout and siesta, a daytime bout of sleep under control of the circadian clock, was calculated by extracting the slope of a line fitted to sleep offset for delays and onset for advances by a manual scorer blind to experimental conditions. In WT mice, re-entrainment of siesta is slower than the primary sleep bout (2-way ANOVA, effect of sleep bout ($p < 0.001$) and interaction with jet lag condition ($p = 0.049$), n = 14 mice for delays, 16 for advances). **B)** Same as A), for DS mouse. Tukey post-hoc comparisons revealed a significant difference in re-entrainment time between main bout and siesta following delay ($p < 0.05$) but not advance jet lags ($p = 0.39$). **C)** DS mice are less likely to have a consolidated siesta than WT controls (Chi-Squared test, $\chi^2(1) = 4.768$, $p = 0.02$).

References

1. Bazil, C.W. (2003). Epilepsy and sleep disturbance. Epilepsy Behav. 4(Suppl 2):S39–45
2. Steriade, M. (2005). Sleep, epilepsy and thalamic inhibitory reticular neurons. Trends Neurosci, 2005 Jun;28(6):317-24
3. Malow, B. (2004) Sleep deprivation and epilepsy. Epilepsy Curr, 2004 Sep; 4(5): 193-195
4. Shouse, M., da Silva, A., Sammaritano, M. (1996) Circadian rhythm, sleep and epilepsy. J Clin Neurophysiol 1996 Jan; 13(1): 32-50
5. Hofstra, W., de Weerd, A. (2009). The circadian rhythm and its interaction with human epilepsy: a review of literature. Sleep Med Rev, 2009 Dec; 13(6): 413-20
6. Cho, C. (2012). Molecular mechanism of circadian rhythmicity of seizures in temporal lobe epilepsy. Front Cell Neurosci 2012 Nov 23; 6:55
7. Mirzoev, A., Bercovici, E., Stewart, L., Cortez, M., Snead, O., Desrocher, M. (2012) Circadian profiles of epileptic seizures: a need for reappraisal. Seizure, 2012 Jul; 21(6):412-6
8. Sanchez-Fernandez, I., Ramgopal, S., Powell, C., et al. (2013). Clinical evolution of seizures: distribution across time of day and sleep/wakefulness cycle. J Neurol, 2013 Feb; 260(2): 549-57
9. Karoly, P., Ung, H., Grayden, D., Kuhlmann, L., Leyde, K., Cook, M., Freestone, D. (2017). The circadian profile of epilepsy improves seizure forecasting. Brain, 2017 Aug 1; 140(8): 2169-2182
10. Dravet, C., Bureau, M., Oguni, H., Fukuyama, Y., Cokar, O. (2005). Severe myoclonic epilepsy in infancy: Dravet syndrome. Adv Neurol. 2005; 95:71–102.
11. Dravet, C. (2011) The core Dravet syndrome phenotype. Epilepsia. 2011 Apr;5 2 Suppl 2:3-9.
12. Licheni, S., McMahon, J., Schneider, A., Davey, M., Scheffer, I. (2018) Sleep problems in Dravet syndrome: a modifiable comorbidity. Dev Med Child Neurol. 2018 Feb; 60(2): 192-198
13. Schoonjans, A., De Keersmaecker, S., Van Bouwel, M., Ceulemams, B. (2018). More daytime sleepiness and worse quality of sleep in patients with Dravet Syndrome compared to other epilepsy patients. Eur J Paediatr Neurol. 2018 Sep 27. Pii: S1090-3798(18)30012-6
14. Nolan, K., Camfield, C., Camfield, P. (2008). Coping with a child with Dravet syndrome: insights from families. J Child Neurol. 2008; 23:690–4
15. Villas, N., Meskis, M., Goodliffe, S. (2017). Dravet syndrome: Characteristics, comorbidities, and caregiver concerns. Epilepsy Behav. 2017 Sep; 74:81-86.
16. Losito, E., Kuchenbuch, M., Chemaly, N., Laschet, J., Chiron, C., Kaminska, A., Nabbout, R. (2017). Age-related "Sleep/nocturnal" tonic and tonic clonic seizure clusters are underdiagnosed in patients with Dravet Syndrome. Epilepsy Behav. 2017 Sep; 74:33-40
17. Claes, L., Del-Favero, J., Ceulemans, B., Lagae, L., Van Broeckhoven, C., De Jonghe, P. (2001). De novo mutations in the sodium-channel gene SCN1A cause severe myoclonic epilepsy of infancy. Am J Hum Genet. 2001; 68:1327–1332.
18. Catterall, W., Kalume, F., Oakley, J. (2010) $Na_V1.1$ channels and epilepsy. J Physiol. 2010; 588:1849–59.

19. Yu, F., Mantegazza, M., Westenbroek, R., et al. (2006). Reduced sodium current in GABAergic interneurons in a mouse model of severe myoclonic epilepsy in infancy. Nat Neurosci. 2006; 9:1142–1149.
20. Ogiwara, I., Miyamoto, H., Morita, N., et al. (2007). $Na_V1.1$ localizes to axons of parvalbumin-positive inhibitory interneurons: a circuit basis for epileptic seizures in mice carrying an Scn1a gene mutation. J Neurosci 2007 May 30; 27(22):5903-14
21. Oakley, J., Kalume, F., Yu, F., Scheuer, T., Catterall, W. (2009). Temperature- and age-dependent seizures in a mouse model of severe myoclonic epilepsy in infancy. Proc Nat Acad Sci U S A. 2009; 106:3994–9
22. Kalume, F., Yu, F., Westenbroek, R., Scheuer, T., Catterall, W. (2007). Reduced sodium current in Purkinje neurons from $Na_V1.1$ mutant mice: implications for ataxia in severe myoclonic epilepsy in infancy. J Neurosci. 2007; 27:11065–74.
23. Han, S., Tai, C., Westenbroek, R., et al. (2012a). Autistic-like behaviour in *Scn1a*$^{+/-}$ mice and rescue by enhanced GABA-mediated neurotransmission. Nature. 2012a; 489:385–90.
24. Tatsukawa, T., Ogiwara, I., Mazaki, E., Shimohata, A., Yamakawa, K. (2018). Impairments in social novelty recognition and spatial memory in mice with conditional deletion of Scn1a in parvalbumin-expressing cells. Neurobiol Dis. 2018 Apr; 112:24-34
25. Kalume, F., Westenbroek, R., Cheah, C., Oakley, J., Scheuer, T., Catterall, W. (2013). Sudden unexpected death in a mouse model of Dravet syndrome. J Clin Invest. 2013 Apr 1; 123(4): 1798-1808
26. Han, S., Yu, F., Schwartz, M., et al. (2012b). $Na_V1.1$ channels are critical for intercellular communication in the suprachiasmatic nucleus and for normal circadian rhythms. Proc Nat Acad Sci U S A 2012b; 109: E368–77.
27. Papale, L., Makinson, C., Christopher Ehlen, J., Tufik, S., Decker, M., Paul, K., Escayg, A. (2013). Altered sleep regulation in a mouse model of SCN1A-derived genetic epilepsy with febrile seizures plus (GEFS+) Epilepsia. 2013; 54:625–34
28. Kalume, F., Oakley, J., Westenbroek, R., Gile, J., de la Iglesia, H., Scheuer, T., Catterall, W. (2015). Sleep impairment and reduced interneuron excitability in a mouse model of Dravet syndrome. Neurobiol Dis. 2015 May; 77: 141-154
29. Cheah, C.S., Yu, F.H., Westenbroek, R.E., et al. (2012). Specific deletion of $Na_V1.1$ sodium channels in inhibitory interneurons causes seizures and premature death in a mouse model of Dravet syndrome. Proc Nat Acad Sci U S A. 2012 Sep 4; 109(36):14646-51
30. Catterall, W.A. (2018). Dravet Syndrome: A Sodium Channel Interneuropathy. Curr Opin Physiol. 2018 Apr; 2:42-50
31. Borbely, A., Achermann, P. (1999) Sleep homeostasis and models of sleep regulation. J Biol Rhythms. 1999 Dec; 14(6): 557-68
32. Luppi, P., Peyron, C., Fort, P. (2016) Not a single but multiple populations of GABAergic neurons control sleep. Sleep Med Rev. 2017 Apr; 32: 85-94
33. Scammell, T., Arrigoni, E., Lipton, J. (2017) Neural circuitry of wakefulness and sleep. Neuron. 2017 Feb 22; 93(4): 747-765
34. Mistlberger, R. (2005) Circadian regulation of sleep in mammals: role of the suprachiasmatic nucleus. Brain Res Rev. 2005 Nov; 49(3): 429-54
35. Hsu, Y., Gile, J., Perez, J., Morton, G., Ben-Hamo, M., Turner, E., de la Iglesia, H. (2017). The dorsal medial habenula minimally impacts circadian regulation of locomotor activity and sleep. J Biol Rhythms. 2017 Oct; 32(5): 444-455

36. Cambras, T., Weller, J., Anglés-Pujorás, et al. (2007) Circadian desynchronization of core body temperature and sleep stages in the rat. Proc Nat Acad Sci U S A. 2007 May 1; 104(18): 7634-9
37. Lee, M., Swanson, B., de la Iglesia, H. (2009) Circadian timing of REM sleep is coupled to an oscillator within the dorsomedial suprachiasmatic nucleus. Curr Biol. 2009 May 26; 19(10): 848-52
38. Lee, M., Katsuyama, Â., Duge, L., Sriram, C., Krushelnytskyy, M., Kim, J., de la Iglesia, H. (2016). Fragmentation of rapid eye movement and nonrapid eye movement sleep without total sleep loss impairs hippocampus-dependent fear memory consolidation. Sleep. 2016 Nov 1; 39(11): 2021-31
39. Esteller, R., Echauz, J., Tcheng, T., Litt, B., Pless, B. (2001). Line length: An efficient feature for seizure onset detection. 2001 Proceedings of the 23rd EMBS International Conference, Oct. 25-28, 2001.
40. Sokolove, P., Bushell, W. (1978). The chi square periodogram: its utility for analysis of circadian rhythms. J Theor Biol. 1978 May 8; 72(1): 131-60
41. Sudbrack-Oliveira, P., Lima Najar, L., Foldvary-Schaefer, N., da Mata Gomes, M. (2019). Sleep architecture in adults with epilepsy: a systematic review. Sleep Med. 53 (2019) 22-27
42. Wobbrock, J.O., Findlater, L., Gergle, D., Higgins, J.J. (2011). The Aligned Rank Transform for nonparametric factorial analyses using only ANOVA procedures. Proceedings of the ACM Conference on Human Factors in Computing Systems.Vancouver, British Columbia (May 7-12, 2011). ACM Press, pp. 143-146.
43. Witting, W., Kwa, I.H., Eikelenboom, P., Mirmiran, M., and Swaab, D.F. (1990) Alterations in the Circadian Rest-Activity Rhythm in Aging and Alzheimer's Disease. Biol Psychiatry, 563, 1990; 27:563-572
44. Duhart, J., Brocardo, L., Caldart, C., Marpegan, L., Golombek, D. (2017). Circadian alterations in a murine model of hypothalamic glioma. Front Physiol. 2017 Oct 30; 8:864
45. Tankersley, C., Irizarry, R., Flanders, S., Rabold, R. (2002). Circadian rhythm variation in activity, body temperature, and heart rate between C3H/HeJ and C57BL/6J inbred strains. J Appl Physiol. 2002 Feb; 92(2): 870-7
46. Stowie, A., Glass, J. (2015). Longitudinal study of changes in daily activity rhythms over the lifespan in individual male and female C57BL/6J mice. J Biol Rhythms. 2015; 30:563–568.
47. Ehlen, C. J., Jones, K.A., Pinckney, L., et al. (2015). Maternal Ube3a Loss Disrupts Sleep Homeostasis But Leaves Circadian Rhythmicity Largely Intact. J Neurosci, 7 Oct 2015, 35 (40) 13587-13598
48. Whitney, M.S., Shemery, A.M., Yaw, A.M., Donovan, L.J., Glass, J.D., Deneris, E.S. (2016) Adult Brain Serotonin Deficiency Causes Hyperactivity, Circadian Disruption, and Elimination of Siestas. J Neurosci, 2016 Sep 21; 36 (38) 9828-9842
49. Collins, B., Brown, S. (2018) A Population of VIPergic Clock Neurons in the Suprachiasmatic Nucleus Consolidate Daily Siesta Sleep. Presentation at Society for Research on Biological Rhythms, May 2018, Amelia Island, FL, USA
50. Vitaterna, M., King, D., Chang, A., et al. (1994). Mutagenesis and mapping of a mouse gene, *Clock*, essential for circadian behavior. Science. 1994; 264:719–725
51. André, E., Conquet, F., Stratton, S., Porciatti, V., Becker-André. (1998). Disruption of retinoid-related orphan receptor beta changes circadian behavior, causes retinal

degeneration and leads to vacillans phenotype in mice. EMBO J. 1998 Jul 15; 17(14): 3867-3877
52. Meng, Q., Logunova, L., Maywood, E., et al. (2008). Setting clock speed in mammals: the *CK1ε* tau mutation in mice accelerates the circadian pacemaker by selectively destabilizing PERIOD proteins. Neuron. 2008 Apr 10; 58(1): 78-88
53. Ritter-Makinson, S., Clemente-Perez, A., Higashikubo, B., Cho, F., Holden, S., Bennet, E., et al. (2019). Augmented Reticular Thalamic Bursting and Seizures in *Scn1a*-Dravet Syndrome. Cell Rep. *26*, 54-65, Jan. 2, 2019.
54. Albus H, Vansteensel MJ, Michel S, Block GD, Meijer JH. (2005). A GABAergic mechanism is necessary for coupling dissociable ventral and dorsal regional oscillators within the circadian clock. Curr Biol. 2005; 15:886–893
55. Liu C, Reppert SM. (2000). GABA synchronizes clock cells within the suprachiasmatic circadian clock. Neuron. 2000; 25:123–128.
56. Welsh DK, Takahashi JS, Kay SA. (2010). Suprachiasmatic nucleus: Cell autonomy and network properties. Annu Rev Physiol. 2010; 72:551–577.
57. Albers, H., Walton, J., Gamble, K., McNeill, J., Hummer, D. (2017). The dynamics of GABA signaling: Revelations from the circadian pacemaker in the suprachiasmatic nucleus. Front Neuroendocrinol. 2017 Jan; 44: 35-82
58. Saper, C., Scammell, T., Lu, J. Hypothalamic regulation of sleep and circadian rhythms. (2005). Nature. 2005 Oct; 437(7063): 1257-63
59. Richardson, G., Moore-Ede, M., Czeisler, C., Dement, W. (1985). Circadian rhythms of sleep and wakefulness in mice: analysis using long-term automated recording of sleep. Am J Physiol 1985 Mar; 248(3 Pt 2): R320-30
60. Brager, A., Ehlen, J., Castanon-Cervantes, O., Natarajan, D., Delisser, P., Davidson, A., Paul, K. (2013). Sleep loss and the inflammatory response in mice under chronic environmental circadian disruption. PLoS One. 2013 May 17; 8(5): e63752
61. Hasan, S., Foster, R., Vyazovskiy, V., Peirson, S. (2018). Effects of circadian misalignment on sleep in mice. Sci Rep. 2018 Oct 26; 8(1): 15343.
62. Casiraghi, L., Alzamendi, A., Giovambattista, A., Chiesa, J., Golombek, D. (2016). Effects of chronic forced circadian desynchronization on body weight and metabolism in male mice. Physiol Rep. 2016 Apr; 4(8): e12743
63. Pallier, P.N., Maywood, E.S., Zheng, Z., et al. (2007). Pharmacological imposition of sleep slows cognitive decline and reverses dysregulation of circadian gene expression in a transgenic mouse model of Huntington's disease. J Neurosci. 2007. 27(29): p. 7869-78.
64. Pallier, P.N. and Morton, A.J. (2009). Management of sleep/wake cycles improves cognitive function in a transgenic mouse model of Huntington's disease. Brain Res, 2009. 1279: p. 90-8.
65. Haynes, P.L., Gengler, D., Kelly, M. (2016). Social Rhythm Therapies for Mood Disorders: An Update. Curr Psychiatry Rep, 2016; 18:75
66. Landgrave-Gómez, J., Mercado-Gómez, O., Vázquez-García, M., et al. (2016). Anticonvulsant effect of time-restricted feeding in a pilocarpine-induced seizure model: metabolic and epigenetic implications. Front Cell Neurosci. 2016 Jan 28; 10:7.

Chapter 2

The role of $Na_V1.1$ sodium channel expression in the SCN in circadian behavior and sleep

Abstract

Dravet syndrome (DS) is a severe form of childhood onset epilepsy accompanied by comorbidities including cognitive deficits and sleep disturbances. DS is caused by loss-of-function mutations in the *Scn1a* gene, coding for the pore-forming alpha subunit of the $Na_V1.1$ sodium channel, found primarily on GABAergic neurons in the brain. Previous work has shown that a mouse model of DS with a heterozygous deletion of *Scn1a* display impairments in the circadian regulation of sleep and behavior, and we hypothesized that these deficits may be result from the reduction of $Na_V1.1$ expression specifically in the suprachiasmatic nucleus (SCN), the master circadian clock located in the hypothalamus. We test predictions of this hypothesis using three complementary approaches. First, we directly assessed the role of SCN GABAergic neurotransmission in the circadian regulation of sleep by conditionally deleting the vesicular GABA transporter (VGAT) from SCN NMS neurons in mice and found that these mice lack circadian rhythmicity of sleep. Next, we evaluated behavioral circadian rhythms in mice with a conditional knockout of the *Scn1a* gene in Neuromedin-S (NMS) neurons of the SCN and find none of the circadian deficits observed in DS mice. Finally, we use an adeno-associated viral (AAV) targeting approach to attempt to delete the *Scn1a* gene in the entirety of the SCN. We report that conditional deletion of the *Scn1a* gene from the SCN is associated with an elongated circadian period of WRA but not sleep. Our results support the idea that both loss of GABAergic neurotransmission and reduction in functional $Na_V1.1$ sodium channel expression in the SCN contributes to circadian and sleep-related disturbances in DS, although several avenues of further inquiry are proposed to further test our central hypothesis.

Introduction

Dravet syndrome (DS) is a severe form of childhood epilepsy characterized by spontaneous and febrile seizures and a high mortality rate[1]. These seizures typically manifest within the first year of life, and as the disease progresses patients develop further co-morbidities including autism-like behaviors, ataxia, psychomotor regression and severe sleep disturbances[2]. While treatment of DS patients tends to focus on ameliorating the primary seizure symptoms, there is increasing attention being paid to the importance of addressing these secondary symptoms to improve patient outcomes and quality of life[3].

DS is caused by loss-of-function mutations in one allele of the *SCN1A* gene, which codes for the pore-forming alpha subunit of the $Na_V1.1$ sodium channel[4]. $Na_V1.1$ is primarily expressed in GABAergic interneurons, and previous work in a mouse model of DS, in which the *Scn1a* gene is heterozygously deleted, has shown that the mutation causes a selective reduction in the excitability of inhibitory interneurons[5]. Several characterizations of the behavior and physiology of DS mice have revealed that, like human patients, they display ataxia[6], autism-like cognitive and social deficits[7,8], sudden unexpected death in epilepsy (SUDEP)[9] and sleep disturbances[10–14] in addition to epilepsy. It has been hypothesized that loss of GABAergic inhibition caused by *Scn1a* mutations contributes to or directly causes these symptoms in DS[15].

The fact that DS is associated with mutations in a single gene make it an ideal model system in which to isolate and further understand the pathophysiology of specific symptoms using conditional knockout approaches. Indeed, a great deal of progress has already been made on this front using the Cre-Lox system[16]. By restricting *Scn1a* deletion to forebrain GABAergic neurons, researchers have been able to recreate many of the most severe phenotypes of DS, including spontaneous and febrile seizures, cognitive deficits and SUDEP[17,18]. More specific

conditional knockouts of the *Scn1a* gene in local brain regions have linked both seizure generation and cognitive deficits in DS mice to somatostatin- and parvalbumin-expressing cortical interneurons[19] as well as the hippocampus[20].

Although sleep disturbances have a severe impact on quality of life for DS patients and caregivers alike[21,22], the mechanisms underlying these symptoms are less well-understood. Previous work from our lab has shown that DS mice display circadian behavioral impairments including an elongated circadian period of wheel-running activity[10] (WRA) and sleep[12]. This work suggested that these impairments are associated with reduced neuronal network synchrony in the suprachiasmatic nucleus (SCN)[10] which is almost entirely GABAergic, although the role of GABAergic neurotransmission in the SCN in the circadian regulation of behavior and sleep remains controversial[23]. Later work showed that DS mice also lack normal homeostatic non-rapid eye movement (NREM) sleep rebound in response to sleep deprivation, as well as fragmented NREM sleep under baseline conditions[11]. This was associated with reduced excitability of GABAergic inhibitory neurons in the thalamic reticular nucleus (TRN), a brain region which contributes to maintaining the slow oscillations characteristic of NREM sleep and the homeostatic sleep response[24,25]. While conditional heterozygous knockout of the *Scn1a* gene in GABAergic forebrain interneurons was sufficient to recreate the deficits in homeostatic sleep regulation seen in DS mice, this was not sufficient to recreate the circadian behavioral deficits, likely because the targeting strategy spares the SCN and surrounding hypothalamic nuclei[11].

Here we test the hypothesis that heterozygous deletion of the *Scn1a* gene and thus reduced GABAergic neurotransmission caused by loss of the $Na_V1.1$ sodium channel in the SCN specifically underlies the circadian behavioral deficits seen in DS mice. We test predictions of this hypothesis using three complementary approaches. First, we directly assessed the role of

GABAergic neurotransmission in the SCN in the circadian regulation of sleep by conditionally deleting the vesicular GABA transporter (VGAT) from Neuromedin-S (NMS)-expressing neurons, which are present with high specificity in the SCN[26], in mice and found that these mice lack intrinsic circadian rhythmicity of sleep. Next, we evaluated behavioral circadian rhythms in mice with a conditional knockout of the *Scn1a* gene in NMS neurons, and find none of the circadian deficits observed in DS mice or NMS-specific *Vgat* KOs. Finally, we use an adeno-associated viral (AAV) targeting approach to delete the *Scn1a* gene in the entirety of the SCN. We report that conditional deletion of the *Scn1a* gene from the SCN is associated with an elongated circadian period of WRA but not sleep. These results highlight the utility of conditional gene knockout approaches both dissecting the phenotypes of DS and the role of GABAergic neurotransmission in the SCN, and further our understanding of the mechanisms underlying sleep disturbances in this debilitating disease.

Methods

Animals and Housing Conditions

All experiments with animals were performed in accordance with animal protocols approved by the Office of Animal Welfare and the Institutional Care and Use Committee at the University of Washington.

To generate mice containing a conditional deletion of the *Vgat* gene in NMS-expressing neurons, we bred *Nms-iCre*$^{+/-}$ mice to *Vgat*$^{fl/fl}$ and *Vgat*$^{fl/+}$ mice obtained from the lab of Charles Allen at Oregon Health Sciences University, and genotyped them as previously described[26,27]. NMS is expressed in ~30-40% of SCN neurons and overlaps with the majority of both vasoactive intestinal polypeptide (VIP) and arginine vasopressin (AVP) neurons[26].

Mice containing heterozygous or homozygous floxed copies of the *Scn1a* gene (*Scn1a*$^{fl/+}$ or *Scn1a*$^{fl/fl}$) were generated and genotyped as previously described[11,17]. Mice expressing Cre-recombinase under the *Nms* promoter (*Nms-iCre*$^{+/-}$ mice) were purchased from Jackson Laboratory (Bar Harbor, ME) and genotyped as previously described[26]. Mice containing a conditional heterozygous (*Nms-iCre*$^{+/-}$-*Scn1a*$^{fl/+}$) or homozygous (*Nms-iCre*$^{+/-}$-*Scn1a*$^{fl/fl}$) deletion of the *Scn1a* gene in NMS neurons were generated (Fig. 1) and genotyped using protocols described above.

Viral Injections

AAV viral vectors were purchased from the Salk Institute for Biological Studies in La Jolla, CA. At 60-90 days of age, either *Scn1a*$^{fl/+}$ or *Scn1a*$^{fl/fl}$ mice were bilaterally injected into the SCN with either an active Cre-expressing virus containing green fluorescent protein (AAVDJ-CAG-Cre-GFP) or a virus not containing Cre but expressing GFP under a ubiquitous promoter (AAVDJ-CAG-GFP). Mice with homozygous or heterozygous conditional deletions of *Scn1a* generated using the viral targeting approach are hereafter referred to as *Scn1a*$^{SCN\text{-}KO}$ and *Scn1a*$^{SCN/+}$ mice, respectively.

Before surgery, mice were anesthetized with isoflurane and placed into a stereotaxic device where isoflurane anesthesia continued throughout surgery. First, a midline incision was made in the skin over the skull. SCN injection coordinates were ± 0.25 mm lateral and -0.5 mm posterior to bregma, and -5.75 mm depth. For each injection site, seven instantaneous injections of 69 nl each were made using a Nanoject II (Drummond Scientific, Broomall, PA), and before removing the injection pipette, we allowed 5 minutes for the solution to settle in the tissue after the first 4 injections and again after the final 3. After surgery, mice were housed in single

recording cages under a 12:12 light-dark (LD) cycle and allowed a recovery period of 3 weeks before beginning behavioral experiments.

Electrocorticographic Recordings

Mice were anesthetized with isoflurane and placed into a stereotaxic device where isoflurane anesthesia continued throughout surgery. Each mouse was implanted with ECoG electrodes, consisting of dental screws (Pinnacle Technology, Lawrence, KS; No. 8209: 0.10-in.). A midline incision was made above the skull. Recording electrodes were screwed through cranial holes as follows: over the left frontal cortex (1.5 mm lateral and 2 mm anterior to bregma) and over the right parietal cortex (1.5 mm lateral and 2 mm posterior to bregma), a ground electrode was placed over the visual cortex (1.5 mm lateral and 4.0 mm posterior to bregma), and a reference electrode was placed over the cerebellum (1.5 mm lateral and 6.5 mm posterior to bregma). Electromyogram (EMG) signals were obtained by placing a pair of silver wires into the neck muscles. The screws were connected, through silver wires, to a common 6-pin connector compatible with the Pinnacle recording device. The screws and connector were fixed to the skull with dental cement. Mice were implanted at between 4 and 5 months of age to account for the long duration of circadian sleep experiments. After surgery, mice were housed in single recording cages under a 12:12 LD cycle.

Mice had a recovery period of 1 week and were then fitted with a preamplifier and tether, and connected to the Pinnacle Technology recording system, where they were allowed 1 day to acclimate before recording started. The ECoG and EMG signals were sampled at 400 Hz with low-pass filters of 80 Hz and 100 Hz, respectively.

Sleep Scoring and Processing

Raw ECoG/EMG data were automatically classified in 10-second bouts as either wake, NREM sleep or REM sleep using a previously described custom algorithm implemented in Python v2.7[28]. Briefly, the power spectrums of the ECoG and EMG signals are calculated using Welch's method with an overlap window of 50%. Then, the following features for each 10-second epoch of sleep are calculated: delta power, the sum of ECoG power at frequencies ranging between 0.5 and 4 Hz; theta power, the sum of ECoG power at frequencies ranging between 6 and 12 Hz; and EMG RMS, the mean square root of the raw EMG signal. If EMG RMS was higher than a visually determined threshold for each 24-h recording session, typically set at 0.4 standard deviations above the mean, the epoch was classified as wake, otherwise it was classified as sleep. Next, sleep stage was classified as REM whenever the theta to delta power ratio during the epoch was higher than the average theta to delta ratio—over the whole 24-h recording session—plus 1 standard deviation. The remaining epochs were classified as NREM sleep. This scoring method was based on heuristics for manually scoring sleep in previous studies, and validated by 2 independent experimenters that visually scored 10-second bins as previously described[29,30], with a minimum of 90% score agreement in both cases.

The 10-s scored epochs were further binned into 1-minute bins, for which we calculated the percentage of each sleep state. A 1-minute bin was classified as REM when more than 20% of the bin was spent in REM sleep. If REM sleep was lower than 20% during the bin, it was classified as either wake or NREM sleep, depending on which of the 2 brain states contributed to a higher percentage of the 1-min bin.

During long-term recording, the recording software was restarted every 24 hours to account for potential software or hardware failures, resulting in a loss of approximately 10-30

seconds of recording time each day. To account for this, missing data points were imputed after scoring by taking the mean of the values for delta, theta and sleep stage calls in the 60 seconds following and preceding the gap using a custom R code. This facilitated the combination of sleep scores into larger bins and enhanced the continuity of the recording.

Behavioral Experiments

We evaluated the behavioral circadian period of mice generated using both the viral approach and *Nms-iCre* mouse line using WRA. We released mice into DD for at least 14 days after they had synchronized to a 12:12 LD cycle. Free running period of activity was recorded using ClockLab (Actimetrics, Wilmette, IL) and was assessed using 15-second bins and Sokolove-Bushell periodogram analysis in El Temps and R version 3.1.2 as previously described[31]. For experiments assessing the circadian period of sleep in $Scn1a^{SCN\text{-}KO}$ and *NmsiCreVgat* mice, behavioral experiments were performed similarly, and periodogram analysis was performed using 1-minute bins of sleep scores obtained as described below.

Sleep deprivation experiments in $Nms\text{-}iCre^{+/-}Vgat^{fl/fl}$ mice and controls were performed as previously described[11]. Briefly, mice were kept awake for 5 hours starting 1 hour after lights on by gentle handling and introduction of novel objects. To evaluate homeostatic sleep rebound, average delta power during two 5-hour windows were compared – one commencing at the conclusion of the deprivation period, and one during the same time window on the day before deprivation.

Immunohistochemistry

At the end of each behavioral experiment, mice were sacrificed by cardiac perfusion and brains were harvested for immunohistochemistry. Deletion of VGAT was confirmed in *NmsVgat* mice by labeling VGAT in brain slices 30 μm thick containing the SCN.

First, slices were subject to permeabilization by incubating in a 0.4% phosphate-buffered saline solution with Tween® 20 (Sigma-Aldrich, St. Louis, MO) detergent (PBST) on a shaker for 15 minutes. After washing four times with PBST 0.04%, 2 instantaneous and 2 five minutes each, slices were subject to a blocking step using 5% normal donkey serum and incubated for 1 hour. Next, slices were incubated with an anti-VGAT antibody (mouse host, Santa Cruz Biotechnology, Santa Cruz, CA) at a concentration of 1:200 in PBST 0.04% for 24 hours at 3° C. After being placed on a shaker for 1 hour at room temperature, slices were then incubated in a solution of 1:300 Alexa 594 antibody (host donkey, anti-mouse, Invitrogen, Carlsbad, CA) in PBST 0.04% for 1 hour before being mounted on slides with DAPI Fluoromount mounting medium (Southern Biotech, Birmingham, AL) and imaged using a Nikon e600 widefield fluorescence microscope (Melville, NY).

To confirm the injection site and assess whether expression of the $Na_V1.1$ channel was successfully reduced in $Scn1a^{SCN\text{-}KO}$ and $Scn1a^{SCN/+}$ mice, brain slices 30 μm thick containing the SCN were double-labeled for the $Na_V1.1$ sodium channel and GFP using a sequential protocol. First, slices were subject to a permeabilization step and washes as described above, then incubated in a solution containing an anti-GFP antibody in PBST 0.04% at a concentration of 1:1000 (anti-mouse, DSHB, University of Iowa) for 24 hours. After being placed on a shaker for 1 hour at room temperature, slices were then incubated with an Alexa 488 secondary antibody (host goat, anti-mouse, Invitrogen, Carlsbad, CA) in PBST 0.04% at a concentration of 1:500 for 1 hour, followed by another 24-hour incubation with an anti-$Na_V1.1$ antibody in PBST 0.04% at

a concentration of 1:200 (anti-rabbit, Pacific Immunology Corp., Ramona, CA) for 24 hours. Finally, after being placed on a shaker for 1 hour at room temperature, slices were incubated with an Alexa 568 secondary antibody (host donkey, anti-rabbit, Invitrogen, Carlsbad, CA) for 1 hour. Slices were then mounted to slides with DAPI Fluoromount (Southern Biotech, Birmingham, AL) mounting medium and imaged. For *Nms-iCre*$^{+/-}$-*Scn1a*$^{fl/+}$ and *Nms-iCre*$^{+/-}$-*Scn1a*$^{fl/fl}$ mice, only immunostaining against the $Na_V1.1$ channel was performed.

SCN injections were classified as being a miss, partial hit or complete hit by an experimenter blind to genotype and behavioral results. To be classified as a hit, GFP expression had to be observed in the SCN that did not overlap with the expression of $Na_V1.1$. Mice injected with the control virus were compared to mice in which the $Na_V1.1$ channel was successfully deleted from the SCN.

Images from SCN slices in which the injection was classified as at least a partial hit were then subject to measurements of intensity of $Na_V1.1$ staining using ImageJ (National Institutes of Health, Bethesda, MD). Regions of interest (ROIs) were drawn around the SCN in images with DAPI staining. These SCN ROIs were transposed onto images containing GFP and $Na_V1.1$ staining and intensity was measured. To account for background fluorescence intensity differences between slices, we also measured intensity within the same ROIs moved to another part of the slice not containing the SCN and lacking of $Na_V1.1$ expression. The SCN measurement was divided by this measurement to obtain a background normalized intensity value that was used for analysis.

Data Analysis and Statistics

Before statistical analysis was performed, the Shapiro-Wilk normality test was performed to confirm data were normally distributed. Data are presented as mean ± SEM, and typically analyzed using one- or two-way ANOVA followed by Tukey, or Student's t-tests for comparisons in which type I error was not possible, unless otherwise indicated. Intensity values of $Na_V1.1$ staining in SCN slices that were identified as at least partial hits were correlated with behavioral free-running period using linear regression analysis. Actograms were created and periodogram analysis was performed in ClockLab Analysis (Actimetrics, Wilmette, IL) and El Temps (Antony Diez-Noguera, University of Barcelona). Individual waveforms of sleep under DD conditions were adjusted for circadian period of each mouse before being incorporated into the mean waveform calculations shown in Figure 2, except in cases for which no significant period was detected. All statistical analyses were performed, and plots were created using R version 3.1.2 or GraphPad Prism 6 (GraphPad Software, Inc., La Jolla, CA).

Results

Mice with a conditional deletion of the *Vgat* gene in NMS-expressing SCN neurons display impaired circadian regulation of sleep

We bred *Nms-iCre*$^{+/-}$ and *Vgat*$^{fl/fl}$ mice to generate mice lacking one (*Nms-iCre*$^{+/-}$*Vgat*$^{fl/+}$) or two (*Nms-iCre*$^{+/-}$*Vgat*$^{fl/fl}$) functional copies of VGAT in NMS-expressing neurons (Fig. 1A). We confirmed successful deletion of VGAT in *Nms-iCre*$^{+/-}$*Vgat*$^{fl/fl}$ mice using immunohistochemistry (Fig. 1B and C). As expected, VGAT expression was significantly reduced in the SCN of mice containing a heterozygous or homozygous deletion of the *Vgat* gene (n = 16 *Vgat*$^{+/+}$ and *Vgat*$^{-/-}$ mice, 14 *Vgat*$^{+/-}$ mice. One-way ANOVA with genotype as a factor, F

= 51.8, $p < 0.001$. Tukey's multiple comparisons: Vgat $^{-/-}$ vs. Vgat $^{+/-}$- $p = 0.0006$, Vgat $^{-/-}$ vs. Vgat $^{+/+}$ $p < 0.0001$, Vgat $^{+/-}$ vs. Vgat $^{+/+}$ $p < 0.0001$).

Based on previous work demonstrating that DS mice (which display reduced excitability in GABAergic neurons due to *Scn1a* deletion[10,32]) have an elongated circadian period of behavior and sleep[10,12], as well as observations that SCN GABA serves to stabilize network synchrony and circadian behavior in mice[23,33,34], we predicted that *Nms-iCre*$^{+/-}$*Vgat*$^{fl/fl}$ mice would display reduced amplitude and elongated circadian period of sleep. We recorded polysomnographic sleep in *Nms-iCre*$^{+/-}$*Vgat*$^{fl/fl}$ mice and littermate controls under DD conditions. Because previous work in our laboratory has established that *Nms-iCre*$^{+/-}$*Vgat*$^{fl/+}$mice display normal circadian rhythms of WRA (Ivana Bussi, data not shown), we treated these mice as littermate controls for DD experiments in which our sample size was low. Interestingly, 3 out of 4 *Nms-iCre*$^{+/-}$*Vgat*$^{fl/fl}$ mice we recorded from displayed no circadian rhythmicity (Fig. 2A and 2C) in DD, compared to littermate controls which all displayed a circadian rhythm (n=4, mean period = 23.77 hours). *Nms-iCre*$^{+/-}$*Vgat*$^{fl/fl}$ mice were still able to synchronize to the LD cycle and displayed no significant differences in amplitude of NREM sleep rhythms (n = 8 *Nms*$^{+/-}$*Vgat*$^{fl/fl}$, 9 *Nms*$^{-/-}$, 3 *Nms*$^{+/-}$*Vgat*$^{fl/+}$ mice, Two-way ANOVA, effect of time [$F_{23,1196} = 32.59$, $p < 0.001$] but not group [$F_{2,17} = 1.05$, $p = 0.37$], effect of the interaction [$F_{46,1196} = 1.95$, $p = 0.002$]) or REM sleep rhythms (Two-way ANOVA, effect of time [$F_{23,1196} = 29.15$, $p < 0.001$] but not group [$F_{2,17} = 0.31$, $p = 0.75$], no effect of the interaction [$F_{46,1196} = 0.87$, $p = 0.71$]) under baseline conditions (Fig. 3A and 3B).

To confirm that conditional deletion of VGAT in the SCN did not have an effect on homeostatic sleep regulation, we performed sleep deprivation experiments in *Nms-iCre*$^{+/-}$*Vgat*$^{fl/fl}$ mice and compared NREM sleep intensity in a 5-hour period after the deprivation and at the

same time on the previous day (Fig. 3C). As expected, *Nms-iCre*$^{+/-}$*Vgat*$^{fl/fl}$ mice had a typical homeostatic sleep response, displaying a significant increase in NREM sleep intensity post sleep deprivation when compared to baseline conditions (n=8, Two-way repeated measures ANOVA, effect of condition [$F_{1,69} = 133.27$, $p < 0.0001$] and time [$F_{1,69} = 13.56$, $p < 0.001$]). To determine whether there were any differences in the homeostatic sleep response of *Nms-iCre*$^{+/-}$*Vgat*$^{fl/fl}$ mice and controls (including both *Nms-iCre*$^{+/-}$*Vgat*$^{fl+l}$ and *Nms*$^{-/-}$ mice, n=14), we compared NREM sleep intensity during baseline and rebound windows between we groups. We found no significant differences in the magnitude of homeostatic sleep response (data not shown, mixed-model two-way ANOVA, no effect of group [$F_{1,20} = 0.044$, $p = 0.85$], condition [$F_{1,20} = 3.62$, $p = 0.07$] or the interaction [$F_{1,20} = 1.64$, $p = 0.22$]). Thus, we concluded that conditional deletion of VGAT from NMS-expressing SCN neurons had a detrimental effect on circadian, but not homeostatic regulation of sleep.

Mice with a conditional deletion of the *Scn1a* gene in NMS-expressing SCN neurons display normal behavioral circadian rhythms

We bred *Scn1a*$^{fl/+}$ and *Scn1a*$^{fl/fl}$ mice to *Nms-iCre*$^{+/-}$ mice to generate *Nms-iCre*$^{+/-}$-*Scn1a*$^{fl/+}$ and *Nms-iCre*$^{+/-}$-*Scn1a*$^{fl/fl}$ mice, in which one or both copies of the *Scn1a* gene were deleted from NMS-expressing SCN neurons (Fig. 4A). To confirm the effectiveness of the conditional deletion strategy, we performed immunostaining against $Na_V1.1$ and found a reduction in expression for *Nms-iCre*$^{+/-}$-*Scn1a*$^{fl/+}$ and *Nms-iCre*$^{+/-}$-*Scn1a*$^{fl/fl}$ mice, but not littermate controls that did not express Cre-recombinase under the *Nms* promoter (Fig. 4A, quantification not shown).

Next, we assessed circadian period using WRA in *Nms-iCre*$^{+/-}$-*Scn1a*$^{fl/+}$ and *Nms-iCre*$^{+/-}$-*Scn1a*$^{fl/fl}$ mice and littermate controls. Mice were placed in a 12:12 LD cycle to confirm their ability to stably entrain and released into DD for at least 14 days (Fig. 4B), and free-running periods were assessed using chi-squared periodogram analysis. We found no significant differences in free-running period between any of the four groups (n=5 per group, one-way ANOVA with genotype as a factor, $p > 0.05$) (Fig. 4C). All mice assessed had robust circadian wheel running and free-running periods of less than 24 hours, in contrast to our previous work demonstrating that DS mice have free-running periods of greater than 24 hours[10] (Fig. 4C).

Conditional deletion of the *Scn1a* gene using viral targeting approaches

Although the *Nms-iCre* driver mouse targets nearly all of the VIP and AVP neurons in the SCN, which are critical for maintaining SCN network synchrony, this targeting strategy spares nearly 60% of SCN neurons[26], including non-oscillating gastrin-releasing peptide (GRP) neurons that are also thought to play an important role in SCN timekeeping[35,36]. Therefore, we sought to delete or reduce expression of $Na_V1.1$ in the entirety of the SCN using Cre-recombinase-expressing AAV vectors (Fig. 5A, top panel) to produce *Scn1a*$^{SCN\text{-}KO}$ mice. We predicted that these mice would have a longer circadian period of WRA and sleep relative to mice injected with a control virus lacking Cre-recombinase.

To confirm successful deletion of the channel, we performed immunohistochemical staining against both GFP and $Na_V1.1$ and analyzed behavioral data only from mice in which we could confirm at least partial deletion of the channel (Fig. 5B). For control virus injected animals (*Scn1a*^{CTRL}), mice in which GFP expression was confirmed in at least part of the SCN were included in the analysis (Fig. 5C). For experiments evaluating circadian period of WRA (Fig.

5A, bottom panel), we included 6 *Scn1a*$^{SCN\text{-}KO}$ mice and 3 *Scn1a*^{CTRL} mice in the analysis. None of the *Scn1a*$^{fl/+}$ mice injected with the Cre-expressing virus displayed successful targeting of the SCN using our criteria.

Circadian period of WRA is not significantly different between *Scn1a*$^{SCN\text{-}KO}$ and *Scn1a*^{CTRL} mice, but circadian period of WRA is negatively correlated with the extent of Na$_V$1.1 sodium channel deletion from the SCN

We first recorded WRA under baseline 12:12 LD conditions for at least 7-10 days to confirm that both groups of mice could synchronize their activity to the LD cycle (Fig. 6A and 6B). We then released mice into DD conditions for at least 21 days and calculated circadian period using Sokolove-Bushell periodograms. We found no significant differences in circadian period of WRA between *Scn1a*$^{SCN\text{-}KO}$ and *Scn1a*^{CTRL} mice (Fig. 6C, one-way ANOVA with group as a factor, $F_{1,7} = 0.46$, $p = 0.52$). We performed a logistic regression to determine if background-normalized Na$_V$1.1 fluorescence intensity, a measure for the extent of the deletion of the Na$_V$1.1 channel from the SCN, was a predictor of the circadian period of WRA. Despite the similarities in circadian period between experimental groups, we found a significant inverse correlation between Na$_V$1.1 intensity and circadian period of WRA (Fig. 6D, $R^2 = 0.7$, $p = 0.04$).

Circadian period of sleep is not significantly correlated with the extent of Na$_V$1.1 sodium channel deletion from the SCN

We implanted 5 *Scn1a*$^{SCN\text{-}KO}$ mice with an ECoG/EMG electrode array and recorded sleep continuously under both LD and DD conditions (Supplementary Fig. 1A). For this experiment we were not able to implant any control-virus injected animals for comparison. Thus, we

predicted that there would be a negative correlation between circadian period of sleep and $Na_V1.1$ intensity, as observed for WRA. Although a trend was observed, using logistic regression we found no significant correlation between these two variables (Supplementary Fig. 1B, n = 5 *Scn1a*$^{SCN\text{-}KO}$ mice, $R^2 = 0.5$, $p = 0.18$).

Discussion

Here we test the hypothesis that loss of GABAergic neurotransmission and deletion of the $Na_V1.1$ sodium channel in the SCN specifically underlies the behavioral circadian rhythm disturbances observed in DS. We assessed circadian period in three complementary mouse models containing conditional gene knockouts in the SCN. First, we found that mice containing a conditional deletion of VGAT from NMS-expressing SCN neurons had severely impaired circadian regulation of sleep. In contrast, we found that *Nms-iCre*$^{+/-}$-*Scn1a*$^{fl/+}$ and *Nms-iCre*$^{+/-}$-*Scn1a*$^{fl/fl}$ mice displayed a free-running period of WRA of less than 24 hours, comparable to their littermate controls, despite the fact that our targeting strategy resulted in significant reduction of $Na_V1.1$ sodium channel expression in the SCN of *Nms-iCre*$^{+/-}$-*Scn1a*$^{fl/+}$ and *Nms-iCre*$^{+/-}$-*Scn1a*$^{fl/fl}$ mice. Finally, we used a viral targeting approach to generate *Scn1a*$^{SCN\text{-}KO}$ mice and evaluated free-running period of WRA and polysomnographically recorded sleep. For mice in which the SCN was successfully targeted, we correlated the extent of $Na_V1.1$ expression with circadian period and found a significant negative correlation between $Na_V1.1$ expression and circadian period of WRA, but not sleep. Although we cannot definitively say that deletion of the $Na_V1.1$ sodium channel from the SCN is sufficient to recreate the circadian behavioral deficits observed in DS, our correlational analyses based on a small number of animals suggest that this deletion at least contributes to the elongated circadian period of sleep and behavior. Future work aims to

replicate these experiments using viral targeting approaches in order to further assess the validity of these preliminary observations.

Of particular note is our finding that *Nms-iCre*$^{+/-}$*Vgat*$^{fl/fl}$ mice displayed no circadian rhythmicity of sleep under constant conditions, despite being able to synchronize to a 12:12 LD cycle and having a normal homeostatic sleep response. This is especially interesting considering that loss of circadian rhythmicity is typically associated only with deletion of or mutations in core circadian clock genes[26,37,38]. Although the SCN is nearly entirely GABAergic, GABA's precise role in the SCN remains an area of great debate[23]. Seemingly contradictory hypotheses have been put forth that GABA alternately serves to synchronize[39,40] and destabilize[41,42] both gene expression and neuronal activity oscillations in the SCN, and it is well documented that GABA displays both inhibitory and excitatory actions in the SCN[43]. Few studies have directly assessed the role of SCN GABA in the circadian regulation of behavior, and those that have typically utilize pharmacological approaches with potential off-target effects and have produced contradictory results[23,42]. Indeed, to the best of our knowledge, the only other study to employ conditional gene deletion to study the role of SCN GABA in circadian behavior utilized Cre-expressing AAVs to delete VGAT from the SCN of adult mice[33]. In contrast to our results from *Nms-iCre*$^{+/-}$*Vgat*$^{fl/fl}$ mice, the authors found that deleting VGAT from the SCN in mice during adulthood resulted in reduced amplitude of circadian rhythms of WRA but not loss of circadian rhythmicity under constant conditions, leading them to conclude that SCN GABA is necessary only to refine circadian behavioral output[33]. Because our *Nms-iCre*$^{+/-}$*Vgat*$^{fl/fl}$ mice lack VGAT in the SCN from development, we hypothesize that VGAT, and thus GABAergic neurotransmission, is necessary for proper development and function of the SCN in mice, as has been proposed in other contexts in the nervous system[44,45]. Ongoing work in our laboratory is

testing predictions of this hypothesis, as well as further characterizing cellular and molecular changes in the SCN of *Nms-iCre*$^{+/-}$*Vgat*$^{fl/fl}$ mice.

In addition to the low sample size in the experiments involving the AAV-mediated deletion of *Scn1a* from the SCN, we propose several potential explanations for results in conditional *Scn1a* deletion models that contradict our central hypothesis. Given the documented importance of NMS-expressing SCN neurons in maintaining both tissue-level and behavioral circadian rhythmicity, the observation that *Nms-iCre*$^{+/-}$-*Scn1a*$^{fl/fl}$ mice displayed normal circadian rhythms was surprising. Previous work characterizing the *Nms*-iCre mouse found that both deleting circadian clock genes from and disrupting synaptic transmission in NMS-expressing neurons was sufficient to abolish behavioral and tissue-level circadian rhythms[26]. Similarly, our finding that deletion of the vesicular GABA transporter VGAT from NMS-expressing neurons was sufficient to abolish circadian rhythmicity of WRA (Ivana Bussi, data not shown) and sleep (Fig. 2) under constant conditions further highlights the importance of NMS SCN neurons in circadian timekeeping. Successful use of the *Nms-iCre* mouse in other contexts within our lab, as well as confirmed reduction of $Na_V1.1$ sodium channel expression shown in Figure 4A, discount the possibility of documented pitfalls of the Cre-Lox system affecting our results[46]. This raises two possibilities in the context of the results presented here: first, that targeting strategies utilizing NMS-expressing neurons spares a sufficient subpopulation of SCN neurons to allow the clock to retain its typical timekeeping abilities, a possibility we evaluated using the viral targeting approach; and second, that the contribution of the $Na_V1.1$ sodium channel to SCN neuronal excitability, and thus circadian timekeeping, is somehow being compensated for during development.

Although $Na_V1.1$ is heavily expressed in GABAergic interneurons throughout the brain, it is hypothesized that in mice the dominant sodium channel found on inhibitory neurons is $Na_V1.3$, and that $Na_V1.1$ only becomes more prominent after postnatal day 14[15]. Indeed, it is well-documented that sodium channel composition in the brain changes throughout the lifespan[47]. Yu & colleagues found that $Na_V1.3$ sodium channel expression was upregulated in the hippocampus of mice containing heterozygous and homozygous global deletions of the *Scn1a* gene[5], suggesting a mechanism by which some of the neuronal excitability lost with the deletion of $Na_V1.1$ may be compensated for. We propose that a similar mechanism may occur in the SCN and underlies the behavioral phenotypes displayed by *Nms-iCre*$^{+/-}$-*Scn1a*$^{fl/fl}$ mice, in which the *Scn1a* gene is absent in the SCN of mice from development. Ongoing work in our lab is testing predictions of this hypothesis by evaluating expression of several voltage-gated sodium channels within the SCN at different developmental timepoints. Previous work has documented the importance of the sodium channels $Na_V1.8$ and $Na_V1.9$ to neuronal excitability within the SCN[48–50], and preliminary qPCR experiments from our lab indicate that $Na_V1.3$ may be more highly expressed in the wild-type adult SCN than $Na_V1.1$, highlighting the value of further probing the contributions of different voltage-gated sodium channels to SCN timekeeping.

Another potential explanation for results contradicting our central hypothesis is that $Na_V1.1$ sodium channel deletion from outputs of the SCN master clock contribute to circadian and sleep disturbances observed in DS. The SCN sends direct and indirect projections to several brain regions involved in the circadian timing of sleep and locomotor activity, many of which are GABAergic[51–53]. Especially important are direct and indirect projections from the SCN to the ventrolateral preoptic area, a GABAergic nucleus critical to the initiation of sleep[54]. Additionally, several GABA-expressing brain regions involved in sleep display circadian

oscillations in neuronal activity and/or clock genes, including the hippocampus[55–57], the nucleus accumbens[58] and the arcuate nucleus of the hypothalamus[59,60]. Although the circadian period of behavior is usually attributed to the SCN master clock only, the possibility remains that sleep and circadian rhythm disturbances in DS result from synergistic effects of $Na_V1.1$ deletion from the SCN and other sleep-related brain areas. This would help to explain our results observed using both the *Nms-iCre* and viral targeting approaches to conditionally knock out the *Scn1a* gene. Further dissection of sleep-related phenotypes of DS using conditional gene deletion should explore this possibility by deleting the *Scn1a* gene from other GABAergic brain areas involved in the regulation of sleep and circadian behavior.

Due to potential compensatory mechanisms at play in the SCN and its outputs, localizing the underlying pathologies leading to circadian and sleep-related DS symptoms using conditional gene deletion approaches may continue to prove difficult. An alternative and complementary approach to these experiments would include targeted genetic rescue experiments in mice with a global deletion of *Scn1a*. Recent work has demonstrated CRISPR/dCas9-mediated *Scn1a* gene activation in GABAergic interneurons alone improved seizures and cognitive deficits in mice with *Scn1a* gene haploinsufficiency[61,62]. Future work should employ these approaches in *Scn1a* gene rescue experiments targeted to the SCN and other sleep-relevant brain regions to continue to disentangle the nature of sleep-related comorbidities of DS. Such experiments would have the added benefit of further validating CRISPR/dCas9-based approaches to gene therapy, which may hold promise for future treatments of DS and other neuronal channelopathies[63].

A key set of experiments missing from the results presented here include characterizations of clock gene expression and neuronal excitability in the SCN of mice with conditional deletions of *Scn1a*. Although the molecular circadian clock drives rhythms of

neuronal firing and excitability in the SCN, it is well documented that neuronal activity can in turn affect the expression of core circadian clock genes[64,65]. Previous work from our lab has indicated that SCN slices obtained from DS mice show reduced signal propagation between dorsal and ventral subregions of the SCN as measured by calcium imaging, as well as reduced amplitude in the expression rhythm of the core circadian clock gene *Per1*[10]. Such experiments performed in SCN slices obtained from *Nms-iCre*$^{+/-}$-*Scn1a*$^{fl/fl}$ mice especially could shed light on the behavioral phenotypes reported here. Ongoing work in our lab is evaluating the rhythms of *Per2-Luciferase*[66] in DS mice (Supplementary Figure 2), and future work will employ these approaches in mouse models with conditional deletions of *Scn1a*.

Taken together, the results presented in this chapter further our understanding of the role of both GABAergic neurotransmission and the $Na_V1.1$ sodium channel in the SCN in circadian regulation of behavior and provide insight into how changes in these processes contribute to the circadian and sleep-related symptoms of DS.

Figures

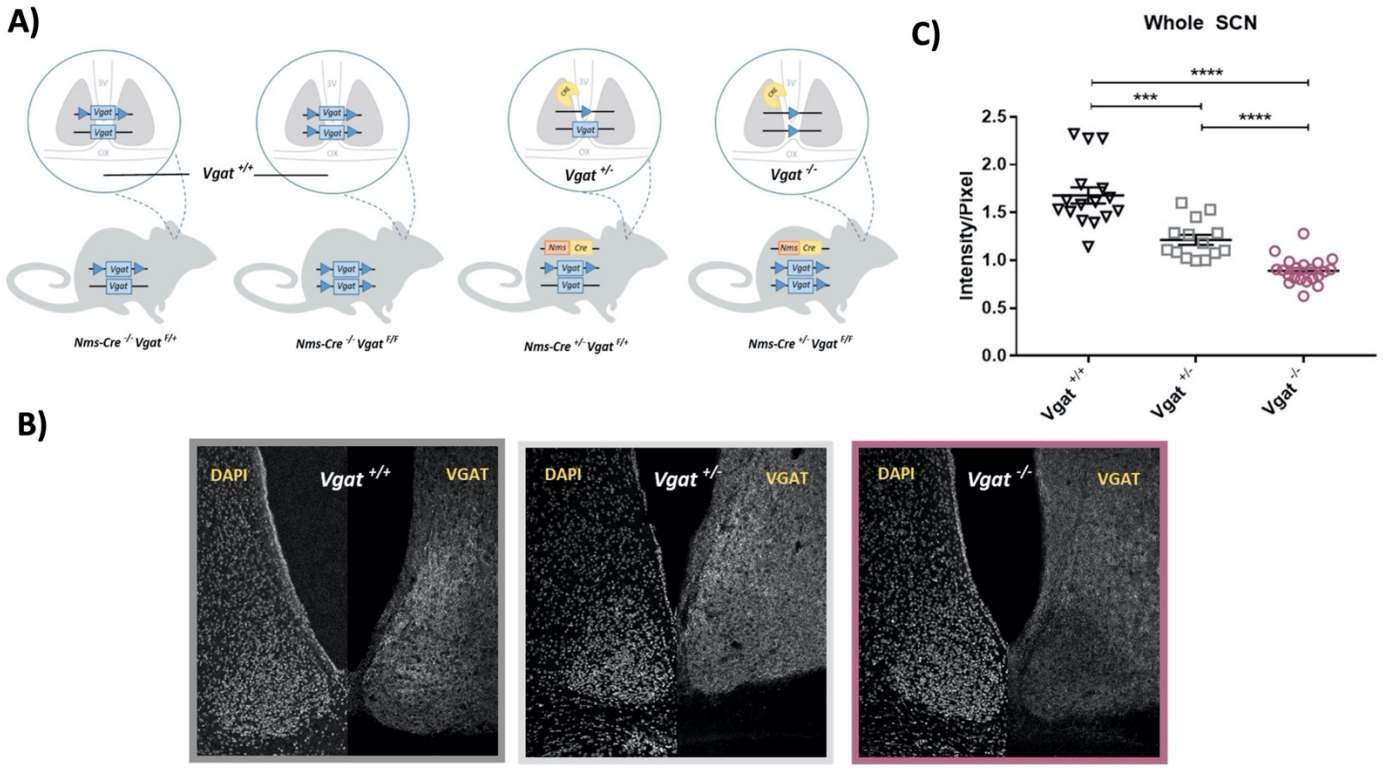

Figure 1. Mice containing a conditional deletion of the vesicular GABA transporter in NMS-expressing SCN neurons synchronize. This figure is adapted with permission from Ivana Bussi. **A)** Breeding scheme for mice containing conditional deletion of VGAT. We bred *Nms-iCre*$^{+/-}$ mice to mice containing one or two "floxed" copies of the vesicular GABA transporter (VGAT) to obtain *NmsiCre*$^{+/-}$*Vgat*$^{fl/fl}$ and *NmsiCre*$^{+/-}$*Vgat*$^{fl/+}$ mice. **B)** Immunohistochemical staining against VGAT in SCN slices obtained from *NmsiCre*$^{-/-}$*Vgat*$^{fl/fl}$ (top), *NmsiCre*$^{+/-}$*Vgat*$^{fl/-}$ (middle), and *NmsiCre*$^{+/-}$*Vgat*$^{fl/fl}$ (bottom) mice confirm successful deletion using this targeting strategy (quantification not shown). **C)** Quantification of immunohistochemical stainings against VGAT in SCN slices. VGAT expression was significantly reduced in the SCN of mice containing a heterozygous or homozygous deletion of the *Vgat* gene. One-way ANOVA with genotype as a factor, $F = 51.8$, $p < 0.001$. Tukey's multiple comparisons: Vgat $^{-/-}$ vs. Vgat $^{+/-}$- $p = 0.0006$, Vgat $^{-/-}$ vs. Vgat $^{+/+}$ $p < 0.0001$, Vgat $^{+/-}$ vs. Vgat $^{+/+}$ $p < 0.0001$.

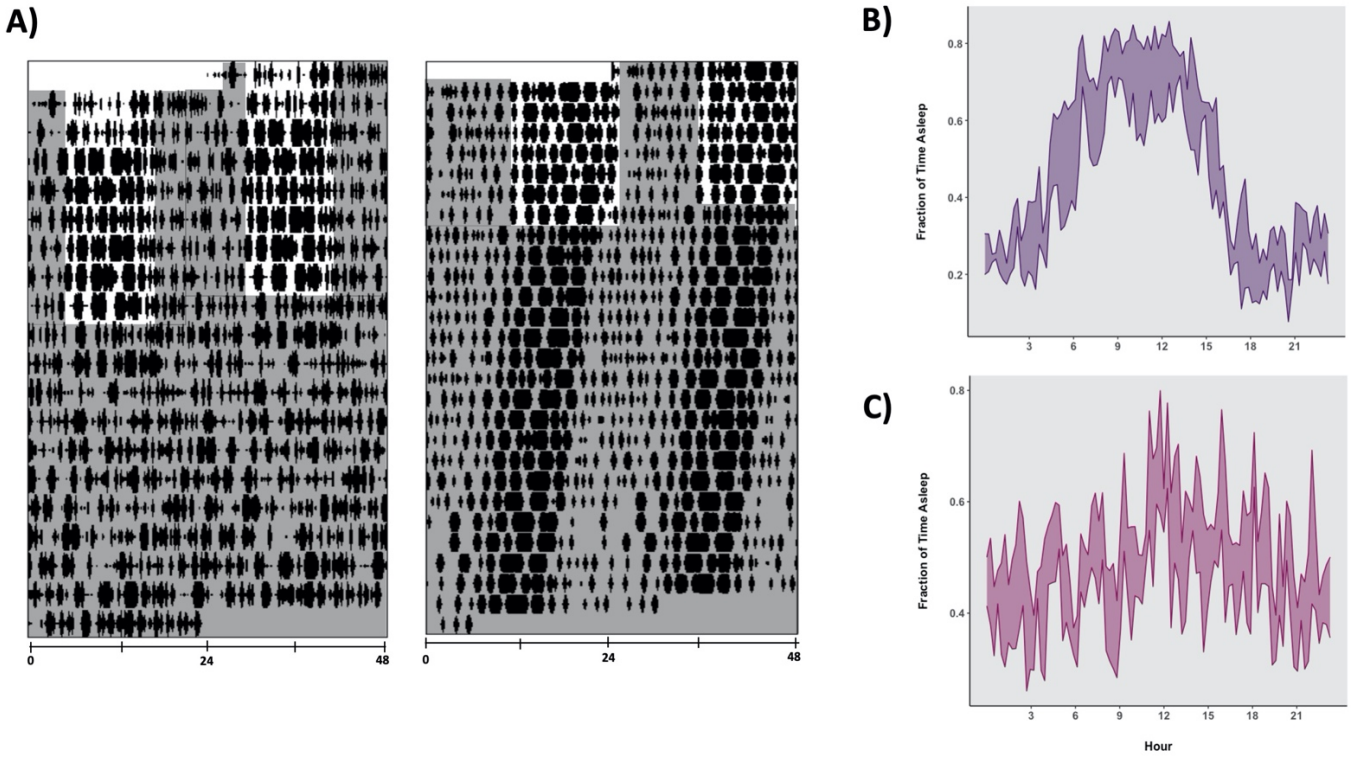

Figure 2. Mice containing a conditional deletion of the vesicular GABA transporter in NMS-expressing SCN neurons display no circadian rhythm of sleep under constant conditions. We evaluated the circadian period of sleep in NmsiCre$^{+/-}$Vgat$^{fl/fl}$ and littermate control mice using polysomnographic recordings. **A)** Left panel: Representative actogram and periodogram of total sleep from a NmsiCre$^{+/-}$Vgat$^{fl/fl}$ mouse. 3 of 4 NmsiCre$^{+/-}$Vgat$^{fl/fl}$ mice recorded from displayed no circadian rhythmicity of sleep under constant conditions. Right panel: Same as A) for a NmsiCre$^{+/-}$Vgat$^{fl/f+}$ mouse. All littermate controls, including mice containing at least one functional copy of the Vgat gene in NMS-expressing SCN neurons retained circadian rhythmicity of sleep under constant conditions (n=4 between all controls, mean sleep period = 23.77 hours). **B)** Mean waveform of time spent asleep in control mice during constant conditions. Individual waveforms are adjusted for circadian period as measured using Sokolove-Bushell periodograms. **C)** Same as B) for NmsiCre$^{+/-}$Vgat$^{fl/fl}$ mice.

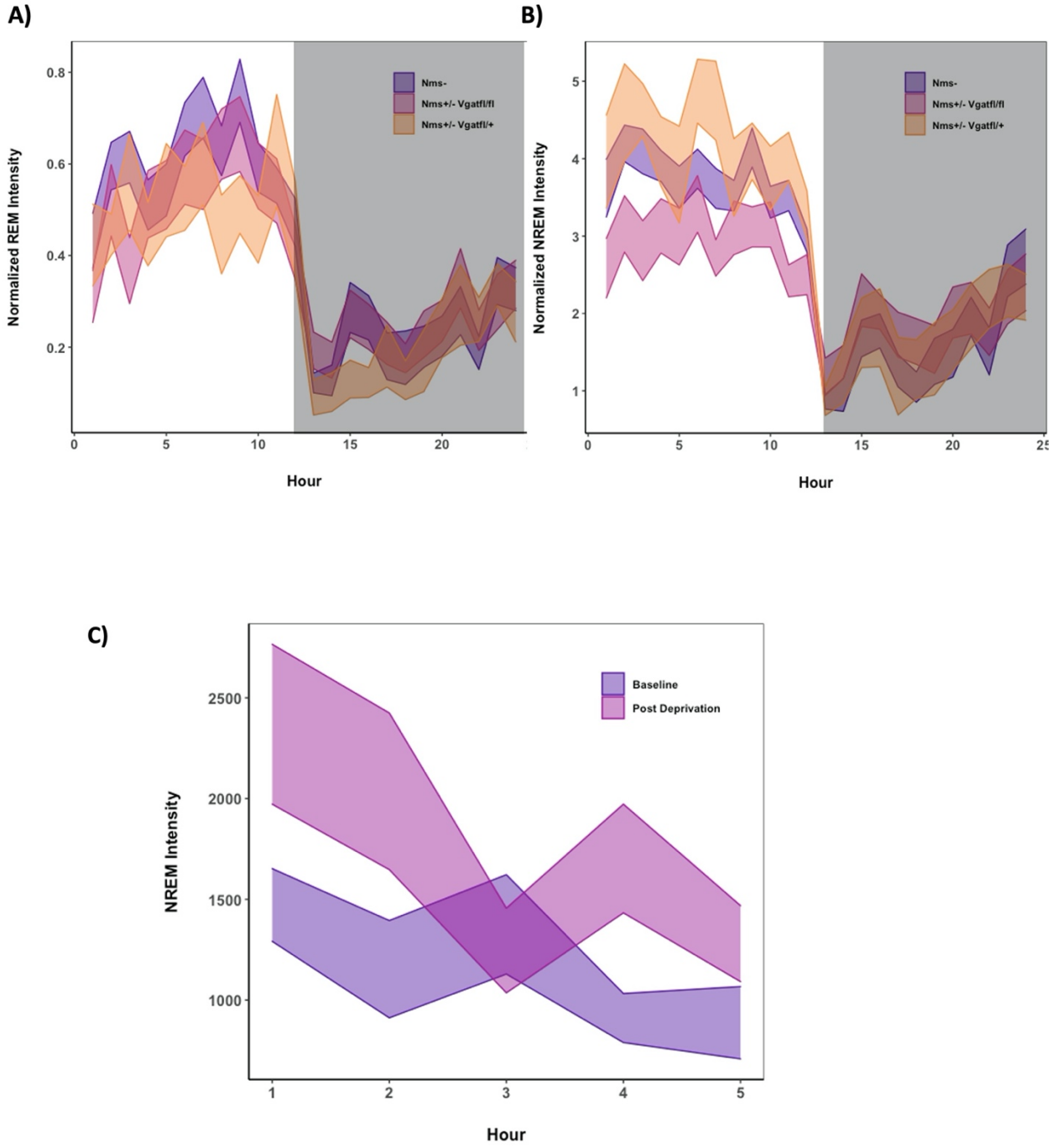

Figure 3. Mice containing a conditional deletion of the vesicular GABA transporter in NMS-expressing SCN neurons synchronize to environmental LD cycles and display normal homeostatic regulation of sleep. A) 24-hour waveforms of NREM sleep intensity under a baseline 12:12 LD cycle. Shaded area indicates period of lights off. There were no significant differences in NREM sleep intensity between groups (n = 8 $Nms^{+/-}Vgat^{fl/fl}$, 9 $Nms^{-/-}$, 3 $Nms^{+/-}Vgat^{fl/+}$). Two-way ANOVA, effect of hour ($F_{23,1196} = 32.59$, $p < 0.001$) but not group ($F_{2,17} = 1.05$, $p = 0.37$). **B)** Same as A) for REM sleep intensity. Two-way ANOVA, effect of hour

($F_{23,1196}$ =29.15, $p < 0.001$) but not group ($F_{2,17} = 0.31$, $p = 0.75$). **C)** Average NREM intensity values during 5 hours of recovery sleep following a 5-hour sleep deprivation period. Relative to baseline sleep recorded at the same ZT during the previous day, $Nms^{+/-}Vgat^{fl/fl}$ mice display a significant increase in NREM sleep intensity post sleep deprivation (n=8). Two-way repeated measures ANOVA, effect of condition ($F_{1,69} = 133.27$, $p < 0.0001$) and hour ($F_{1,69} = 13.56$, $p < 0.001$).

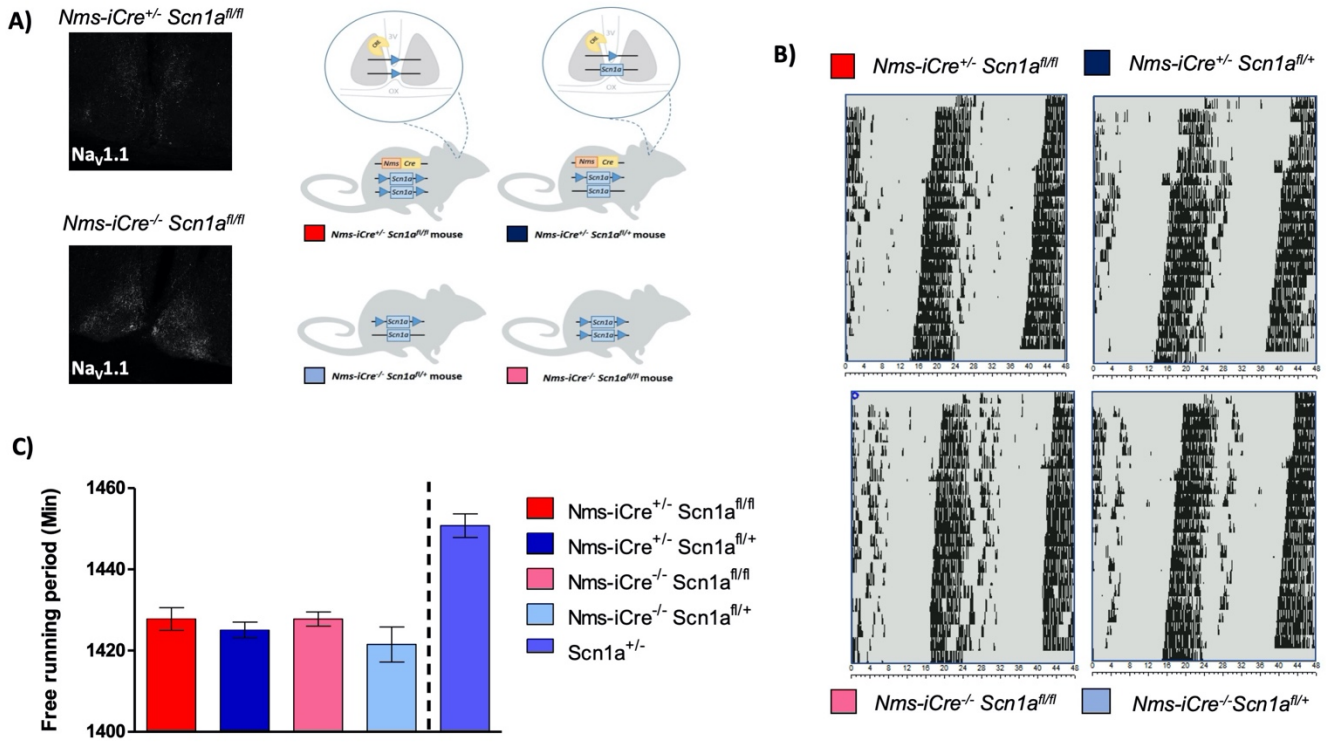

Figure 4. Mice containing a conditional deletion of the Scn1a gene in NMS-expressing SCN neurons display normal behavioral circadian rhythms. This figure is adapted with permission from Ivana Bussi. **A)** Breeding strategy to obtain Nms-iCre$^{+/-}$ / Scn1a$^{fl/fl}$ and Nms-iCre$^{+/-}$ / Scn1a$^{fl/+}$ mice. Relative to littermate controls, both experimental animal groups display a reduction in the expression of $Na_V1.1$. **B)** Representative actograms from all four genotypes released into constant conditions to evaluate the circadian period of wheel running activity (WRA). **C)** There was no significant difference in circadian period of WRA between any of the four groups (one-way ANOVA, genotype as factor, $p > 0.05$, $n = 5$ per group), and none of the mice displayed a circadian period comparable to that of the Scn1a$^{+/-}$ Dravet syndrome mouse model.

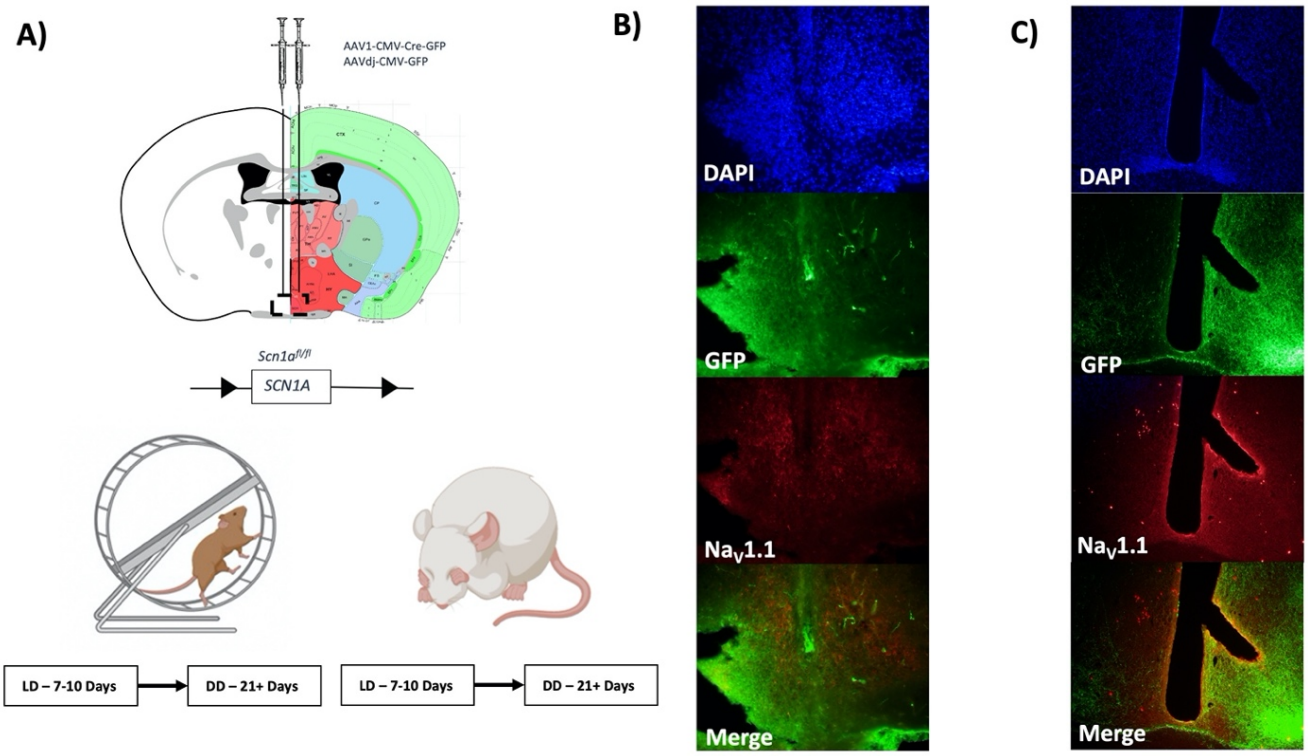

Figure 5. Conditional deletion of the Scn1a gene from the SCN of mice using AAV vectors. **A)** Mice containing two "floxed" copies of the Scn1a gene ($Scn1a^{fl/fl}$) received a bilateral injection of either a Cre-expressing AAV or a control virus lacking Cre-recombinase into the SCN (top panel). After 3 weeks recovery to allow for recombination to occur, mice were evaluated first for circadian period of wheel-running activity and then for circadian period of sleep (bottom panel). **B)** Example SCN slices stained for DAPI, GFP and $Na_V1.1$ proteins from a mouse injected with a Cre-expressing AAV. To be included in the analysis, an experimenter blinded to genotype and behavioral phenotype had to describe coverage of the SCN by the virus as at least partial. In this example, one full SCN and a small section of the other was successfully targeted. There is no overlap between staining against GFP and $Na_V1.1$ suggesting successful deletion of the channel from the neurons in the SCN that the virus was able to penetrate. **C)** Same as B) for a mouse injected with control virus lacking Cre-recombinase. In this example, one side of one SCN was successfully targeted, as the injection site was slightly lateral to both nuclei.

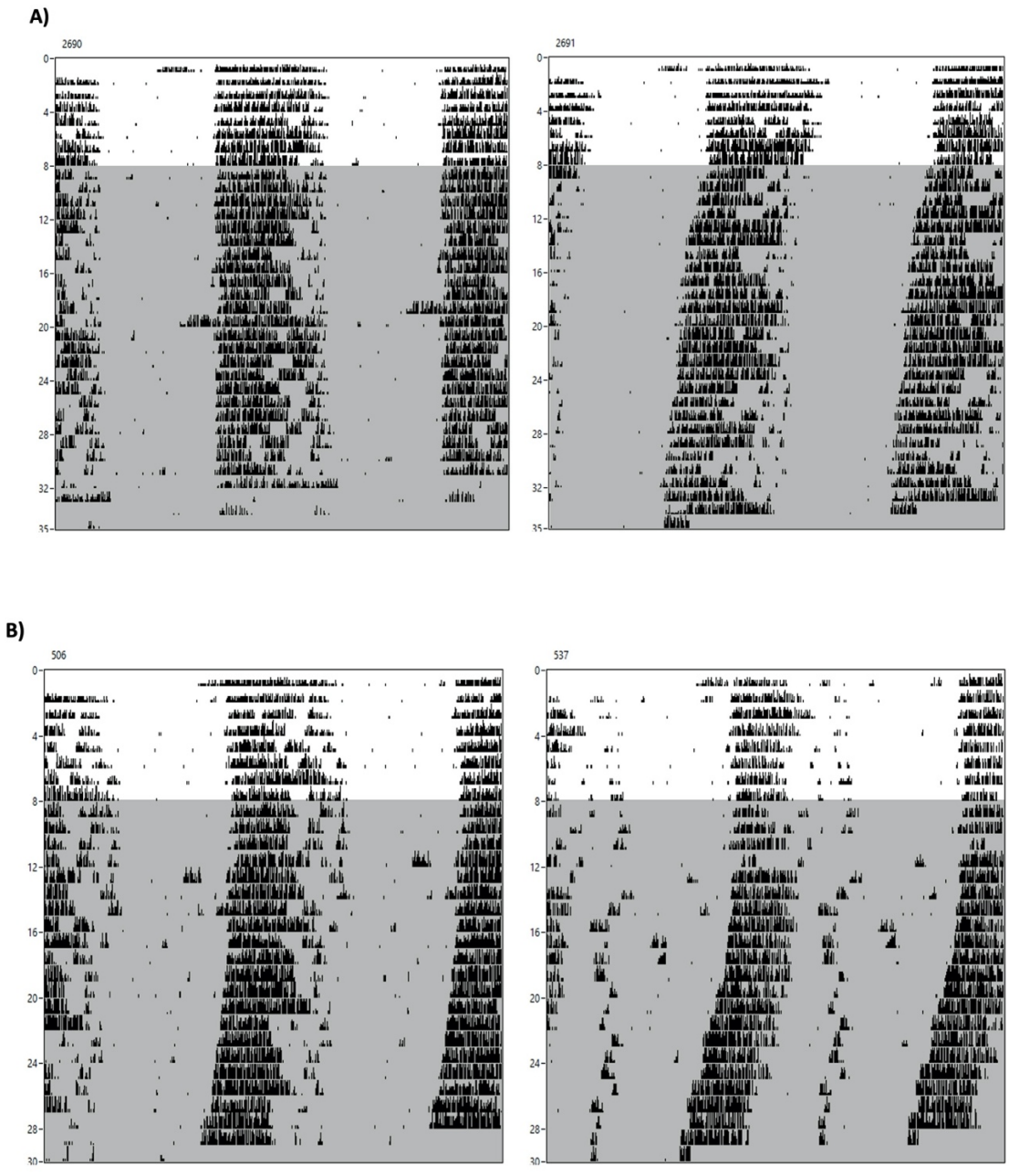
A)
2690
2691
B)
506
537

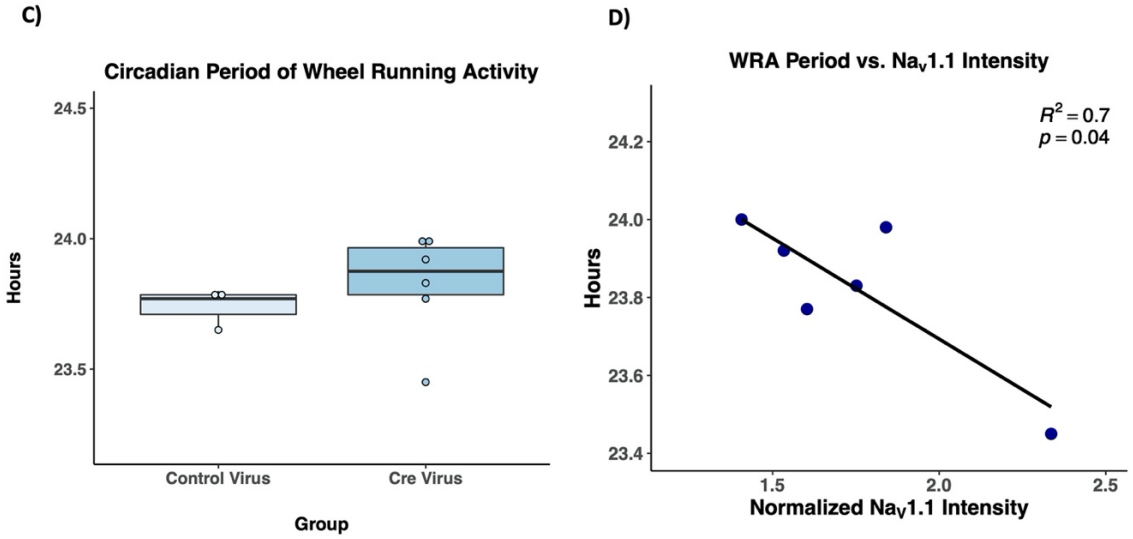

Figure 6. Circadian period of wheel-running activity in Scn1afl/fl mice injected with Cre-expressing is negatively correlated with the extent of NaV1.1 sodium channel deletion. A) Representative actograms of wheel-running activity (WRA) from mice injected with a Cre-expressing AAV. Shaded areas indicate periods of constant darkness. **B)** Same as A for mice injected with a control virus lacking Cre-recombinase. **C)** Comparison of circadian period of WRA between groups (n = 6 Cre virus group, 3 control virus group) reveals no significant differences (one-way ANOVA with group as a factor, $F_{1,7} = 0.46$, $p = 0.52$). None of the mice with successful targeting of the SCN displayed a WRA period comparable to the Scn1a$^{+/-}$ mouse model of DS. **D)** Logistic regression between circadian period of WRA and background-subtracted intensity of antibody staining against Na$_V$1.1 reveals a significant negative correlation between the two variables ($R^2 = 0.7$, $p = 0.04$).

Supplementary Materials

Supplementary Methods

Animals and Behavioral Experiments

To generate DS mice expressing the *Per2-Luciferase* fusion reporter protein, we bred *Scn1a*$^{+/-}$ mice with *mPer2*^{Luc} mice, and genotyped breeding pairs and progeny as previously described[5,66]. We evaluated circadian period of WRA in both *Scn1a*$^{+/-}$*-mPer2*^{Luc} mice (n=1) and littermate *mPer2*^{Luc} controls (n=2) to confirm that *Scn1a*$^{+/-}$*-mPer2*^{Luc} mice displayed the same behavioral phenotype.

Per2-Luciferase Imaging

At the conclusion of behavioral experiments, animals were briefly anesthetized with CO_2 and rapidly decapitated and the brain was dissected out. 300 μm-thick coronal brain sections containing the SCN were prepared with a Vibratome and transferred to cold HBSS buffer. The SCN was dissected out of the brain slice under a dissecting scope using a scalpel and placed on a Millicell culture membrane with a buffer containing DMEM, luciferin, HEPES, penicillin and streptomycin. SCN explants were sealed in Petri dishes using vacuum grease and placed in an incubator kept at 36° C. Slices were imaged using a camera every 30 minutes and images were analyzed for luminescence intensity using ROIs drawn around the SCN in imageJ (National Institutes of Health, Bethesda, MD). Luminescence measurements were subjected to linear detrending as previously described[38] and plotted using R version 3.1.2.

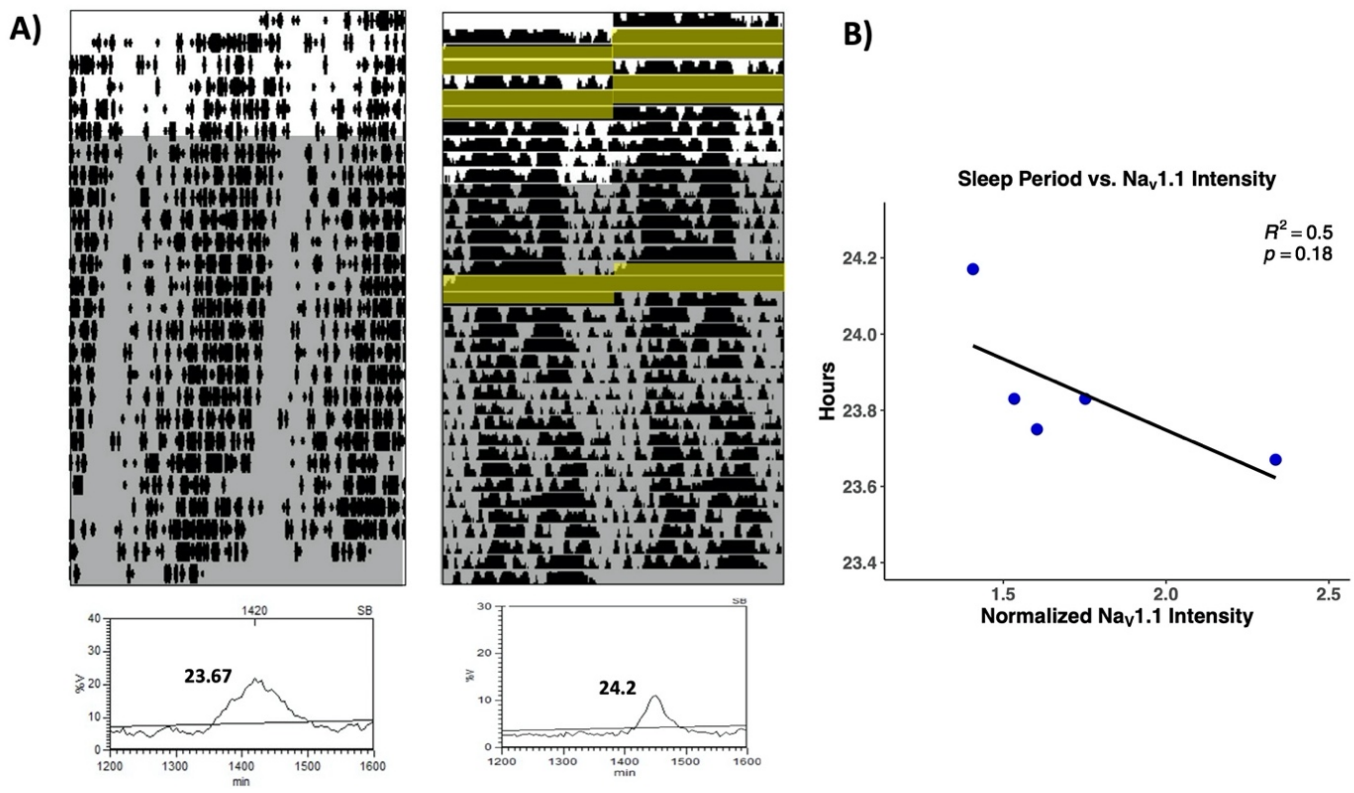

Supplementary Figure 1. Circadian period of polysomnographically recorded sleep in Scn1afl/fl mice injected with Cre-expressing virus. A) Top panels: Representative actograms of total sleep (including NREM and REM sleep stages) from cohort of 5 injected mice. Shaded areas indicate periods of constant darkness. Yellow bars in right actogram indicate missing days of recording due to computer error. Bottom panels: Sokolove-Bushell periodograms indicating circadian period of sleep calculated from each actogram. **B)** Logistic regression between circadian period of sleep and background-subtracted intensity of antibody staining against $Na_V1.1$ reveals no significant negative correlation between the two variables ($R^2 = 0.5$, $p = 0.18$).

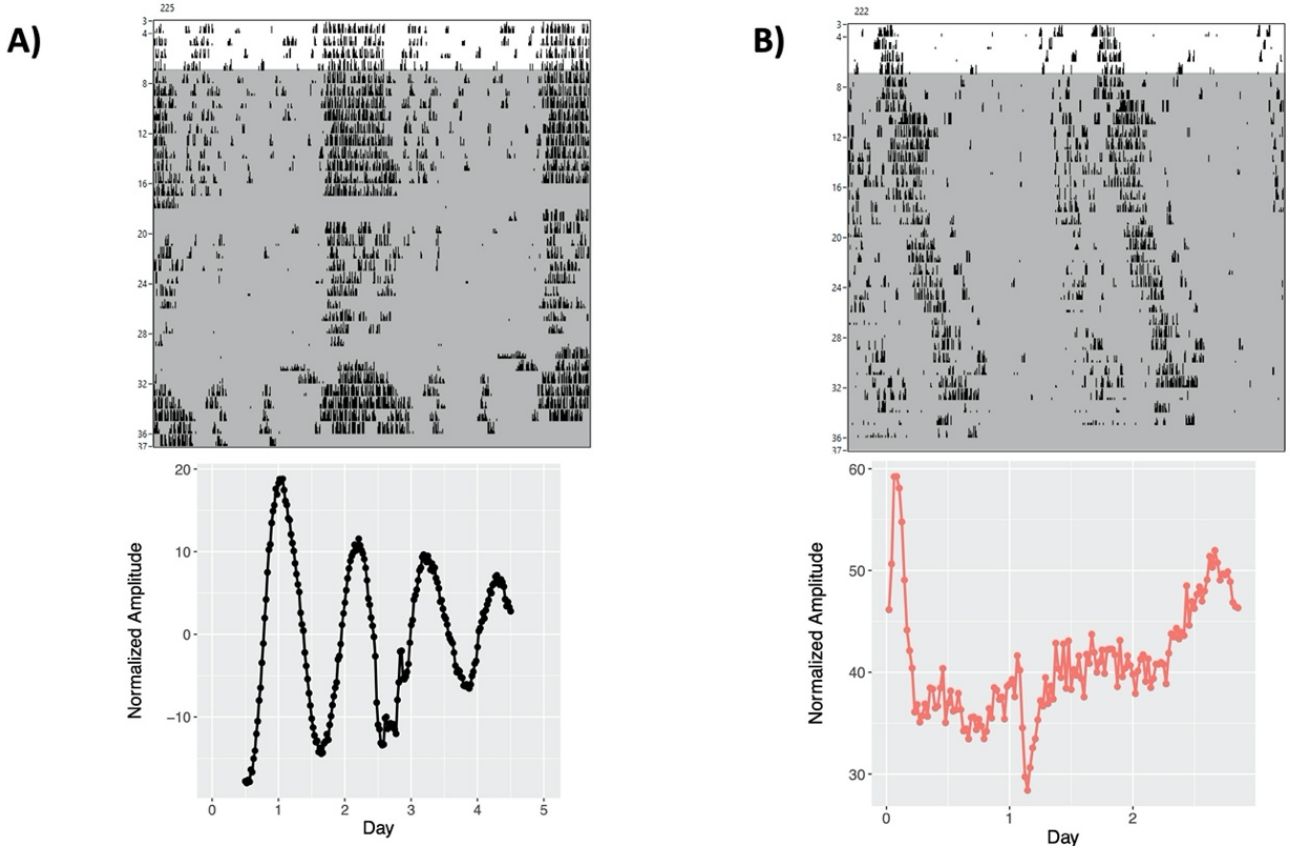

Supplementary Figure 2. Preliminary evaluation of rhythms of Per2-Luciferase expression in Scn1a+/- mice. We recorded wheel-running activity (WRA) and imaged Per2-Luciferse (PER2::LUC) expression in 2 mPer2^{Luc} mice and one mPer2^{Luc}/Scn1a$^{+/-}$ mouse. **A)** Top panel: actogram from one of the two mPer2^{Luc} mice imaged, which displayed a circadian period of WRA of 23.93 hours. Shaded areas indicate periods of constant darkness. Bottom panel: Normalized amplitude of ex vivo luminescence measurements of brain slice containing the SCN from the behavioral data shown in the top panel. **B)** Same as A) for the mPer2^{Luc}/Scn1a$^{+/-}$ mouse.

References

1 Fujiwara T. Clinical spectrum of mutations in SCN1A gene: severe myoclonic epilepsy in infancy and related epilepsies. *Epilepsy Res* 2006;**70 Suppl 1**:S223-30. https://doi.org/10.1016/j.eplepsyres.2006.01.019.

2 Dravet C. The core Dravet syndrome phenotype. *Epilepsia* 2011;**52**:3–9. https://doi.org/10.1111/j.1528-1167.2011.02994.x.

3 Nolan K, Camfield CS, Camfield PR. Coping With a Child With Dravet Syndrome: Insights From Families 2008. https://doi.org/10.1177/0883073808314162.

4 Claes L, Del-Favero J, Ceulemans B, Lagae L, Van Broeckhoven C, De Jonghe P. De novo mutations in the sodium-channel gene SCN1A cause severe myoclonic epilepsy of infancy. *Am J Hum Genet* 2001;**68**:1327–32. https://doi.org/10.1086/320609.

5 Yu FH, Mantegazza M, Westenbroek RE, Robbins CA, Kalume F, Burton KA, *et al.* Reduced sodium current in GABAergic interneurons in a mouse model of severe myoclonic epilepsy in infancy. *Nat Neurosci* 2006. https://doi.org/10.1038/nn1754.

6 Kalume F, Yu FH, Westenbroek RE, Scheuer T, Catterall WA. Reduced sodium current in Purkinje neurons from Nav1.1 mutant mice: Implications for ataxia in severe myoclonic epilepsy in infancy. *J Neurosci* 2007;**27**:11065–74. https://doi.org/10.1523/JNEUROSCI.2162-07.2007.

7 Han S, Tai C, Westenbroek RE, Yu FH, Cheah CS, Potter GB, *et al.* Autistic-like behaviour in Scn1a +- mice and rescue by enhanced GABA-mediated neurotransmission. *Nature* 2012;**489**:385–90. https://doi.org/10.1038/nature11356.

8 Tatsukawa T, Ogiwara I, Mazaki E, Shimohata A, Yamakawa K. Impairments in social novelty recognition and spatial memory in mice with conditional deletion of Scn1a in parvalbumin-expressing cells. *Neurobiol Dis* 2018;**112**:24–34. https://doi.org/10.1016/j.nbd.2018.01.009.

9 Kalume F, Scheuer T, Catterall WA, Kalume F, Westenbroek RE, Cheah CS, *et al.* Sudden unexpected death in a mouse model of Dravet syndrome Find the latest version : Sudden unexpected death in a mouse model of Dravet syndrome 2013;**123**:1798–808. https://doi.org/10.1172/JCI66220.1798.

10 Han S, Yu FH, Schwartz MD, Linton JD, Bosma MM, Hurley JB, *et al.* Na V 1.1 channels are critical for intercellular communication in the suprachiasmatic nucleus and for normal circadian rhythms n.d. https://doi.org/10.1073/pnas.1115729109.

11 Kalume F, Oakley JC, Westenbroek RE, Gile J, de la Iglesia HO, Scheuer T, *et al.* Sleep impairment and reduced interneuron excitability in a mouse model of Dravet Syndrome. *Neurobiol Dis* 2015;**77**:141–54. https://doi.org/10.1016/j.nbd.2015.02.016.

12 Sanchez REA, Bussi IL, Ben-Hamo M, Caldart CS, Catterall WA, De La Iglesia HO. Circadian regulation of sleep in a pre-clinical model of Dravet syndrome: dynamics of sleep stage and siesta re-entrainment. *Sleep* 2019;**42**:. https://doi.org/10.1093/sleep/zsz173.

13 Papale LA, Makinson CD, Christopher Ehlen J, Tufik S, Decker MJ, Paul KN, *et al.* Altered sleep regulation in a mouse model of SCN1A -derived genetic epilepsy with febrile seizures plus (GEFS+). *Epilepsia* 2013;**54**:625–34. https://doi.org/10.1111/epi.12060.

14 Cheah CS, Lundstrom BN, Catterall WA, Oakley JC. Impairment of Sharp-Wave Ripples in a Murine Model of Dravet Syndrome. *J Neurosci* 2019;**39**:9251–60.

https://doi.org/10.1523/JNEUROSCI.0890-19.2019.
15 Catterall WA, Kalume F, Oakley JC. NaV1.1 channels and epilepsy. *J Physiol* 2010:1849–59. https://doi.org/10.1113/jphysiol.2010.187484.
16 Yarmolinsky M, Hoess R. The Legacy of Nat Sternberg: The Genesis of Cre- lox Technology . *Annu Rev Virol* 2015;**2**:25–40. https://doi.org/10.1146/annurev-virology-100114-054930.
17 Cheah CS, Yu FH, Westenbroek RE, Kalume FK, Oakley JC, Potter GB, *et al.* Specific deletion of NaV1.1 sodium channels in inhibitory interneurons causes seizures and premature death in a mouse model of Dravet syndrome. *Proc Natl Acad Sci U S A* 2012;**109**:14646–51. https://doi.org/10.1073/pnas.1211591109.
18 Kalume F, Westenbroek RE, Cheah CS, Yu FH, Oakley JC, Scheuer T, *et al.* Sudden unexpected death in a mouse model of Dravet syndrome. *J Clin Invest* 2013;**123**:1798–808. https://doi.org/10.1172/JCI66220.
19 Rubinstein M, Han S, Tai C, Westenbroek RE, Hunker A, Scheuer T, *et al.* Dissecting the phenotypes of Dravet syndrome by gene deletion n.d. https://doi.org/10.1093/brain/awv142.
20 Stein RE, Kaplan JS, Li J, Catterall WA. Hippocampal deletion of NaV1.1 channels in mice causes thermal seizures and cognitive deficit characteristic of Dravet Syndrome. *Proc Natl Acad Sci U S A* 2019;**116**:16571–6. https://doi.org/10.1073/pnas.1906833116.
21 Losito E, Kuchenbuch M, Chemaly N, Laschet J, Chiron C, Kaminska A, *et al.* Age-related "Sleep/nocturnal" tonic and tonic clonic seizure clusters are underdiagnosed in patients with Dravet Syndrome. *Epilepsy Behav* 2017;**74**:33–40. https://doi.org/10.1016/j.yebeh.2017.05.037.
22 Villas N, Meskis MA, Goodliffe S. Dravet syndrome: Characteristics, comorbidities, and caregiver concerns. *Epilepsy Behav* 2017;**74**:81–6. https://doi.org/10.1016/j.yebeh.2017.06.031.
23 Albers HE, Walton JC, Gamble KL, McNeill JK, Hummer DL. The dynamics of GABA signaling: Revelations from the circadian pacemaker in the suprachiasmatic nucleus. *Front Neuroendocrinol* 2017:35–82. https://doi.org/10.1016/j.yfrne.2016.11.003.
24 Fuentealba P, Steriade M. The reticular nucleus revisited: Intrinsic and network properties of a thalamic pacemaker. *Prog Neurobiol* 2005:125–41. https://doi.org/10.1016/j.pneurobio.2005.01.002.
25 Borbély AA. A Two Process Model of Sleep Regulation. *Hum Neurobiol* 1982;**1**:.
26 Lee IT, Chang AS, Manandhar M, Shan Y, Fan J, Izumo M, *et al.* Neuromedin s-producing neurons act as essential pacemakers in the suprachiasmatic nucleus to couple clock neurons and dictate circadian rhythms. *Neuron* 2015;**85**:1086–102. https://doi.org/10.1016/j.neuron.2015.02.006.
27 Tong Q, Ye CP, Jones JE, Elmquist JK, Lowell BB. Synaptic release of GABA by AgRP neurons is required for normal regulation of energy balance. *Nat Neurosci* 2008;**11**:998–1000. https://doi.org/10.1038/nn.2167.
28 Hsu YWA, Gile JJ, Perez JG, Morton G, Ben-Hamo M, Turner EE, *et al.* The Dorsal Medial Habenula Minimally Impacts Circadian Regulation of Locomotor Activity and Sleep. *J Biol Rhythms* 2017;**32**:444–55. https://doi.org/10.1177/0748730417730169.
29 Cambras T, Weller JR, Anglès-Pujoràs M, Lee ML, Christopher A, Díez-Noguera A, *et al.* Circadian desynchronization of core body temperature and sleep stages in the rat. *Proc Natl Acad Sci U S A* 2007;**104**:7634–9. https://doi.org/10.1073/pnas.0702424104.

30 Lee ML, Swanson BE, de la Iglesia HO. Circadian Timing of REM Sleep Is Coupled to an Oscillator within the Dorsomedial Suprachiasmatic Nucleus. *Curr Biol* 2009;**19**:848–52. https://doi.org/10.1016/j.cub.2009.03.051.
31 Sokolove PG, Bushell WN. The chi square periodogram: Its utility for analysis of circadian rhythms. *J Theor Biol* 1978;**72**:131–60. https://doi.org/10.1016/0022-5193(78)90022-X.
32 Yu FH, Mantegazza M, Westenbroek RE, Robbins CA, Kalume F, Burton KA, *et al.* Reduced sodium current in GABAergic interneurons in a mouse model of severe myoclonic epilepsy in infancy. *Nat Neurosci* 2006;**9**:1142–9. https://doi.org/10.1038/nn1754.
33 Ono D, Honma K ichi, Yanagawa Y, Yamanaka A, Honma S. GABA in the suprachiasmatic nucleus refines circadian output rhythms in mice. *Commun Biol* 2019;**2**:1–12. https://doi.org/10.1038/s42003-019-0483-6.
34 Albus H, Vansteensel MJ, Michel S, Block GD, Meijer JH. A GABAergic mechanism is necessary for coupling dissociable ventral and dorsal regional oscillators within the circadian clock. *Curr Biol* 2005;**15**:886–93. https://doi.org/10.1016/j.cub.2005.03.051.
35 Mcarthur AJ, Coogan AN, Ajpru S, Sugden D, Biello SM, Piggins HD. *Gastrin-Releasing Peptide Phase-Shifts Suprachiasmatic Nuclei Neuronal Rhythms In Vitro*. 2000.
36 Drouyer E, Lesauter J, Hernandez AL, Silver R. Specializations of gastrin-releasing peptide cells of the mouse suprachiasmatic nucleus. *J Comp Neurol* 2010;**518**:1249–63. https://doi.org/10.1002/cne.22272.
37 Lowrey PL, Takahashi JS. Genetics of circadian rhythms in mammalian model organisms. *Adv. Genet.*, vol. 74. Academic Press Inc.; 2011. p. 175–230.
38 Izumo M, Pejchal M, Schook AC, Lange RP, Walisser JA, Sato TR, *et al.* Differential effects of light and feeding on circadian organization of peripheral clocks in a forebrain Bmal1 mutant. *Elife* 2014;**3**:. https://doi.org/10.7554/eLife.04617.
39 C Liu SR. GABA synchronizes clock cells within the suprachiasmatic circadian clock. *Neuron* 2000;**25**:123–8.
40 Aton SJ, Huettner JE, Straume M, Herzog ED. GABA and Gi/o differentially control circadian rhythms and synchrony in clock neurons. *Proc Natl Acad Sci U S A* 2006;**103**:19188–93. https://doi.org/10.1073/pnas.0607466103.
41 Freeman GM, Krock RM, Aton SJ, Thaben P, Herzog ED. GABA networks destabilize genetic oscillations in the circadian pacemaker. *Neuron* 2013;**78**:799–806. https://doi.org/10.1016/j.neuron.2013.04.003.
42 Ono D, Honma K ichi, Yanagawa Y, Yamanaka A, Honma S. Role of GABA in the regulation of the central circadian clock of the suprachiasmatic nucleus. *J Physiol Sci* 2018:333–43. https://doi.org/10.1007/s12576-018-0604-x.
43 Hee JC, Lee CJ, Schroeder A, Yoon SK, Seung HJ, Jeong SK, *et al.* Excitatory actions of GABA in the suprachiasmatic nucleus. *J Neurosci* 2008;**28**:5450–9. https://doi.org/10.1523/JNEUROSCI.5750-07.2008.
44 Saito K, Kakizaki T, Hayashi R, Nishimaru H, Furukawa T, Nakazato Y, *et al.* The physiological roles of vesicular GABA transporter during embryonic development: A study using knockout mice. *Mol Brain* 2010;**3**:40. https://doi.org/10.1186/1756-6606-3-40.
45 Deidda G, Bozarth IF, Cancedda L. Modulation of GABAergic transmission in development and neurodevelopmental disorders: Investigating physiology and pathology

to gain therapeutic perspectives. *Front Cell Neurosci* 2014:119. https://doi.org/10.3389/fncel.2014.00119.

46 Song AJ, Palmiter RD. Detecting and Avoiding Problems When Using the Cre–lox System. *Trends Genet* 2018:333–40. https://doi.org/10.1016/j.tig.2017.12.008.

47 Yu FH, Catterall WA. Overview of the voltage-gated sodium channel family. *Genome Biol* 2003:207. https://doi.org/10.1186/gb-2003-4-3-207.

48 Jackson AC, Yao GL, Bean BP. Mechanism of spontaneous firing in dorsomedial suprachiasmatic nucleus neurons. *J Neurosci* 2004;**24**:7985–98. https://doi.org/10.1523/JNEUROSCI.2146-04.2004.

49 Kononenko NI, Shao LR, Dudek FE. Riluzole-Sensitive Slowly Inactivating Sodium Current in Rat Suprachiasmatic Nucleus Neurons. *J Neurophysiol* 2004;**91**:710–8. https://doi.org/10.1152/jn.00770.2003.

50 Lein ES, Hawrylycz MJ, Ao N, Ayres M, Bensinger A, Bernard A, *et al.* Genome-wide atlas of gene expression in the adult mouse brain. *Nature* 2007;**445**:168–76. https://doi.org/10.1038/nature05453.

51 Mistlberger RE. Circadian regulation of sleep in mammals: Role of the suprachiasmatic nucleus. *Brain Res Rev* 2005:429–54. https://doi.org/10.1016/j.brainresrev.2005.01.005.

52 Saper CB, Scammell TE, Lu J. Hypothalamic regulation of sleep and circadian rhythms. *Nature* 2005;**437**:1257–63. https://doi.org/10.1038/nature04284.

53 Luppi PH, Peyron C, Fort P. Not a single but multiple populations of GABAergic neurons control sleep. *Sleep Med Rev* 2017;**32**:85–94. https://doi.org/10.1016/j.smrv.2016.03.002.

54 Deurveilher S, Burns J, Semba K. Indirect projections from the suprachiasmatic nucleus to the ventrolateral preoptic nucleus: A dual tract-tracing study in rat. *Eur J Neurosci* 2002;**16**:1195–213. https://doi.org/10.1046/j.1460-9568.2002.02196.x.

55 Jilg A, Lesny S, Peruzki N, Schwegler H, Selbach O, Dehghani F, *et al.* Temporal dynamics of mouse hippocampal clock gene expression support memory processing. *Hippocampus* 2010;**20**:377–88. https://doi.org/10.1002/hipo.20637.

56 Harbour VL, Weigl Y, Robinson B, Amir S. Phase differences in expression of circadian clock genes in the central nucleus of the amygdala, dentate gyrus, and suprachiasmatic nucleus in the rat. *PLoS One* 2014;**9**:. https://doi.org/10.1371/journal.pone.0103309.

57 Smarr BL, Jennings KJ, Driscoll JR, Kriegsfeld LJ. A time to remember: The role of circadian clocks in learning and memory. *Behav Neurosci* 2014;**128**:283–303. https://doi.org/10.1037/a0035963.

58 Landgraf D, Long JE, Welsh DK. Depression-like behaviour in mice is associated with disrupted circadian rhythms in nucleus accumbens and periaqueductal grey. *Eur J Neurosci* 2016;**43**:1309–20. https://doi.org/10.1111/ejn.13085.

59 Guilding C, Hughes AT, Brown TM, Namvar S, Piggins HD. A riot of rhythms: Neuronal and glial circadian oscillators in the mediobasal hypothalamus. *Mol Brain* 2009;**2**:. https://doi.org/10.1186/1756-6606-2-28.

60 Padilla SL, Perez JG, Ben-Hamo M, Johnson CW, Sanchez REA, Bussi IL, *et al.* Kisspeptin Neurons in the Arcuate Nucleus of the Hypothalamus Orchestrate Circadian Rhythms and Metabolism. *Curr Biol* 2019;**29**:. https://doi.org/10.1016/j.cub.2019.01.022.

61 Yamagata T, Raveau M, Kobayashi K, Miyamoto H, Tatsukawa T, Ogiwara I, *et al.* CRISPR/dCas9-based Scn1a gene activation in inhibitory neurons ameliorates epileptic and behavioral phenotypes of Dravet syndrome model mice. *Neurobiol Dis* 2020;**141**:104954. https://doi.org/10.1016/j.nbd.2020.104954.

62 Colasante G, Lignani G, Brusco S, Di Berardino C, Carpenter J, Giannelli S, *et al.* dCas9-Based Scn1a Gene Activation Restores Inhibitory Interneuron Excitability and Attenuates Seizures in Dravet Syndrome Mice. *Mol Ther* 2019;**28**:. https://doi.org/10.1016/j.ymthe.2019.08.018.

63 Wykes RC, Lignani G. Gene therapy and editing: Novel potential treatments for neuronal channelopathies. *Neuropharmacology* 2018:108–17. https://doi.org/10.1016/j.neuropharm.2017.05.029.

64 Colwell CS. Linking neural activity and molecular oscillations in the SCN. *Nat Rev Neurosci* 2011:553–69. https://doi.org/10.1038/nrn3086.

65 Allen CN, Nitabach MN, Colwell CS. Membrane currents, gene expression, and circadian clocks. *Cold Spring Harb Perspect Biol* 2017;**9**:a027714. https://doi.org/10.1101/cshperspect.a027714.

66 Yoo SH, Yamazaki S, Lowrey PL, Shimomura K, Ko CH, Buhr ED, *et al.* PERIOD2::LUCIFERASE real-time reporting of circadian dynamics reveals persistent circadian oscillations in mouse peripheral tissues. *Proc Natl Acad Sci U S A* 2004;**101**:5339–46. https://doi.org/10.1073/pnas.0308709101.

Chapter 3: Novel supervised machine learning-based methods for sleep stage classification to aid in studies of circadian sleep regulation

Note to the reader: This work is a collaboration resulting in a co-first author manuscript with Carlos Caldart, a former postdoctoral researcher in our lab, and is available on biorXiv as a preprint at the time of writing.

Abstract

The temporal distribution of sleep stages is critical for the study of sleep function, regulation, and disorders in higher vertebrates. This temporal distribution is typically determined polysomnographically. In laboratory rodents, scoring of electrocorticography (ECoG) and electromyography (EMG) recordings is usually performed manually, where 5-10 second epochs are categorized as one of three specific stages: wakefulness, rapid-eye-movement (REM) sleep and non-REM (NREM) sleep. This process is laborious, time-consuming, and particularly impractical for large experimental cohorts with recordings lasting longer than 24 hours.

To circumvent this problem, we developed an open-source Python toolkit, **Sleep Identification Enabled by Supervised Training Algorithms** (SIESTA), that automates the detection of these three main behavioral stages in mice. Our supervised machine learning algorithm extracts features from the ECoG and EMG signals, then automatically scores recordings with a hierarchical classifier based on Bagging Random Forest approaches. We evaluated this approach on data collected from wild-type mice housed under both normal and different lighting conditions, as well as from a mutant mouse line with abnormal sleep phenotypes. To validate its performance on test data, we compared SIESTA with manually scored data and obtained F_1 scores of 0.92 for wakefulness, 0.81 for REM, and 0.93 for NREM.

SIESTA has a user-friendly interface that can be used without coding expertise. To our knowledge, this is the first time that such a strategy has been developed using all open-source and freely available resources, and our aim is that SIESTA becomes a useful tool that facilitates further research of sleep in rodent models.

Introduction

Sleep is a highly adaptive process that plays an important role in numerous physiological functions. Sleep generally occurs in two stages: rapid eye movement (REM) and non-rapid eye movement (NREM). These stages are characterized by distinct electrophysiological signatures, and the temporal distribution of these stages during sleep defines a 'sleep architecture' that can have important consequences for critical physiological and behavioral processes including memory consolidation, mood and cognitive function.

The study of sleep architecture in the context of disease is an area of great interest. Sleep disorders are extremely common, impacting over 100 million individuals in the United States alone, and contribute to or are co-morbid with a wide range of neurological, metabolic and psychiatric conditions.[1]

Sleep disorders are usually diagnosed using polysomnography, which measures multiple physiological signals including electroencephalography (EEG), electrooculography (EOG), chin and leg electromyography (EMG), electrocardiography (ECG), breathing effort, oxygen saturation and airflow.[2] However, most experts regard EEG and EMG as the essential signals for the classification of behavioral states as either wake, NREM or REM.[3] The characteristics of each stage are currently standardized and defined by the American Academy of Sleep Medicine (AASM) Scoring Manual.[4] In humans NREM can be further subdivided into four distinct stages (N1 to N3), but this distinction is lost or ignored in studies of rodent models, with very few exceptions.[5]

Despite this standardization, trained professionals exhibit an overall inter-scorer agreement of 82.6%, which decreases to around 70% for N1, N3[6] and sleep spindles.[7] Recent findings suggest that this variability can be largely attributed to epochs that could legitimately be assigned to multiple sleep stages.[8] Unlike human sleep data, there is currently no "gold standard" for the manual classification of rodent sleep stage [9] and manual scoring of sleep recordings is often error-prone, time-consuming, and generally must be done offline.

Attempts to develop automated algorithms for sleep staging date back to 1969,[10] and have incorporated a wide range of approaches with varying degrees of success.[11] Previous protocols have been developed and validated using both human and rodent data,[12] often with good results but low adoption by the field. One reason for this limited reach could be because many methods were developed and described assuming the user has expertise in mathematics and computer programming. While more user-friendly approaches have been developed,[13] they are often validated only on data acquired from wild-type (WT) animals or under standard laboratory conditions, or require the purchase of a commercial license and give little to no information about the underlying algorithm or training data used to validate the approach.

Considering the state of the field, and specifically the value to the circadian biology community of long-term chronic polysomnographic recording in studying the role of the circadian clock in regulating sleep/wake cycles, we have developed Sleep Identification Enabled by Supervised Training Algorithms (SIESTA): an open-source, automated sleep stage classification software toolkit in Python.

We first generated a training dataset consisting of 20 days of ECoG and EMG recordings obtained from both WT and transgenic mice with disturbed sleep under multiple experimental lighting conditions. For every 10 seconds of recording, we extracted 54 total features from ECoG and EMG signals, and used these data to evaluate a battery of supervised machine learning algorithms. We selected the bagging classifier using random forest, which showed the highest performance as determined by the F_1 score. We aimed to reach an accuracy of at least 83% across behavioral states, reflecting the average inter-scorer reliability reported by the AASM.[6] When evaluated on test data withheld from the training set, this classifier performed well, achieving F_1 scores of 0.92 for wakefulness, 0.81 for REM, and 0.93 for NREM.

SIESTA is an open-source platform developed in Python. Our user-friendly graphical interface provides an intuitive workflow from data selection to final scored output and includes an optional training module where users can both train SIESTA on their own data and contribute to our freely available database of training data.

Methods

Animals and Housing Conditions

All experiments with animals were performed in accordance with animal protocols approved by the Office of Animal Welfare at the University of Washington. Mice with a heterozygous deletion of the *Scn1a* gene (*Scn1a*$^{+/-}$), which are a model for an intractable form of epilepsy called Dravet syndrome (DS) and are hereafter referred to as DS mice, were generated by targeted deletion of the last exon, encoding domain IV from the S3 to S6 segment and the entire

C-terminal tail of $Na_V1.1$ channel, as previously described.[14] The mice used in this study were generated by crossing heterozygous mutant mice of C57BL/6 background with wild-type (WT) C57BL/6 mice (both males and females of each genotype), resulting in only WT or heterozygous *Scn1a* mutant offspring.[15] The DS mouse has been previously described to have deficits in both the circadian and homeostatic regulation of sleep.[15-17]

Electrocorticographic Recordings

Sleep was recorded as previously described[18]. Briefly, mice were anesthetized with isoflurane and placed into a stereotaxic device where isoflurane anesthesia continued throughout surgery. Each mouse was implanted with ECoG electrodes, consisting of dental screws (Pinnacle Technology, Lawrence, KS; No. 8209: 0.10-in.). A midline incision was made above the skull. Recording electrodes were screwed through cranial holes as follows: over the left frontal cortex (1.5 mm lateral and 2 mm anterior to bregma) and over the right parietal cortex (1.5 mm lateral and 2 mm posterior to bregma), a ground electrode was placed over the visual cortex (1.5 mm lateral and 4.0 mm posterior to bregma), and a reference electrode was placed over the cerebellum (1.5 mm lateral and 6.5 mm posterior to bregma). EMG signals were obtained by placing a pair of silver wires into the neck muscles. The screws were connected, through silver wires, to a common 6-pin connector compatible with the Pinnacle recording device. The screws and connector were fixed to the skull with dental cement. Mice were implanted at between 3 and 4 months of age to account for the long duration of circadian sleep experiments. After surgery, mice were housed in single recording cages under a 12:12 light-dark (LD) cycle. Mice had a recovery period of 1 week and were then fitted with a preamplifier and tether, and connected to the Pinnacle Technology recording system, where they were allowed 1 day to acclimate before

recording started. The ECoG and EMG signals were sampled at 400 Hz with low-pass filters of 80 Hz and 100 Hz, respectively. All recordings are saved and exported for processing using the European Data Format (EDF), an open-source file format commonly used in polysomnographic recording.

Behavioral Experiments and Environmental Conditions

Our recordings came from experiments maintained in a ventilated, light-tight room under either a 12:12 LD cycle with 200-lux intensity or DD. To determine the effect of abrupt LD phase shifts on the phase of the circadian rhythm of sleep, we used a delay and advance "jetlag" protocol. After mice were entrained to a 12:12 LD cycle, a delay jetlag was initiated by extending the light phase by 6 hours (i.e. delaying the time of lights off by 6 hours). The mice stayed under this new 12:12 LD cycle until they re-entrained to the new cycle. The advance jetlag was initiated by shortening the light phase by 6 hours (i.e. advancing the time of lights off by 6 hours). To assess the endogenous circadian period of sleep, we released mice into DD for at least 14 days after they had synchronized to a 12:12 LD cycle.

Signal Processing and Feature Engineering

We used a total of 54 features extracted for each 10-second epoch, calculated from raw ECoG and EMG data. ECoG and EMG signals were prefiltered using a Hanning filter with a moving window of one minute.

From ECoG signals, we calculated power, energy and amplitude values for a series of spectral bands as described in previous studies of the ECoG and EMG signatures of sleep stages[19]. We

defined the alpha band as 8-13 Hz, beta as 20-40 Hz, sigma as 11-15 Hz, gamma as 35-45 Hz,[20] and a frequency band indicating the occurrence of sleep spindles as 12-14 Hz. Because there is little consensus on the definition of mouse theta in the literature, we incorporated several previously described definitions as features (4-12 Hz,[21] 6-9 Hz,[22] 5.5-8.5 Hz [19] 7-10 Hz[21]). Next, we calculated three different power ratios between frequency bands. The first is the theta-delta ratio, which is commonly incorporated into heuristics used to discriminate sleep and wake states[5]. The other two have been used for sleep spindle detection[23] and are defined as the ratio of power values of frequencies between 0.5-20 Hz to those between 0.5-50 Hz; and the ratio of those between 11-16 Hz to those between 0.5-40 Hz. Additional features included the 90% spectral edge, 50% spectral mean, mean and median amplitude, the root mean square, variance, skewness, and kurtosis of the signal. Finally, we incorporated the number of zero crossings, the peak-to-peak range, and the spectral entropy of the signal.

From the EMG signal, we calculated the amplitude, signal variance, skewness, kurtosis, root mean square amplitude and the spectral entropy. A list of all the features and their descriptions can be found in Supplementary Table 1.

Software Development

All the codes were written and tested in Python 2.7 and 3.7.3, using Spyder 3.3.2 and Jupyter 5.7.2 on Windows, MacOS and Linux operating systems. The scikit.learn package version 0.20.1 was used for validating the machine learning algorithms and Kivy 1.10.1 for designing the graphical interface. We used Pandas 0.23.4, Pickle 3.0, Numpy 1.15.4 and Scipy 1.1.0 for data management and signal processing.

Supervised Learning Algorithm Selection

Using our manually-scored sleep data, we tested the ability of several algorithms to identify each sleep stage. We used methods of one-step classification, wherein an epoch was classified as either wake, REM or NREM in a single step using one classifier; and two-level hierarchical classification, wherein one classifier was used to score an epoch as either wake or sleep, and a second classifier was used to further divide the bouts of sleep as either NREM or REM. The full list of classifiers tested is given in Table 1[24-36].

Because the random forest algorithm is at the core of SIESTA, we provide a brief discussion of its implementation as follows. The random forest algorithm is an ensemble learning method that takes into account the classification results of multiple decision trees[27]. Although effective, decision trees often generalize poorly and underperform on classification problems with a large number of input variables.[31] To compensate for this, random forest classifiers utilize a combination of decision trees such that each tree depends on a random, independently sampled vector of the dataset that has the same distribution for all decision trees. After several trees are created, the random forest algorithm "votes" on the most popular class. A margin function is used to determine by how much the average number of votes from decision trees for the right class exceeds the vote total for any of the other classes (e.g. wake, NREM or REM).[31]

SIESTA employs two other similarly structured ensemble learning methods called bagging and gradient boosting,[37] using random forest as the base classifier for each. A bagging classifier[33] is an ensemble meta-estimator method that creates random individual results by training each

classifier on a random redistribution of the training dataset, and then aggregating their individual predictions (by a vote) to form a final prediction. This meta-estimator is typically used to reduce the variance of the core method (in this case Random Forest). Similarly, gradient boosting is an ensemble learning method that boosts the performance of "weak learners" such as decision trees using a loss function, which determines how well the model fits the training data.[33]

In the screening for all algorithms we performed 20-fold cross validation with shuffle and used F_1 score to assess performance. The F_1 score is the harmonic mean of the precision and recall of the test. Precision is given by the number of true positives (TP) divided by the sum of false positives and TP, and recall is calculated as the number of TPs divided by the sum of false negatives and TPs. Assessing test performance using F_1 score compensates for the imbalance in the occurrences of wake, NREM and REM bouts, and as such is widely used in machine learning-based approaches to automatic sleep scoring.[11] All results are shown as mean with standard deviation.

Inter- and intra-scorer reliability

To calculate inter-scorer reliability, we randomly selected a 24-hour recording from our training dataset and compared the agreement between 4 experienced manual scorers using both percent agreement and Fleiss' kappa.[38] In accordance with previous reports[39] of inter-scorer reliability for sleep scoring between multiple scorers, we set the following levels of agreement for evaluating κ: 0-0.20 = slight agreement, 0.21-0.40 = fair agreement, 0.41-0.60 = moderate agreement, 0.61-0.80 = substantial agreement, 0.81-1.0 = near perfect agreement. κ values are reported as being within a 95% confidence interval (CI).

We then calculated intra-scorer reliability, or how consistently each manual scorer classified a single epoch as being the same state when presented with the epoch multiple times. We wrote a custom R script to randomly select 600 10-second epochs from the same 24-hour recording session, duplicate each of these epochs 5 times, randomly insert them into the original data file, and finally randomize the order of all epochs in the data file. This new file was then scored by 4 experienced manual scorers, and the score consistency between duplicate epochs was evaluated using percent agreement for each individual scorer.

Training Dataset

The training dataset consisted of 20 total days of recording from 20 different mice, scored by 4 different experts blind to experimental conditions. Each recording was a day long (24 hours), under several different environmental lighting conditions including LD (12h light – 12h dark), Constant Darkness (DD), and in the days immediately following induced jet lag. These conditions covered the most common light cycle paradigms used in the study of behavioral circadian rhythms, with DD and jet lag particularly being known to induce changes in sleep timing and quantity.[40] Data from these experiments were selected to make the dataset more generalizable to recordings obtained under diverse experimental conditions.

Correlation Matrix and Dendrogram

We generated a correlation matrix to visualize the Pearson correlation coefficients calculated for pairs of features. We used single linkage clustering to generate the feature order.[41] The

dendrogram measures the pairwise distance between the features using a threshold and metric to divide the measurements called the cophenetic correlation coefficient. This allowed us to cluster the variables according to the average distance between each subset of merged features.

Dimensionality Reduction using Sequential Feature Selection

Sequential Feature Selection belongs to a family of greedy search algorithms that are used to reduce an initial d-dimensional feature space (where d is the number of features extracted from the EDF file) to a k-dimensional subset (where k is the target number of features, and $k < d$). These methods select an initial size for the subset of features, and sequentially find the features[42] that are most informative at this timestep. The process is repeated at the next timestep, choosing the next feature subset depending on the previously selected features and the metric of the classifier. In the forward sequential selector, a small feature subset is selected, and the algorithm adds a single feature at a time to the initial subset. This process is repeated until all features are added back in. For the backward sequential selector, the initial subset is of size d or near d, and the algorithm removes one feature at each timestep.

Results

Inter- and intra-scorer reliability

To evaluate the consistency of manual scoring and ensure the robustness of our training dataset, we first calculated measures for both inter-scorer and intra-scorer reliability. Four experienced manual scorers from our laboratory were asked to score a total of 12,608 10-second epochs as wake, NREM or REM, and inter-scorer reliability was determined using both Fleiss' kappa and

percent agreement (Table 1). Across all three stages, manual scorers displayed substantial Fleiss' kappa agreement particularly in epochs scored as wake and REM, with NREM Fleiss' kappa agreement being slightly lower (Table 2). Interestingly, wake and NREM showed the highest percent agreement, with the lowest for REM bouts (Table 1).

Next, we evaluated intra-rater reliability using percent agreement. We found that on average our four manual scorers were highly consistent in their scoring across all three states (Table 2). This agreement was slightly higher for wake bouts, and slightly lower for NREM and REM bouts (Table 2).

Table 1. Inter- and intra-rater reliability metrics for manual scores used in training datasets

	Inter-Rater Reliability			
	Total	Wake	NREM	REM
Fleiss Kappa [95% CI]	0.75 [0.744-757]	0.76 [0.758-0.770]	0.73 [0.726-0.738]	0.78 [0.773-0.786]
Agreement	87.34%	93.55%	89.04%	84.73%
# Epochs (% of Total)	12608	5934 (47.07%)	6047 (47.96%)	627 (4.97%)
	Intra-Rater Reliability			
Rater	All	Wake	NREM	REM
A	98.53%	98.89%	98.62%	95.14%
B	91.60%	93.62%	87.71%	95.00%
C	96.17%	96.21%	96.32%	93.85%
D	96.90%	97.47%	97.12%	89.33%
Average	95.80%	96.55%	94.94%	93.33%

Cells under intra-rater reliability represent % agreement. NREM = non-rapid eye movement; REM = rapid eye movement.

One-step classifier with complete dataset

Once we established consistency and high inter-rater reliability in our manual scoring, we examined which commonly used supervised learning algorithms performed with the highest accuracy in sleep stage classification when trained on our dataset (see Table 2 and Methods

section for complete list). We tested each algorithm with the feature values both scaled and without scaling, as the performance of some algorithms changed depending on scaling; the results of both cases are displayed in Table 2 and Supplementary Table 2. Although several algorithms produced an F_1 score that was better than chance using the one-step approach, GBC and BCRF performed the highest F_1 score.

Because both GBC and BCRF do not require scaled data as a prerequisite to their use[31,35] they did not show a change in performance whether the data were scaled or unscaled.

Table 2. Classification accuracy by algorithm and method.

Algorithm	One-step	Hierarchical	Hierarchical + 2 hrs.
Logistic Regression	0.78 (0.081)	0.35 (0.074)	0.86 (0.060)
Linear Discriminant Analysis	0.77 (0.090)	0.85 (0.077)	0.85 (0.077)
K-nearest Neighbors Classifier	0.76 (0.074)	0.51 (0.009)	0.84 (0.060)
Decision Tree Classifier	0.72 (0.076)	0.84 (0.043)	0.84 (0.038)
Gaussian Naïve Bayes	0.52 (0.18)	0.35 (0.87)	0.60 (0.149)
Passive Aggressive Classifier	0.71 (0.079)	0.48 (0.055)	0.77 (0.0113)
Ridge Classifier	0.70 (0.082)	0.85 (0.077)	0.85 (0.077)
Logistic Regression, cross validation	0.79 (0.077)	0.36 (0.086)	0.86 (0.062)
Bernoulli Naïve Bayes	0.60 (0.163)	0.50 (0.032)	0.75 (0.118)
Nearest Centroid	0.54 (0.129)	0.49 (0.013)	0.67 (0.135)
Random Forest Classifier	0.80 (0.061)	0.89 (0.030)	0.89 (0.028)
Ada Boost Classifier	0.79 (0.066)	0.88 (0.040)	0.88 (0.040)
Bagging Classifier, Decision Tree	0.79 (0.061)	0.89 (0.030)	0.88 (0.033)
Extra Trees Classifier	0.80 (0.063)	0.89 (0.031)	0.89 (0.033)
Gradient Boosting Classifier	0.83 (0.057)	0.90 (0.035)	0.90 (0.035)
Perceptron	0.72 (0.112)	0.49 (0.006)	0.78 (0.077)
Bagging Classifier, Random Forest	**0.83 (0.060)**	**0.91 (0.032)**	**0.91 (0.032)**
Bagging Classifier, Extra Trees	0.82 (0.062)	0.90 (0.034)	0.90 (0.032)

Values represent F_1 scores (with standard deviation in parentheses). Hierarchical + 2 hrs. methods refers to the method of adding two hours of manually scored data to the training set for the classifier. All data are unscaled.

Hierarchical classifier with complete dataset

With this approach, we observed improved detection of NREM and REM states using most of the algorithms we tested, with a F_1 score of 0.907 ± 0.032 in the case of BCRF, an improvement from the F_1 score of 0.827 ± 0.059 obtained using the one-step approach (Table 2). This improvement was not of equal magnitude in all three states scored. Table 2 and Supplemental Table 2 illustrate the performance of each classifier in first distinguishing sleep and wake, and second distinguishing between NREM and REM. The BCRF algorithm was the highest performing in terms of classification speed and accuracy (Sup. Table 3) and was subsequently selected as the classifier for SIESTA.

Generalization of algorithm across genotypes and training datasets

We validated the performance of SIESTA using a test dataset excluded from the training dataset. This test data included WT and DS mice, manually scored by the same experts that labeled the original training dataset.

First, we tested SIESTA with only the WT data, training the algorithm with all but one WT mouse, using the scores from these new data as targets to validate the scoring method. This process was repeated 20 times, with both the one-step and hierarchical classifiers. Complete results of the scoring can be seen in Table 3. Finally, we added the first 2 hours of the manually scored data of the target mice to the dataset to reduce the interindividual variability of the individual mice in the training process,[48] and then re-trained the BCRF in the hierarchical

classifier with this new dataset. Using this approach, we increased classification performance for all three stages (Awake: 0.942 [±0.017] to 0.956 [±0.031]; NREM: 0.936 [±0.019] to 0.952 [±0.039]; REM: 0.811 [±0.036] to 0.844 [±0.054]).

These three different approaches (One-step classifier, hierarchical classifier and hierarchical classifier with the first 2 hours to the dataset) were repeated using a dataset consisting of only DS mice. Compared to WT data, these F_1 scores were lower than for the WT database in the first two methods, but increased in the last method (Table 3). This discrepancy could be due to the known circadian rhythm and sleep disturbances present in DS mice.

Lastly, we attempted to use a training dataset consisting of only data from WT mice to classify data from DS mice. Once again, the best method was the hierarchical classifier using the first 2 hours of the target mice (Table 3). Based on these results, we concluded that the performance of the algorithm is best when the target data and the data in the training dataset are similar, and that adding scores for the first 2 hours of the target data increases the scores in all cases (Table 3).

Table 3. Sleep stage classification accuracy using subsets of the training data.

Wild Type Training/Wild Type Validation				
Method	Wake	Sleep	NREM	REM
One-Step	0.94 (0.015)		0.90 (0.017)	0.77 (0.038)
Hierarchical	0.94 (0.017)	0.92 (0.021)	0.94 (0.019)	0.81 (0.036)
Hierarchical + 2 hrs.	0.96 (0.031)	0.94 (0.038)	0.95 (0.039)	0.84 (0.054)
Dravet Syndrome Training/Dravet Syndrome Validation				
Method	Wake	Sleep	NREM	REM
One-Step	0.85 (0.059)		0.82 (0.094)	0.60 (0.048)
Hierarchical	0.85 (0.061)	0.82 (0.115)	0.91 (0.054)	0.70 (0.084)

Hierarchical + 2 hrs.	0.94 (0.013)	0.93 (0.028)	0.95 (0.016)	0.81 (0.054)
Wild Type Training/Dravet Syndrome Validation				
Method	Wake	Sleep	NREM	REM
One-Step	0.84 (0.091)		0.86 (0.048)	0.68 (0.081)
Hierarchical	0.85 (0.097)	0.88 (0.058)	0.88 (0.072)	0.75 (0.082)
Hierarchical + 2 hrs.	0.88 (0.049)	0.89 (0.030)	0.89 (0.037)	0.76 (0.061)

Cells contain F_1 accuracy scores (and standard deviation in parentheses). Hierarchical + 2 hrs. methods refers to the method of adding two hours of manually scored data to the algorithm. All data is unscaled. Wild type database n= 14, Dravet syndrome database n=6. NREM = non-rapid eye movement; REM = rapid eye movement.

Although scoring sleep in 10-second increments is common, this temporal resolution can result in the misclassification of boundary epochs, as sleep stage transitions can happen on rapid timescales. Therefore, we also tested the performance of the algorithm when tasked with scoring data in 5-second epochs. We normalized the database and validated the scores with a wild-type and a DS mouse. The F_1 scores for these mice were similar to those obtained using 10-second epochs, with a score for REM of 0.75 in WT and 0.83 in DS using the One-step classifier; and 0.76 in WT and 0.85 in DS with the hierarchical classifier (Supplementary Table 5). These results validated the utility of this method even when changing the epoch size.

Feature evaluation and reduction

Next, we decided to further characterize the features that we extracted from our raw data for training. Most features were empirically chosen based on features used to identify sleep stages according to the AASM, as well as previously developed methods for automatic sleep scoring in rodents. The aim of this feature characterization was to find a subset of the most important features for successful classification. Reducing the number of features used for scoring would

allow for a faster and more flexible method that could work in a real-time scoring paradigm without significantly reducing classification accuracy.

We computed a correlation matrix to determine the extent of the similarity between features used in training, and found highly correlated features ($r>0.9$) that appeared to cluster primarily in two main groups: one with features describing the amplitude of the signal (in several frequency bands of both the ECoG signal and EMG signals), and a second cluster that included the relative power of all but the delta band of the ECoG signal, along with other features that describe the frequency domain of the signal (the spectral mean and spectral entropy of ECoG).

To further characterize the clustering and correlation of the features used for training, we constructed a dendrogram (Sup. Fig. 2). We found 3 clusters and 1 independent variable. The first cluster consisted primarily of variables related to the amplitude of the signals, similar to the correlation matrix. The second cluster contained a mix of the relative power and the energy of most frequency bands. The third cluster contained the fewest features and included the relative power and amplitude of the delta band and the spectral characteristics of the EMG. The only feature that did not belong to any cluster was the second ECoG index ('ECOGrel2', the ratio of the relative power of the 0.5-20 Hz band and the 0.5-50 Hz band), which has been previously identified as being useful in automated approaches to sleep scoring[49].

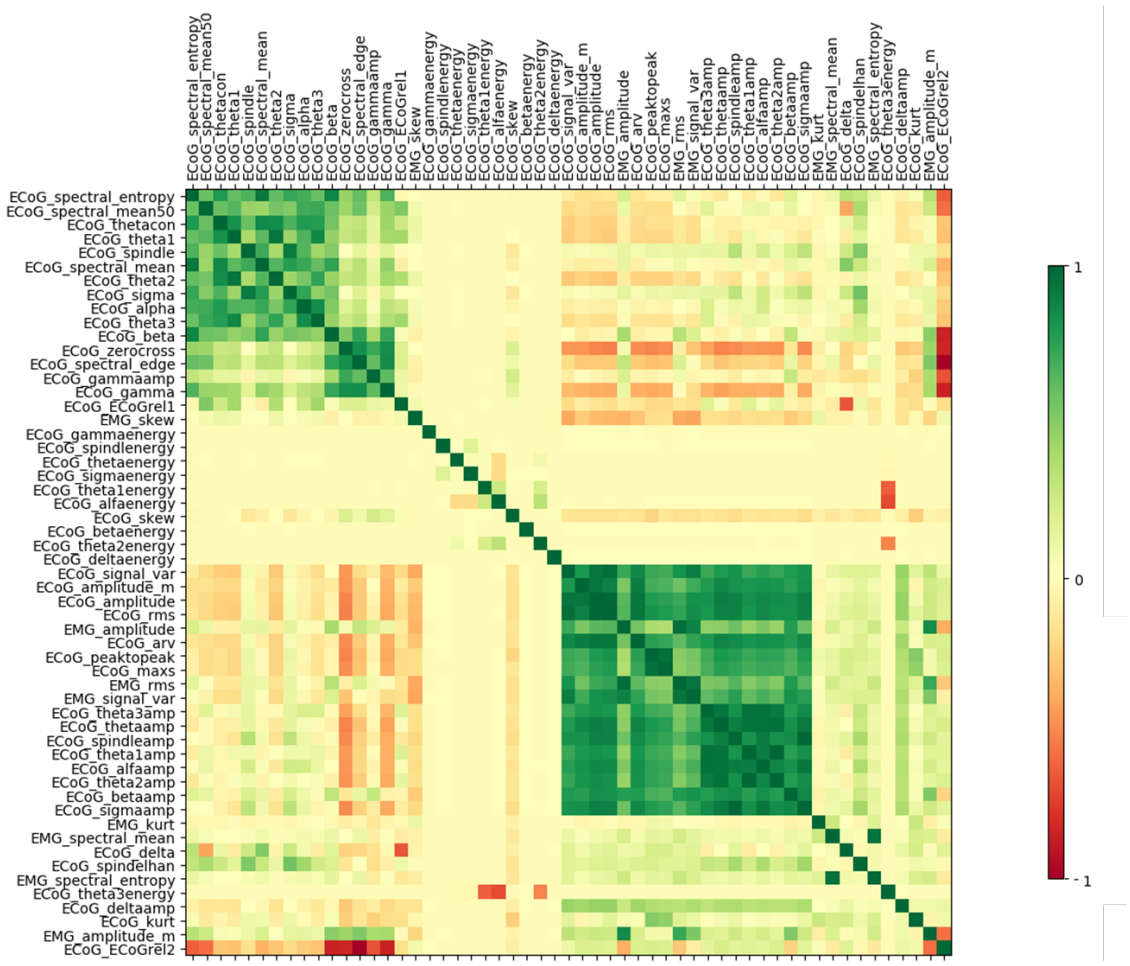

Figure 1 – Correlation matrix of the features from the complete dataset. The data was reorganized via the clustering algorithm described in the Methods section to identify highly correlated subsets of features (in both positive – green - and negative – red - correlation). Each of the above features is described in detail in Supplementary Table 1.

After identifying subsets of features that were highly correlated, we next sought to find the optimal subset of features for classifying sleep stages. We used both Sequential Forward Selection (SFS) and Sequential Backward Selection (SBS) to identify the features that were the most critical for sleep stage identification. In both selection algorithms the inflection point (the number of features at which increasing the size of the feature subset does not significantly improve the performance of the classifier[50]) of the performance curve was around 6 features (Figure 2). Both algorithms were run with the one-step classifier using BCRF three times, each

with cross-validation performed five times, to evaluate the robustness of the feature selection (Sup. Table 2). In most cases the same features were identified as being the most important for algorithm performance, and the inflection point of the performance curve always occurred at 6-8 features. The list of all features found by the sequential selection algorithm can be found in Sup. Fig. 1. The top 5 features consistently identified by both SFS and SBS as being most important were: ECoG Zero crossing, EMG Amplitude, ECoG Sleep Spindle Hanning window (listed as 'ECoG Spindlehan' in Fig. 1 and Sup. Table 1), ECoG Delta power and EMG Spectral Entropy. Most of the features identified have been already reported to be relevant for classifying sleep stages, either by being used to score sleep (ECoG Delta[51]) or being present mainly in certain stages (sleep spindles[52]).

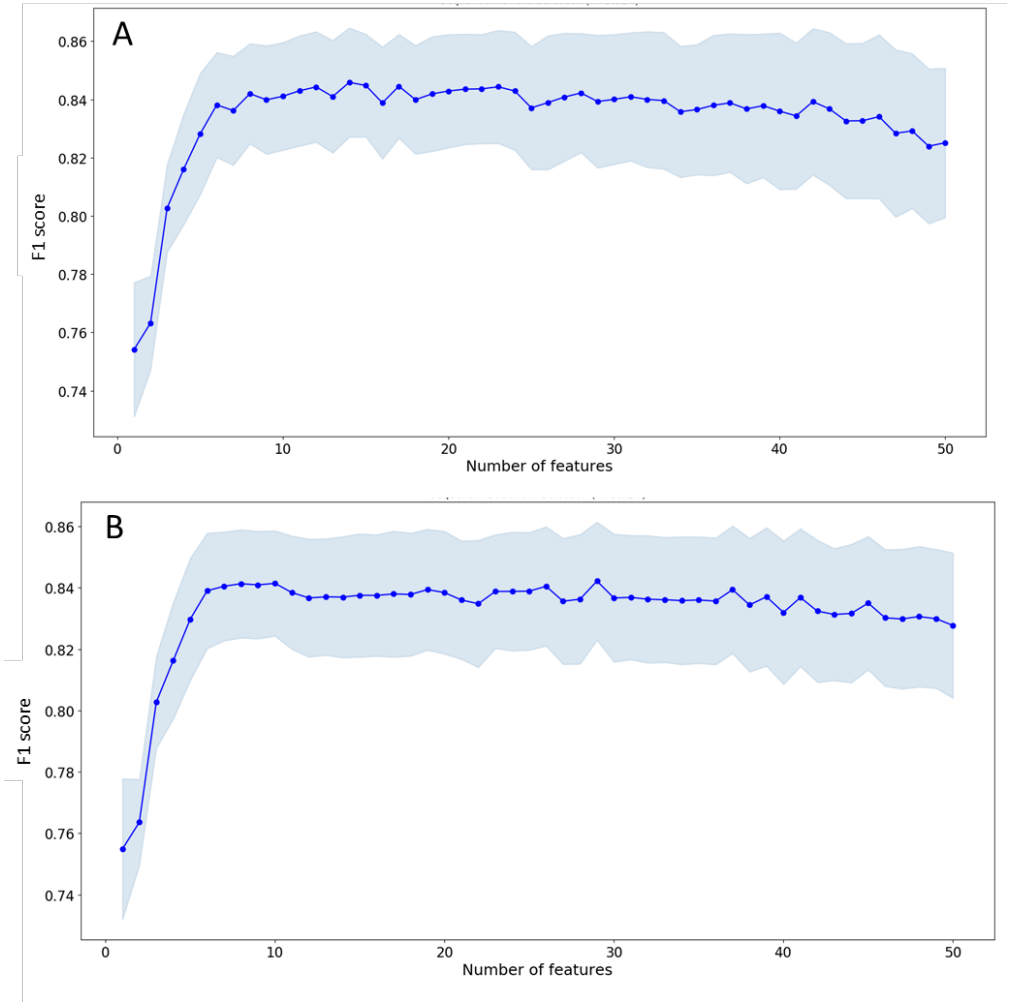

Figure 2 – Performance under sequential feature selection of the BCRF algorithm trained on the complete training dataset using a One-Step approach to classification. The blue dots indicate the mean F_1 values from 3 runs of the sequential feature selection method, and the light blue shaded area represents the standard deviation in each case. **A)** Sequential Forward Selection, **B)** Sequential Backward Selection.

As expected, several of the highest-rated features in all the iterations of the sequential search method were the same. We found 5 features that were present in all cases, and these features were spread across the three clusters identified in the dendrogram (Sup. Fig. 2) as well as the two most correlated clusters of the correlation matrix. Similarly, the correlation matrix revealed one feature identified by SBS and SFS in each cluster while the rest were not highly correlated with any other feature (Sup. Fig. 3).

Graphical interface

Given the success of SIESTA in sleep stage classification, we sought to ease the access of our code to the broader sleep and circadian biology community. We developed a graphical interface that allows researchers to use our method, from pre-processing to scoring. SIESTA takes European Data Format (EDF) files as input, an open-source file format commonly used in both human and animal polysomnographic recordings. Each widget of the interface performs a different function, starting with either the feature extraction of new test data or training on a new dataset input by the user, to score new recordings. Users have the option to input parameters that are specific to their experimental needs, including the sampling frequency used in their recording and their desired epoch length. Both the features and final score files are output in .csv format. The stored database uses the Pickle library of Python to store the training results in a non-binary file so that users do not need to re-train the algorithm each time they want to score new data. A flow diagram of the complete training process and the actions available in the graphical interface is illustrated in Figure 3.

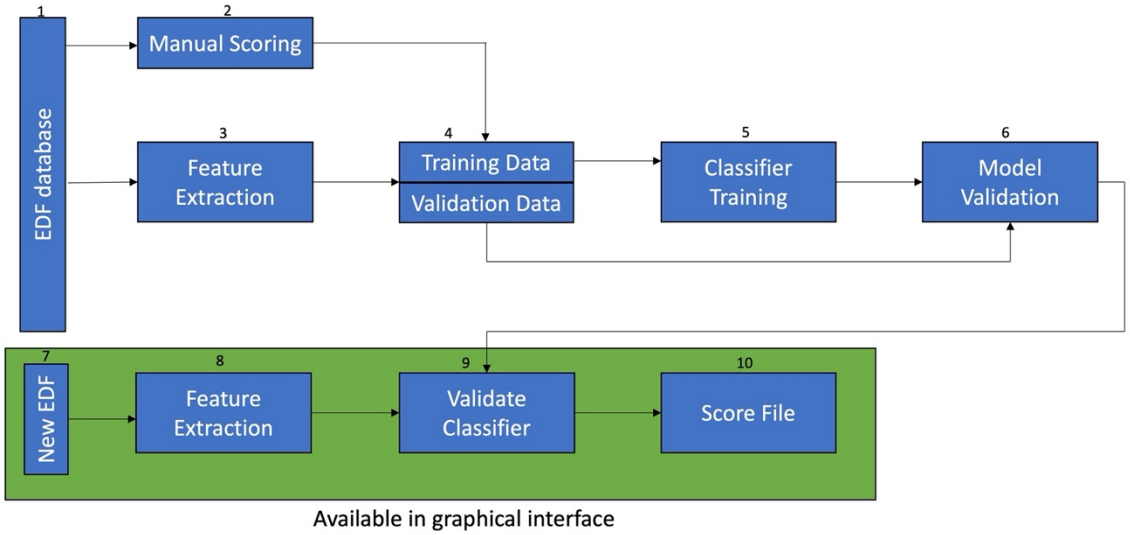

Figure 3 – Overview of the SIESTA workflow. To train the model, we start with raw ECoG/EMG recordings in EDF file format **(1)**. Our dataset is manually scored by one of four human experts **(2)**. From data in the same EDF files, we calculated features used for scoring **(3).** Next, we split the data into training and validation sets **(4).** Using only the training set, we trained the BCRF classifier and obtain our model **(5).** We then evaluate model performance on the validation set **(6).** When a user wants to score data from their own experiment, they first upload their raw recording in EDF format **(7).** Feature extraction occurs as in Step 2, which generates a timestamped file containing feature values for every epoch in the recording. **(8).** Next, users can load the working model from our dataset. They will be informed of the validation results of the model as well as information about the underlying dataset (number and genotype of the animals included) **(9).** Users will also have the option to train a new classifier on their own manually scored dataset or combine their data with ours. Finally, users can upload the newly generated feature data to create a final output file containing timestamped scores and several metrics commonly used in sleep analysis, including ECoG delta power and theta power **(10).**

We freely provide the source code for the graphical interface, a user's manual, and the database that we used to train our algorithm, as well as the base code that we used outside the graphical interface to validate SIESTA on GitHub®.

Discussion

Using open-source coding and data management tools, we developed a novel automated sleep stage classification system for rodent polysomnographic data we call SIESTA. First, we

compared the performance of a set of commonly used classifiers in identifying sleep stages from a training dataset containing data from both WT and transgenic mice with disturbed sleep. From this comparison, we identified the highest-performing classifier: the bagging classifier using random forest as the base classifier. We demonstrated that the accuracy of several classifiers was heavily influenced by the pre-processing of the signals, but the chosen method was not affected by this process. While other groups have reported using the random forest classifier to score sleep[43-45] fewer have used the bagging[46] or gradient boosting ensemble classification methods.[47] To our knowledge, even fewer approaches have used the bagging classifier with random forest as the base classifier. We obtained high classification accuracy on par with AASM inter-rater reliability standards using a one-step classifier for all stages, and this score was further improved using a hierarchical classifier. We were able to improve classification accuracy even further when using a small amount (2 hours) of manually scored epochs from the data needing to be scored.

We have used this method to score data obtained in our laboratory, including continuous long-term polysomnographic recordings lasting over 3 weeks. Scoring this data manually is normally a tedious, error prone and time-consuming process. The run time for the feature extraction with the SIESTA code is less than a minute. In other words, we can score 24 hours of recording in under 1 minute if we use our complete training data set. If the algorithm is trained on new data, scoring 24 hours of recording takes approximately 5 minutes. Information on computational times associated with training and scoring with the different methods and subset of data can be found in Sup. Tables 3 and 4.

We welcome users to contribute both data and code to SIESTA to improve its performance and better suit their own needs. Accordingly, we provide the manually scored data we used to train the algorithm, as well as the source code of the classifier and feature extraction methods. We hope that as SIESTA is used in a wider range of experimental conditions and mouse lines, it will become more robust with a more comprehensive training dataset. A key feature of this code is that we do not use a time-dependent model, meaning the score of each epoch is independent from the previous epoch, so data from experimental animals with altered sleep architecture can be scored in an unbiased way. This characteristic allows for the training dataset to be replaced, modified or expanded with ease, allowing for more flexible scoring. Even though scoring can be improved when taking the previous epoch into account,[53] this can lead to mistakes when the sleep architecture is atypical.

Scoring with SIESTA can be done without extensive coding knowledge, and our goal is that our simple interface and transparent analysis pipeline can make a novel contribution to the field of automatic sleep scoring and facilitate studies involving the chronic monitoring of sleep in the research community.[54] Additionally, SIESTA dramatically reduces the time needed to obtain sleep scores from raw data compared to manual scoring. Our code is modular and separated into 3 main processes that comprise our analysis pipeline: feature extraction, training of the algorithm with the dataset and scoring of the experimental data file. All of the input and output files are in standardized open-source formats, making the manipulation of data using SIESTA easy. The motivation behind this open-source approach and the free release of SIESTA is to provide a trustworthy application that can be understood and validated by the community, encouraging any comment or modification that could improve the scoring process.

One of the main limitations of our approach is that we are not taking in account boundary epochs (epochs that include more than one state or a state change). These epochs can be difficult for both human and machine scorers to classify, and as such may decrease the efficiency of our algorithm. Additionally, neither our manual or automatic scorers have a criterion for the rejection of an epoch, so all data is stored in one of the predetermined labels (including epochs containing artifacts and transition epochs), which could also lower the performance of the algorithm. Even though we were aware of this limitation, we opted for this approach to simplify the use of the software and manual scoring of the recording. Even with this limitation, we obtain F_1 scores of between 0.83 and 0.93 in all states.

Although we present only one pathological model in which we have validated our method, we are working on expanding the training dataset to include more data from additional mouse lines with altered sleep phenotypes. Additionally, we are looking to test the algorithm with data obtained from humans and other animal models, but there is recent work using similar approaches that lead us to believe our method can be effective in other models.[55,56] Indeed, a recent study demonstrated that another supervised learning algorithm, deep convolutional neural networks, can be used to predict sleep stages from manually scored data in narcoleptic mice with a comparable degree of success as our own approach.[57]

An additional value of this work is the characterization of the features we use to train our model and score recordings. Through feature correlation and reduction, we specify a small subset of features needed to maintain high accuracy of SIESTA. Most of these features have been

described in the literature to have a biological meaning (e.g. the relative power of the delta frequency band in the ECoG signal, EMG amplitude, and sleep spindles), which served to further validate our approach when they were found to be key in successful scoring. Other features are usually more prominently associated with other neural phenomena, as in the case of ECoG Zero-Crossing in the context of seizure and interictal spike detection.[58] This might point to underlying biological processes that we have yet to fully characterize and are being identified by an unbiased machine learning algorithm. These supervised classifiers could also be finding success in scoring using the interaction between different features in the subset identified by SFS and SBS, as an emergent property of the complex ECoG and EMG features that by itself might not have a direct biological interpretation.[59,60] Finally, the reduced subset of features we identified can be useful in the development of a real-time scoring paradigm, allowing more easily for long-term closed-loop manipulations of sleep stages in rodent models with both normal and pathological sleep, a potentially valuable tool for the sleep and circadian biology communities. One method that may increase availability of such real-time scoring is compressed sensing, which can reduce computational complexity and thereby computational time needed for sleep-scoring analyses[63]. This is effectively accomplished by only gathering data relevant to the task of interest, which tends to be a fraction of the overall data collected.

Although deep learning approaches have shown recent success in automated sleep scoring in both human patients[61] and animal models[62] (with large datasets and promising results), we opted for a shallow-learning approach without dimensionality reduction, allowing for greater interpretability of the results. The knowledge that the algorithm is using features with known biological relevance makes these results easier to approach and understand by the medical and

research communities. Still, future studies should continue to directly compare the efficacy of supervised, unsupervised and deep learning approaches to scoring rodent polysomnographic data from diverse mouse lines and experimental conditions.

Finally, the study of the circadian regulation of sleep can produce long time series data that are often cumbersome to analyze. Our hope for SIESTA is not only to create an open-source community driven tool for sleep and circadian biologists, but also to encourage other researchers in the field not to shy away from performing experiments that would produce otherwise unwieldy datasets. These approaches are extremely valuable in furthering our understanding of the relationship between sleep, the circadian system and neurological and psychiatric conditions. Long-term monitoring of sleep in pre-clinical models of disease is an indispensable tool in understanding and leveraging these interactions to address the impact of sleep on health.

References

1. Ohayon MM. Epidemiology of insomnia: what we know and what we still need to learn. *Sleep medicine reviews.* Apr 2002;6(2):97-111.

2. Grigg-Damberger MM. Atlas of Clinical Sleep Medicine, 2nd edition. *J Clin Neurophysiol.* Oct 2015;32(5):440-440.

3. Schulz H, Salzarulo P. The Development of Sleep Medicine: A Historical Sketch. *Journal of clinical sleep medicine : JCSM : official publication of the American Academy of Sleep Medicine.* Jul 15 2016;12(7):1041-1052.

4. Berry RB. *The AASM manual for the scoring of sleep and associated events: rules, terminology and technical specifications*: American Academy of Sleep Medicine; 2018.

5. Katsageorgiou VM, Sona D, Zanotto M, et al. A novel unsupervised analysis of electrophysiological signals reveals new sleep substages in mice. *PLoS biology.* May 2018;16(5):e2003663.

6. Danker-Hopfe H, Anderer P, Zeitlhofer J, et al. Interrater reliability for sleep scoring according to the Rechtschaffen & Kales and the new AASM standard. *Journal of sleep research.* Mar 2009;18(1):74-84.

7. Wendt SL, Welinder P, Sorensen HB, et al. Inter-expert and intra-expert reliability in sleep spindle scoring. *Clinical neurophysiology : official journal of the International Federation of Clinical Neurophysiology.* Aug 2015;126(8):1548-1556.

8. Younes M, Raneri J, Hanly P. Staging Sleep in Polysomnograms: Analysis of Inter-Scorer Variability. *Journal of clinical sleep medicine : JCSM : official publication of the American Academy of Sleep Medicine.* Jun 15 2016;12(6):885-894.

9. Robert C, Guilpin C, Limoge A. Automated sleep staging systems in rats. *Journal of neuroscience methods.* May 1 1999;88(2):111-122.

10. Smith JR, Negin M, Nevis AH. Automatic analysis of sleep electroencephalograms by hybrid computation. *IEEE transactions on systems science and cybernetics.* 1969;5(4):278-284.

11. Faust O, Razaghi H, Barika R, Ciaccio EJ, Acharya UR. A review of automated sleep stage scoring based on physiological signals for the new millennia. *Computer methods and programs in biomedicine.* Jul 2019;176:81-91.

12. Miladinovic D, Muheim C, Bauer S, et al. SPINDLE: End-to-end learning from EEG/EMG to extrapolate animal sleep scoring across experimental settings, labs and species. *PLoS computational biology.* Apr 2019;15(4):e1006968.

13. Allocca G, Ma S, Martelli D, et al. Validation of 'Somnivore', a Machine Learning Algorithm for Automated Scoring and Analysis of Polysomnography Data. *Frontiers in Neuroscience.* 2019-March-18 2019;13(207).

14. Yu FH, Mantegazza M, Westenbroek RE, et al. Reduced sodium current in GABAergic interneurons in a mouse model of severe myoclonic epilepsy in infancy. *Nature neuroscience.* Sep 2006;9(9):1142-1149.

15. Kalume F, Oakley JC, Westenbroek RE, et al. Sleep impairment and reduced interneuron excitability in a mouse model of Dravet Syndrome. *Neurobiology of disease.* May 2015;77:141-154.

16. Sanchez REA, Bussi IL, Ben-Hamo M, Caldart CS, Catterall WA, de la Iglesia HO. Circadian Regulation of Sleep in a Pre-Clinical Model of Dravet Syndrome: Dynamics of Sleep Stage and Siesta Re-entrainment. *Sleep.* Jul 26 2019.

17. Han S, Yu FH, Schwartz MD, et al. Na(V)1.1 channels are critical for intercellular communication in the suprachiasmatic nucleus and for normal circadian rhythms. *Proceedings of the National Academy of Sciences of the United States of America.* Feb 7 2012;109(6):E368-377.

18. Hsu YA, Gile JJ, Perez JG, et al. The Dorsal Medial Habenula Minimally Impacts Circadian Regulation of Locomotor Activity and Sleep. *Journal of biological rhythms.* Oct 2017;32(5):444-455.

19. Katsageorgiou VM, Lassi G, Tucci V, Murino V, Sona D. Sleep-stage scoring in mice: The influence of data pre-processing on a system's performance. *Conference proceedings : ... Annual International Conference of the IEEE Engineering in Medicine and Biology Society. IEEE Engineering in Medicine and Biology Society. Annual Conference.* Aug 2015;2015:598-601.

20. Marrosu F, Santoni F, Fa M, et al. Beta and gamma range EEG power-spectrum correlation with spiking discharges in DBA/2J mice absence model: role of GABA receptors. *Epilepsia.* Mar 2006;47(3):489-494.

21. Franken P, Malafosse A, Tafti M. Genetic variation in EEG activity during sleep in inbred mice. *The American journal of physiology.* Oct 1998;275(4):R1127-1137.

22. Feng ZX, Dong H, Qu WM, Zhang W. Oral Delivered Dexmedetomidine Promotes and Consolidates Non-rapid Eye Movement Sleep via Sleep-Wake Regulation Systems in Mice. *Frontiers in pharmacology.* 2018;9:1196.

23. Lacourse K, Delfrate J, Beaudry J, Peppard P, Warby SC. A sleep spindle detection algorithm that emulates human expert spindle scoring. *Journal of neuroscience methods.* Mar 15 2019;316:3-11.

24. Yu HF, Huang FL, Lin CJ. Dual coordinate descent methods for logistic regression and maximum entropy models. *Mach Learn.* Oct 2011;85(1-2):41-75.

25. Pedregosa F, Varoquaux G, Gramfort A, et al. Scikit-learn: Machine Learning in Python. *J Mach Learn Res.* Oct 2011;12:2825-2830.

26. Yang W, Wang KQ, Zuo WM. Fast neighborhood component analysis. *Neurocomputing.* Apr 15 2012;83:31-37.

27. Hastie T, Tibshirani R, Friedman JH. *The elements of statistical learning : data mining, inference, and prediction*. 2nd ed. New York, NY: Springer; 2009.

28. Crammer K, Dekel O, Keshet J, Shalev-Shwartz S, Singer Y. Online Passive-Aggressive Algorithms. *J. Mach. Learn. Res.* 2006;7:551-585.

29. McCallum A, Nigam K. A comparison of event models for naive bayes text classification. Paper presented at: AAAI-98 workshop on learning for text categorization1998.

30. Tibshirani R, Hastie T, Narasimhan B, Chu G. Diagnosis of multiple cancer types by shrunken centroids of gene expression. *Proceedings of the National Academy of Sciences of the United States of America.* May 14 2002;99(10):6567-6572.

31. Breiman L. Random Forests. *Mach Learn.* October 01 2001;45(1):5-32.

32. Freund Y, Schapire RE. A Decision-Theoretic Generalization of On-Line Learning and an Application to Boosting. *J. Comput. Syst. Sci.* 1997;55(1):119-139.

33. Breiman L. Bagging Predictors. *Mach Learn.* August 01 1996;24(2):123-140.

34. Geurts P, Ernst D, Wehenkel L. Extremely randomized trees. *Mach Learn.* April 01 2006;63(1):3-42.

35. Friedman JH. Greedy Function Approximation: A Gradient Boosting Machine. *The Annals of Statistics.* 2001;29(5):1189-1232.

36. Freund Y, Schapire RE. Large Margin Classification Using the Perceptron Algorithm. *Mach Learn.* December 01 1999;37(3):277-296.

37. Dietterich TG. An Experimental Comparison of Three Methods for Constructing Ensembles of Decision Trees: Bagging, Boosting, and Randomization. *Mach Learn.* August 01 2000;40(2):139-157.

38. Landis JR, Koch GG. The measurement of observer agreement for categorical data. *Biometrics.* Mar 1977;33(1):159-174.

39. Magalang UJ, Chen NH, Cistulli PA, et al. Agreement in the Scoring of Respiratory Events and Sleep Among International Sleep Centers. *Sleep.* Apr 1 2013;36(4):591-596.

40. Hasan S, Foster RG, Vyazovskiy VV, Peirson SN. Effects of circadian misalignment on sleep in mice. *Sci Rep.* Oct 26 2018;8(1):15343.

41. Murtagh F, Contreras P. Algorithms for hierarchical clustering: an overview, II. *Wires Data Min Knowl.* Nov-Dec 2017;7(6).

42. Ferri FJ, Pudil P, Hatef M. Comparative Study of Techniques for Large-Scale Feature Selection. *Pattern Recognition in Practice, IV: Multiple Paradigms, Comparative Studies and Hybrid Systems.* 2001;16.

43. Klok AB, Edin J, Cesari M, Olesen AN, Jennum P, Sorensen HBD. A New Fully Automated Random-Forest Algorithm for Sleep Staging. *Conference proceedings : ... Annual International Conference of the IEEE Engineering in Medicine and Biology Society. IEEE Engineering in Medicine and Biology Society. Annual Conference.* Jul 2018;2018:4920-4923.

44. Cooray N, Andreotti F, Lo C, Symmonds M, Hu MTM, De Vos M. Detection of REM sleep behaviour disorder by automated polysomnography analysis. *Clinical neurophysiology : official journal of the International Federation of Clinical Neurophysiology.* Apr 2019;130(4):505-514.

45. Sen B, Peker M, Cavusoglu A, Celebi FV. A comparative study on classification of sleep stage based on EEG signals using feature selection and classification algorithms. *Journal of medical systems.* Mar 2014;38(3):18.

46. Gao V, Turek F, Vitaterna M. Multiple classifier systems for automatic sleep scoring in mice. *Journal of neuroscience methods.* May 1 2016;264:33-39.

47. Hassan AR, Bhuiyan MIH. Automated identification of sleep states from EEG signals by means of ensemble empirical mode decomposition and random under sampling boosting. *Computer methods and programs in biomedicine.* Mar 2017;140:201-210.

48. Allocca G, Ma S, Martelli D, et al. Validation of 'Somnivore', a Machine Learning Algorithm for Automated Scoring and Analysis of Polysomnography Data. *Front Neurosci.* 2019;13:207.

49. Libourel PA, Corneyllie A, Luppi PH, Chouvet G, Gervasoni D. Unsupervised online classifier in sleep scoring for sleep deprivation studies. *Sleep.* May 1 2015;38(5):815-828.

50. Mayer J, Rahman R, Ghosh S, Pal R. Sequential feature selection and inference using multi-variate random forests. *Bioinformatics.* Apr 15 2018;34(8):1336-1344.

51. Silber MH, Ancoli-Israel S, Bonnet MH, et al. The visual scoring of sleep in adults. *Journal of clinical sleep medicine : JCSM : official publication of the American Academy of Sleep Medicine.* Mar 15 2007;3(2):121-131.

52. Jiang X, Gonzalez-Martinez J, Halgren E. Coordination of human hippocampal sharpwave-ripples during NREM sleep with cortical theta bursts, spindles, downstates and upstates. *The Journal of neuroscience : the official journal of the Society for Neuroscience.* Sep 18 2019.

53. Fiorillo L, Puiatti A, Papandrea M, et al. Automated sleep scoring: A review of the latest approaches. *Sleep medicine reviews.* Aug 9 2019;48:101204.

54. Kemp B, Varri A, Rosa AC, Nielsen KD, Gade J. A simple format for exchange of digitized polygraphic recordings. *Electroencephalography and clinical neurophysiology.* May 1992;82(5):391-393.

55. Gangstad SW, Mikkelsen KB, Kidmose P, et al. Automatic sleep stage classification based on subcutaneous EEG in patients with epilepsy. *Biomedical engineering online.* Oct 30 2019;18(1):106.

56. Skorucak J, Hertig-Godeschalk A, Schreier DR, Malafeev A, Mathis J, Achermann P. Automatic detection of microsleep episodes with feature-based machine learning. *Sleep.* Jan 13 2020;43(1).

57. Exarchos I, Rogers AA, Aiani LM, et al. Supervised and unsupervised machine learning for automated scoring of sleep-wake and cataplexy in a mouse model of narcolepsy. *Sleep.* May 12 2020;43(5).

58. Shahidi Zandi A, Tafreshi R, Javidan M, Dumont GA. Predicting epileptic seizures in scalp EEG based on a variational Bayesian Gaussian mixture model of zero-crossing intervals. *IEEE transactions on bio-medical engineering.* May 2013;60(5):1401-1413.

59. Garcia-Cairasco N. Learning about brain physiology and complexity from the study of the epilepsies. *Braz J Med Biol Res.* Jan 2009;42(1):76-86.

60. Wong V. Biology in a gray box: targeting the emergent properties of protein complexes: 2011 Yale Chemical Biology Symposium. *The Yale journal of biology and medicine.* Dec 2011;84(4):491-495.

61. Human immunodeficiency virus and other blood-borne pathogens in sports. The American Medical Society for Sports Medicine (AMSSM) and the American Academy of Sports Medicine (AASM). *Clinical journal of sport medicine : official journal of the Canadian Academy of Sport Medicine.* Jul 1995;5(3):199-204.

62. Yamabe M, Horie K, Shiokawa H, Funato H, Yanagisawa M, Kitagawa H. MC-SleepNet: Large-scale Sleep Stage Scoring in Mice by Deep Neural Networks. *Sci Rep.* Oct 31 2019;9(1):15793.'

63. Huang, L., Lin, Q., Zhang, X., & Shuai, P. (2017). Fast Ambiguity Resolution for Pulsar-Based Navigation by Means of Hypothesis Testing. *IEEE Transactions on Aerospace and Electronic Systems*, *53*(1), 137–147. https://doi.org/10.1109/TAES.2017.2649698

64. Mohren, T., Daniel, T., Brunton, S., Brunton, B. (2018). Neural-inspired sensors enable sparse, efficient classification of spatiotemporal data. *Proceedings of the National Academies of Sciences United States of America,* Oct 16 2018;115(42) E10564-10569

Supplementary Materials

Supplementary Table 1 – List of Signal Features used by SIESTA

ECoG_delta	Relative power of the 0.5-4 Hz frequency band
ECoG_delta_energy	Energy of the 0.5-4 Hz frequency band
ECoG_delta_amp	Mean amplitude of the signal in the 0.5-4 Hz frequency band
ECoG_thetacon	Relative power of the 4-12 Hz frequency band
ECoG_thetaenergy	Energy of the 4-12 Hz frequency band
ECoG_thetaenergy	Energy of the 4-12 Hz frequency band
ECoG_thetamp	Mean amplitude of the 4-12 Hz frequency band
ECoG_theta1	Relative power of the 6-9 Hz frequency band
ECoG_theta1_energy	Energy of the 6-9 Hz frequency band
ECoG_theta1amp	Mean amplitude of the 6-9 Hz frequency band
ECoG_theta2	Relative power of the 5.5-8.5 Hz frequency band
ECoG_theta2energy	Energy of the 5.5-8.5 Hz frequency band
ECoG_theta2amp	Mean amplitude of the 5.5-8.5 Hz frequency band
ECoG_theta3	Relative power of the 7-10 Hz frequency band
ECoG_theta3energy	Energy of the 7-10 Hz frequency band
ECoG_theta3amp	Mean amplitude of the 7-10 Hz frequency band
ECoG_beta	Relative power of the 20-40 Hz frequency band
ECoG_betaenergy	Energy of the 20-40 Hz frequency band
ECoG_betamp	Amplitude of the 20-40 Hz frequency band
ECoG_alpha	Relative power of the 8-13 Hz frequency band
ECoG_alphaenergy	Energy of the 8-13 Hz frequency band
ECoG_alphaamp	Mean amplitude of the 8-13 Hz frequency band

ECoG_sigma	Relative power of the 11-15 Hz frequency band
ECoG_sigmaenergy	Energy of the 11-15 Hz frequency band
ECoG_sigmaamp	Mean amplitude of the 11-15 Hz frequency band
ECoG_spindle	Relative power of the 12-14 Hz frequency band, the frequency at which NREM sleep spindles typically occur
ECoG_spindlenergy	Energy of the 12-14 Hz frequency band
ECoG_spindleamp	Mean amplitude of the 12-14 Hz frequency band
ECoG_gamma	Relative power of the 35-45 Hz frequency band
ECoG_gammaenergy	Energy of the 35-45 Hz frequency band
ECoG_gammaamp	Mean amplitude of the 35-45 Hz frequency band
ECoG_ECoGrel1	Ratio of the relative power value of the thetacon band (4-12 Hz) to that of the delta band (0.5-4 Hz)
ECoG_ECoGrel2	Ratio of the relative power value of the 0.5-20 Hz band to that of the 0.5-50 Hz band
ECoG_Spindlehan	Ratio of 11-16 Hz power to 0.5-40 Hz power smoothed with a 12-point Hanning filter
ECoG_spectral_edge	90% spectral edge of the ECoG signal
ECoG_spectral_mean50	50% spectral mean of the ECoG signal
ECoG_zerocross	Counts of the number of times the amplitude of the ECoG signal falls above or below the mean of the ECoG signal for any given epoch
ECoG_maxs	Maximum amplitude of the raw ECoG signal
ECoG_peaktopeak	Peak-to-peak amplitude of the ECoG signal
ECoG_arv	Arithmetic mean of the absolute values of the ECoG signal in a given epoch
ECoG_rms	Root mean square value of the ECoG signal
ECoG_amplitude	Mean amplitude of the ECoG signal in a given epoch

ECoG_amplitude_m	Median amplitude of the ECoG signal in a given epoch
ECoG_signal_var	Spectral variance of the ECoG signal
ECoG_skew	Skewness of the ECoG signal
ECoG_kurt	Kurtosis of the ECoG signal
ECoG_spectral_mean	Mean of the spectral power distribution of the ECoG signal for a given epoch
ECoG_spectral_entropy	Entropy of the spectral power distribution of the ECoG signal for a given epoch
EMG_amplitude	Mean amplitude of the EMG signal
EMG_signal_var	Spectral variance of the EMG signal
EMG_skew	Skewness of the EMG signal
EMG_kurt	Kurtosis of the EMG signal
EMG_spectral_mean	Mean of the spectral power distribution of the EMG signal for a given epoch
EMG_spectral_entropy	Entropy of the spectral power distribution of the EMG signal for a given epoch
EMG_amplitude_m	Median amplitude of the EMG signal in a given epoch

Supplementary Table 2. Classification accuracy by algorithm and method when data are scaled.

Algorithm	One-step	Hierarchical	Hierarchical + 2 hrs.
Logistic Regression	0.80 (0.067)	0.47 (0.005)	0.87 (0.054)
Linear Discriminant Analysis	0.77 (0.090)	0.86 (0.056)	0.86 (0.056)
K-nearest Neighbors Classifier	0.76 (0.075)	0.48 (0.003)	0.85 (0.050)
Decision Tree Classifier	0.72 (0.078)	0.80 (0.061)	0.80 (0.063)
Gaussian Naïve Bayes	0.52 (0.18)	0.48 (0.005)	0.79 (0.136)
Passive Aggressive Classifier	0.68 (0.11)	0.46 (0.033)	0.84 (0.052)
Ridge Classifier	0.70 (0.083)	0.78 (0.072)	0.78 (0.072)
Logistic Regression, cross validation	0.79 (0.077)	0.48 (0.005)	0.87 (0.062)
Bernoulli Naïve Bayes	0.60 (0.163)	0.48 (0.009)	0.69 (0.123)
Nearest Centroid	0.54 (0.129)	0.39 (0.012)	0.79 (0.125)
Random Forest Classifier	0.80 (0.063)	0.86 (0.051)	0.86 (0.051)
Ada Boost Classifier	0.79 (0.066)	0.86 (0.05)	0.86 (0.050)
Bagging Classifier, Decision Tree	0.79 (0.06)	0.85 (0.054)	0.85 (0.054)
Extra Trees Classifier	0.80 (0.062)	0.86 (0.053)	0.86 (0.053)
Gradient Boosting Classifier	0.83 (0.057)	0.86 (0.051)	0.86 (0.051)
Perceptron	0.72 (0.11)	0.40 (0.01)	0.84 (0.057)
Bagging Classifier, Random Forest	**0.83 (0.060)**	**0.87 (0.055)**	**0.87 (0.055)**
Bagging Classifier, Extra Trees	0.82 (0.061)	0.87 (0.052)	0.87 (0.054)

Values represent F_1 scores (with standard deviation in parentheses). Hierarchical + 2 hrs. methods refers to the method of adding two hours of manually scored data to the training set for the classifier. All data are scaled.

Supplementary Table 3 – Training time for each classification method using the complete training dataset.

Method	One-step Training (min)	Hierarchical classifier Training (min)		
		Sleep vs. Wake	NREM vs. REM	Total
Logistic Regression	1.305017	0.56646388	0.5664639	1.132928
Linear Discriminant Analysis	0.325585	0.44011573	0.4401157	0.880231
K-nearest Neighbors Classifier	0.494233	0.64531681	0.6453168	1.290634
Decision Tree Classifier	3.087765	3.36282204	3.362822	6.725644
Gaussian Naïve-Bayes	0.169616	0.2236391	0.2236391	0.447278
Passive Aggressive Classifier	0.330701	0.25370451	0.2537045	0.507409
Ridge Classifier	0.215765	0.28431216	0.2843122	0.568624
Logistic Regression with cross-validation	2.72975	1.11243985	1.1124398	2.22488
Bernoulli Naïve Bayes	0.194801	0.23899159	0.2389916	0.477983
Nearest Centroid	0.138609	0.19050883	0.1905088	0.381018
Random Forest Classifier	2.204762	2.46243883	2.4624388	4.924878
Ada Boost Classifier	13.14571	15.7994703	15.79947	31.59894
Bagging Classifier with decision tree	19.74422	20.9569206	20.956921	41.91384
Extra Trees Classifier	0.650872	0.77603496	0.776035	1.55207
Gradient Boosting Classifier	50.63355	19.0567781	19.056778	38.11356
Perceptron	0.409127	0.22129073	0.2212907	0.442581
Bagging Classifier with Random Forest Classifier	**14.21601**	**13.9431089**	**13.943109**	**27.88622**
Bagging Classifier with Extra Trees Classifier	4.14548	4.19125078	4.1912508	8.382502

Supplementary Table 4 – Scoring time of the BCRF algorithm on subsets of the training and scoring data.

Database	Classifier	Sleep Stages	Training Time	Scoring Time (24 hours)	Training Time with 2 hours of manual score	Scoring Time of 24 hours with 2 hours of manual score
WT	One-Step	Awake / NREM/REM	0.8150	0.0086		
DS	One-Step	Awake / NREM/REM	0.3515	0.0108	-	-
WT+DS	One-Step	Awake / NREM/REM	1.5338	0.0127	-	-
WT	Hierarchical	Sleep/Awake	0.9320	0.0107	0.8998	0.0089
		NREM/REM	0.9651	0.0082	0.9894	0.0089
		Total	1.8972	0.0189	1.8892	0.0178
DS	Hierarchical	Sleep/Awake	0.2839	0.0085	0.2905	0.0087
		NREM/REM	0.2979	0.0074	0.3332	0.0074
		Total	0.5818	0.0159	0.6236	0.0160
WT+DS	Hierarchical	Sleep/Awake	1.4357	0.0092	1.4296	0.0080
		NREM/REM	1.6556	0.0083	1.5358	0.0076
		Total	3.0914	0.0175	2.9654	0.0156

Runtimes are listed in minutes.

Supplementary table 5 – SIESTA performance using data binned in 5-second epochs.

One-Step Approach

Using complete database to score WT mice		Using complete database to score DS mice	
Awake	0.94	**Awake**	0.91
NREM	0.90	**NREM**	0.87
REM	0.75	**REM**	0.83

Hierarchical Approach

Using complete database to score WT mice		Using complete database to score DS mice	
Awake	0.93	**Awake**	0.93
Sleep	0.91	**Sleep**	0.91
NREM	0.91	**NREM**	0.84
REM	0.76	**REM**	0.85

These tests use the complete dataset (WT n=14 , DS n=6) to score one mouse of each genotype.

A

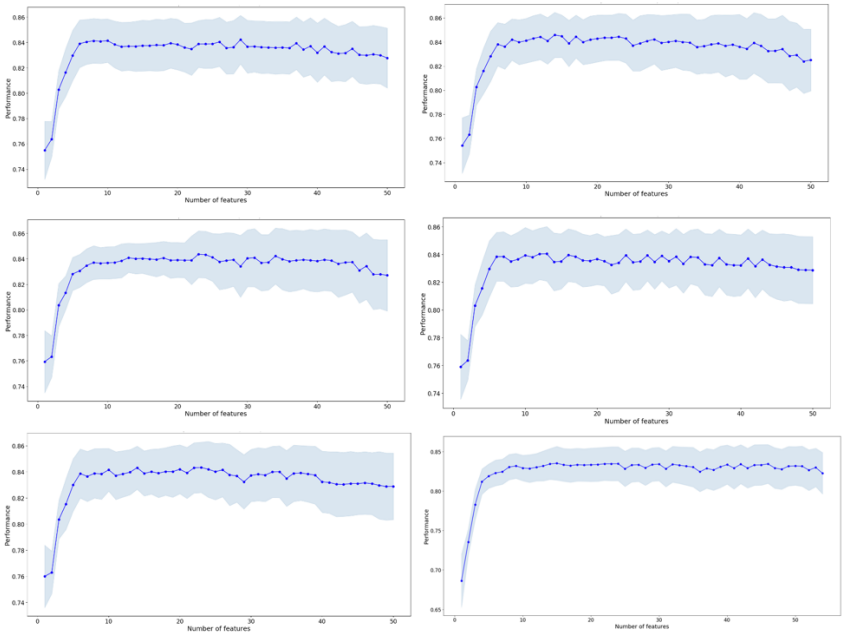

B

C

Sequential Forward Selection		
ECoG_zerocross	ECoG_zerocross	ECoG_zerocross
ECoG_spindelhan	EMG_amplitude	ECoG_spindelHan
EMG_amplitude	ECoG_spindelhan	ECoG_spectral_mean
ECoG_delta	ECoG_delta	ECoG_delta
EMG_spectral_entropy	EMG_spectral_entropy	EMG_sepctral_entropy
ECoG_thetacon	ECoG_beta	ECoG_theta3
ECoG_spectral_edge	EMG_signal_var	ECoG_spectral_edge
ECoG_deltaenergy	ECoG_spectral_edge	ECoG_theta2

D

Sequential Backward Selection.		
ECoG_zerocross	ECoG_zerocross	ECoG_zerocross
EMG_amplitude	ECoG_spindelhan	EMG_amplitude
ECoG_spindelhan	ECoG_theta3amp	ECoG_spindelhan
ECoG_delta	EMG_spectral_entropy	ECoG_delta
EMG_spectral_entropy	ECoG_rms	ECoG_theta3amp
ECoG_theta2	ECoG_sigma	ECoG_theta2
ECoG_betaenergy	ECoG_theta2amp	ECoG_theta3
ECoG_sigmaenergy	ECoG_signal_var	ECoG_sigmaamp

Supplementary Figure 1 – Sequential feature selection test using the BCRF algorithm trained on the complete dataset, with a One-Step approach. The blue dots are the mean performance and the light blue shaded area is the STD in each case. **A)** Three repetitions of the Sequential Forward Selection. **B**) Three repetitions of the Sequential Backward Selection. **C)** Table with the top 8 features of each run of the Sequential Forward Selection in order of importance. **D**) Table with the top 8 features of each run of the Sequential Backward Selection in order of importance in C and D. Features highlighted in green occurred in 2 or more runs of any Sequential Selection Algorithm.

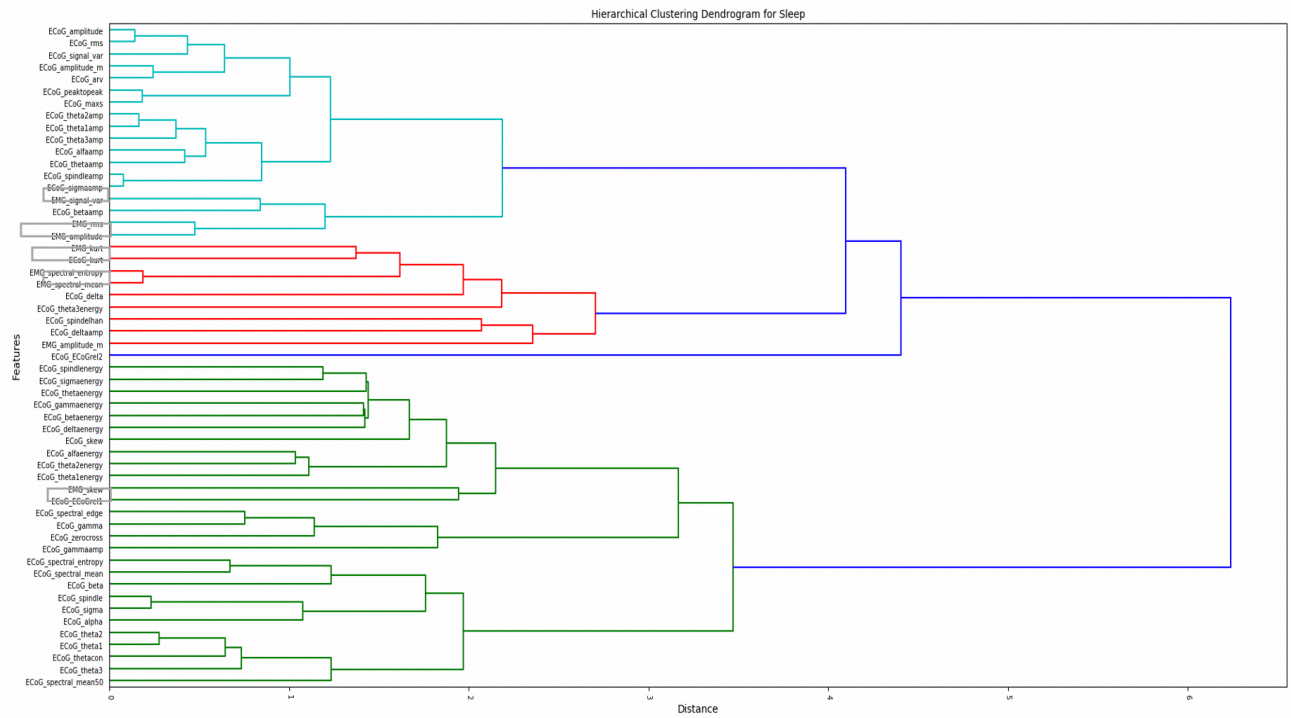

Supplementary Figure 2 – Cluster dendrogram of the pair-wise distance of the features from the complete dataset. In light blue, red and light green are the branches of the identified clusters. In blue the distance branches of the cluster features over the threshold. The most important features identified by SFS and SBS are boxed in grey on the y-axis.

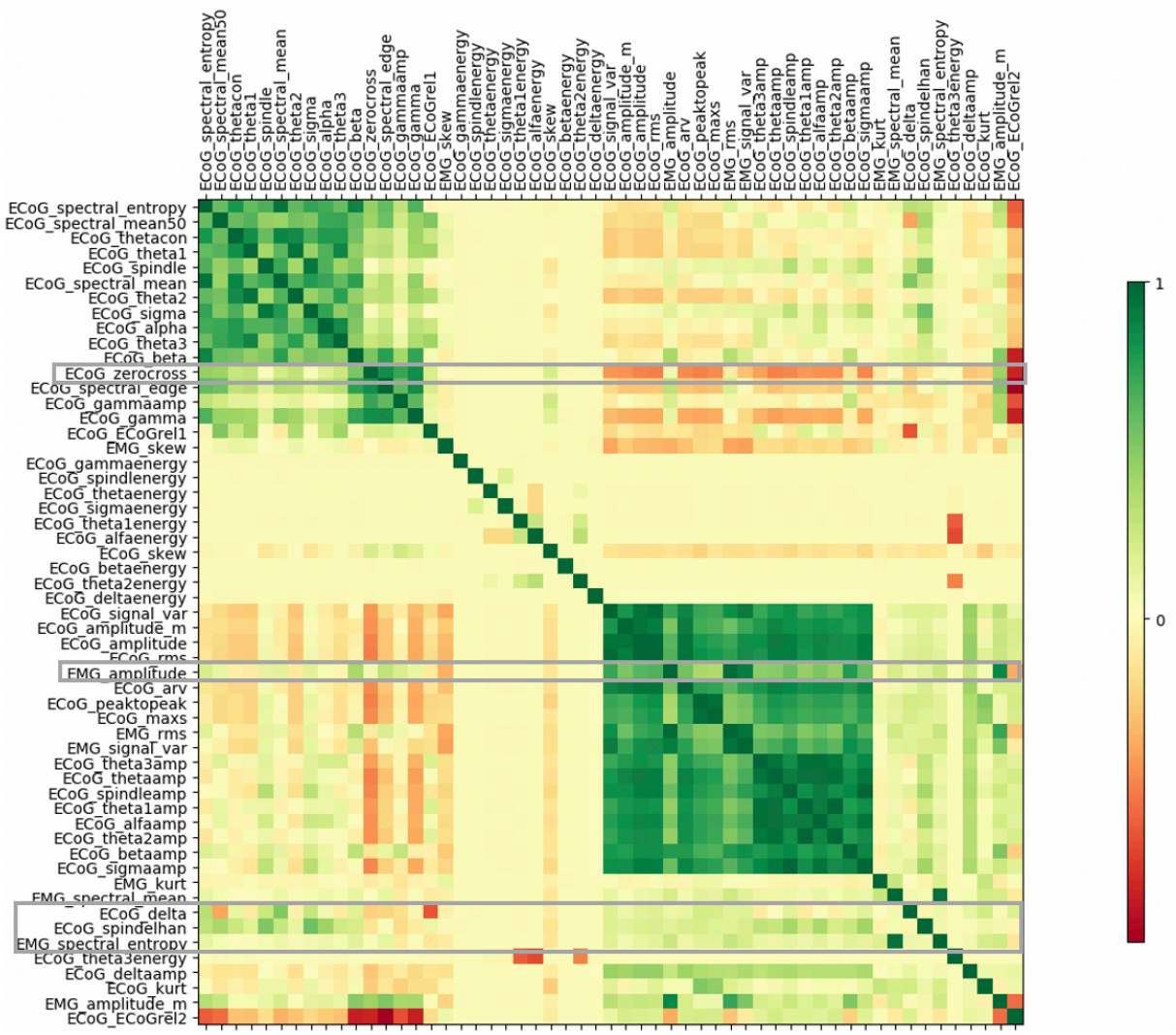

Supplementary Figure 3 – Same as Figure 1 in primary manuscript, with gray boxes surrounding the features consistently identified by sequential feature selection as being critical for classification performance.

Final Discussion

Summary of Findings

The relationship between sleep, circadian rhythms and epilepsy is well established but incompletely understood. Sleep disturbances are among the most common comorbidities of epilepsy syndromes, and sleep deprivation is associated with increased risk of seizures and poor cognitive outcomes. Understanding and addressing sleep-related symptoms of epilepsy is critical to improving outcomes and quality of life for patients and caregivers alike. In this thesis, I explored unanswered questions about the mechanisms underlying sleep and circadian rhythm disturbances in a severe form of epilepsy called Dravet syndrome (DS).

In Chapter 1, I present a set of experiments in which we performed long-term continuous polysomnographic recordings from a mouse model of DS and identified deficits in the circadian regulation of sleep. We found that although DS mice displayed the same amount of total sleep as wild-type (WT) controls, they displayed a higher intradaily variability of NREM sleep that was not correlated with the frequency of interictal epileptic events. In contrast to previous reports that DS mice display delayed re-entrainment of wheel-running activity (WRA) to phase shifts of the light-dark (LD) cycle simulating jet lag, we found no difference in time to re-entrainment of sleep stages between DS and WT mice, for both advance and delay jet lags. Additionally, we found that rapid eye movement (REM) and non-rapid eye movement (NREM) sleep re-entrain to jet lag at the same rate in mice, in contrast to reports that REM re-entrains more slowly than NREM in rats. However, we found that the siesta, a short bout of daily sleep that occurs during the dark phase in mice, re-entrains more slowly to both advance and delay jet lag than the primary bout of sleep. DS mice were less likely to have a consolidated siesta, and the differences

in re-entrainment rate between the siesta and the main bout of sleep were not present in DS mice for advance jet lags. Finally, we found the DS mice have a longer circadian period of sleep than WT controls.

In Chapter 2, I hypothesized that these sleep disturbances and previously reported deficits in circadian behavior observed in DS mice were the result of reduced GABAergic neurotransmission caused by the lack of functional $Na_V1.1$ sodium channels specifically in the suprachiasmatic nucleus (SCN). We tested predictions of this hypothesis by first generating a mouseline in which mice contained a heterozygous or homozygous deletion of the *Vgat* gene in Neuromedin-S (NMS) expressing neurons of the SCN. To our surprise, we found that these mice displayed no circadian rhythmicity of sleep under constant darkness conditions. Next, we use a similar approach to conditionally delete *Scn1a* from NMS-expressing SCN neurons. We found that these mice displayed none of the circadian behavioral deficits observed in DS mice, including the elongated circadian period of activity. Although NMS is co-expressed in ~90% of vasoactive intestinal polypeptide (VIP) and arginine vasopressin (AVP) neurons, which are critical in the maintenance of SCN network synchrony, the NMS targeting strategy spares ~60% of SCN neurons. Therefore, we sought to delete or reduce the expression of the $Na_V1.1$ channel in the entirety of the SCN using a viral targeting approach and tested the prediction of my hypothesis that mice with this conditional deletion would display an elongated circadian period of WRA and sleep. We found a significant correlation between the extent of $Na_V1.1$ channel deletion and circadian period of WRA but not sleep. Although we propose several explanations for these results in the Discussion section of Chapter 2, this particular study is limited by its low sample size and the primary aim of future research in this area will be to replicate the experiments performed using the viral targeting approach.

In Chapter 3 we leverage data collected in Chapters 1 and 2 to develop a novel method for the automatic classification of sleep stages from rodent polysomnographic data in an effort to encourage further characterizations of circadian sleep regulation in mouse models of disease. We trained a battery of supervised machine learning algorithms on a dataset collected from DS and WT mice under a range of experimental conditions and identified a method that scored sleep with an accuracy comparable to inter-rater reliability metrics obtained from experienced manual scorers in our lab. Using dimensionality reduction techniques, we identified 6 signal features that were essential to accurate scoring performance, enabling rapid sleep stage classification from test data. We have developed an open-source application based on our findings that sleep and circadian biology researchers can freely download and use to analyze their own data.

Taken together, this thesis presents novel findings about sleep and circadian rhythm disturbances in Dravet syndrome (DS) from both descriptive and mechanistic perspectives. The results presented here suggest that the lack of functional $Na_V1.1$ sodium channels in the SCN contributes to but is likely not solely responsible for the deficits in circadian sleep regulation observed in DS. Additionally, my findings in the *NmsiCre*$^{+/-}$*Vgat*$^{fl/fl}$ mouse model represent a major contribution to the longstanding debate about the role of SCN GABA in the circadian regulation of behavior, and complement the findings in our two mouse models containing conditional deletions of *Scn1a*. In addition to furthering our basic understanding of sleep and circadian biology, findings from both Chapters 1 and 2 may provide critical insight to future researchers and clinicians seeking to develop targeted therapies for circadian sleep disorders and sleep-related symptoms of DS. Finally, it is my hope that the novel data analysis methods presented in Chapter 3, which we are making free to the research community, will encourage further study of sleep disturbances in rodent models of disease, which is an increasingly

important endeavor especially in the context of neurological and psychiatric diseases that represent a significant burden to public health.